École doctorale 072 : Sciences pour l'Ingénieur

THÈSE

pour obtenir le grade de docteur délivré par

l'Université de Lille

Sciences et Technologies

Spécialité "Génie Électrique"

présentée et soutenue publiquement par

Martin Legry

le 25 novembre 2019

Control of distributed energy resources for primary response of grid-interactive micro-grids

Commande de ressources d'énergie distribuées pour la réponse primaire de micro-réseaux interactifs et connectés

Directeur de thèse : **Christophe Saudemont**
Co-encadrants de thèse : **Frederic Colas, Jean-Yves Dieulot**
Co-encadrant industriel : **Olivier Ducarme**

Membres du Jury

Serge Pierfederici,	Professeur	Président
Manuela Sechilariu,	Professeur	Rapporteur
Lieven Vandevelde,	Professeur	Rapporteur
Christophe Saudemont,	Professeur	Examinateur
Frederic Colas,	Docteur	Examinateur
Jean Yves Dieulot,	Maitre de Conférence HDR	Examinateur

Laboratoire d'Électrotechnique et d'Électronique de Puissance de Lille - L2EP
Univ. Lille, Centrale Lille, Arts et Métiers Paris Tech, HEI, EA 2697

Abstract

Control of distributed energy resources for primary response of grid interactive micro-grid

This work focuses on the control of a grid-interactive micro-grid to provide ancillary services to a weak power system, and more particularly a primary frequency and voltage response at the point of common coupling (PCC). The first objective of this thesis is to supervise a micro-grid in order to ensure stable operation while enforcing the economic objectives defined by an external optimizer.
Then, a novel three-step methodology has been developed.First, to provide the ancillary services at the PCC, it is necessary to estimate and coordinate the flexibility of heterogeneous equipment such as distributed generators, renewables, storages, etc. An optimization algorithm is proposed for the aggregation of these flexibilities to deduce the maximum active and reactive power flows that the micro-grid can provide. The second step determines the possible behavior of the micro-grid at its PCC. Finally, two new control algorithms have been developed to ensure a droop-like behavior at the PCC. A first solution, based on a centralized Model Predictive Control based supervisor, ensures a real-time adjustment of the set-points. The second one is a distributed solution that determines new primary local control laws for DERs. The effectiveness of the two control architectures has been validated by simulation with a benchmark micro-grid model.

Keywords

«Grid-interactive Micro-grid», «DER Primary Control», «Model Predictive Control», «Nonlinear Primary Control».

List of publications

Conference

M. Legry, F. Colas, C. Saudemont, J. Y. Dieulot, and O. Ducarme, *“Improved Real-Time Operation of Microgrids With Integrated Economic Constraints,”* in CIRED Workshop 2018, 2018, no. 0488, pp. 7–8.

M. Legry, F. Colas, C. Saudemont, J. Y. Dieulot, and O. Ducarme, *“A Two-layer Model Predictive Control Based Secondary Control with Economic Performance Tracking for Islanded Microgrids,”* in IECON 2018 - 44th Annual Conference of the IEEE Industrial Electronics Society, 2018, vol. 1, no. c, pp. 77–82.

M. Legry, F. Colas, C. Saudemont, J. Y. Dieulot, and O. Ducarme, *“Mixed integer quadratic programming receding horizon microgrid supervisor,”* 2019 IEEE Milan PowerTech, PowerTech 2019, 2019.

H. Fakham, T. Qoria, **M. Legry**, O. Ducarme, F. Colas, *"Development of a power hardware in the loop simulation of an islanded microgrid,"* in IECON 2019 - 45th Annual Conference of the IEEE Industrial Electronics Society, 2019, (to be published)

Journal

M. Legry, J. Y. Dieulot, F. Colas, C. Saudemont, and O. Ducarme, *“Non-linear primary control mapping for droop-like behavior of micro-grid systems”*. (Submitted to IEEE Transactions on Smart Grid)

Contents

Acronym

DER	Distributed Energy Resources.
EMS	Energy Management System.
ESS	Energy Storage System.
GAMS	General Algebraic Modeling System.
IP	Interior Point method.
LP	Linear Programming.
LV	Low Voltage.
MILP	Mixed Integer Linear Programming.
MINLP	Mixed Integer Non Linear Programming.
MIQP	Mixed Integer Quadratic Programming.
MPC	Model Predictive Control.
NLP	Non Linear Programming.
OPF	Optimal Power Flow.
PCC	Point of Common Coupling.
PMS	Power Management System.
QP	Quadratic Programming.
ROCOF	Rate Of Change Of Frequency.
SCR	Short Circuit Ratio.
SQP	Sequential Quadratic Programming method.
UC	Unit Commitment problem.
VPP	Virtual Power Plant.

Nomenclature

$(\cdot)^*$	Expected value/reference for the variable $(\cdot)$
$(\cdot)^0$	Initial state of variable $(\cdot)$
$(\cdot)_i^g$	Variable $(\cdot)$ related to the generation at node i
$(\cdot)_i^l$	Variable $(\cdot)$ related to the load at node i
$\mathcal{N}$	Set of grid nodes
$\Delta P_i,\ \Delta Q_i$	Modulated active and reactive power at node i
δ_i	Phase angle of node i
$\hat{(\cdot)}$	Predicted value of variable $(\cdot)$
$\lambda_{(\cdot)}$	Weighting factors of variable $(\cdot)$
ω	Synchronous speed
ω^n	Nominal synchronous speed
$\overline{(\cdot)}$	Maximum allowed of variable $(\cdot)$
θ_{ij}	Transmission angle of the line between node i and j
f	System frequency
f^n	Nominal system frequency
$G_{ij},\ B_{ij}$	Real and imaginary part of the bus admittance matrix of the line ij
k_i^p	Active power droop coefficient at note i
k_i^q	Reactive power droop coefficient at note i
N_c	Control horizon
N_p	Prediction horizon
$P_i^{ref},\ Q_i^{ref}$	Active and reactive power references at node i
$P_i,\ Q_i$	Active and reactive power at node i
S_{base}	Apparent base power
V_i	Voltage magnitude of node i
V_i^n	Nominal voltage magnitude of node i
$\mathcal{N}_d$	Set of inverter-controlled nodes
$\mathbf{A}$	State matrix

$\mathbf{B}$	Input matrix
$\mathbf{C}$	Output matrix
$\mathbf{D}$	Disturbance matrix
$\underline{(\cdot)}$	Minimum allowed of variable $(\cdot)$

List of Figures

List of Tables

Remerciements

Au moment ou j'écris ces dernières lignes, vient le temps de se remémorer cette expérience extremment enrichissante et si particulière qu'est une thèse. Je voudrais donc remercier tout ceux sans qui ce voyage n'aurait pu être possible.

Je commencerai donc par remercier l'ensemble des membres du jury, Mme Manuela Sechilariu et Mr Lieven Vendevelde pour avoir accepté de relire, commenter et apporter un retour sur ce manuscript, ainsi que pour les échanges durant la soutenance, et Mr Serge Pierfederici pour m'avoir fait l'honneur de présider ce jury.

Je tiens à remercier également mes encadrants, à commencer par Christophe, qui m'a fait confiance tout au long de cette thèse et pour toutes les discussions qui m'auront permis de poser et préciser mes idées. Merci également à Jean Yves pour ton regard et tous tes commentaires sur mes travaux qui m'ont permis d'avancer et de clarifier énormement le chaos qui survient parfois dans ma tête. Enfin, un immense merci à Frédéric pour toute ton implication durant ces trois ans, que ce soit scientifiquement ou pour les activités et la vie au sein du laboratoire.

Cette thèse n'aurait également jamais pu avoir lieu sans les efforts et le suivi de Yann Pankow et Olivier Ducarme, qui m'ont tout deux d'abord fait confiance pour un poste de consultant au sein de Laborelec, puis pour ces trois années de thèse.

Tout au long de ces trois dernières années passées à l'Ensam, j'ai pu côtoyer de nombreuses personnes que je voudrais également remercier. Un grand merci donc aux voisins de bureau, Jérôme, Quentin, Pierre pour toutes ces discussions toujours intéressantes (bon, peut être pas Jérôme), et ces grands moments lors des pauses le midi. Merci également à Gabriel, Tiago, David, Arthur, Amélie, Gil, Joris, Julian, Haibo, Michel, Nnaemeka, Artur, et toute la bande... pour tous les moments passés au labo, à l'ensam, dans les bars ou autour d'un jeu.

General introduction

Power system history

Back in late 19th, beginning of 20th century, the boom in electricity uses (transports, residential, industry) marked the development and growth of electric companies. At first, these developed and operated large production units close to the consumers – the cities and industries. Technologies, voltages and frequency differed from a company to another. The idea of interconnecting generation units and developing networks later appeared as a solution to increase the quality of supply and decreasing outages. The electric companies decided to adopt the same technical standards, thus making it possible to connect power networks together. Then, transmission systems and high voltage power transfer were developed with the benefits we know. New mechanisms and the first operating rules, also known as Grid Codes appeared to manage and control the power system and more specifically the interconnections (see Figure 1). They specify the requirements for a generation unit to behave on a specific power system and interact with transmission system operators and between two different areas managed by different system operators.

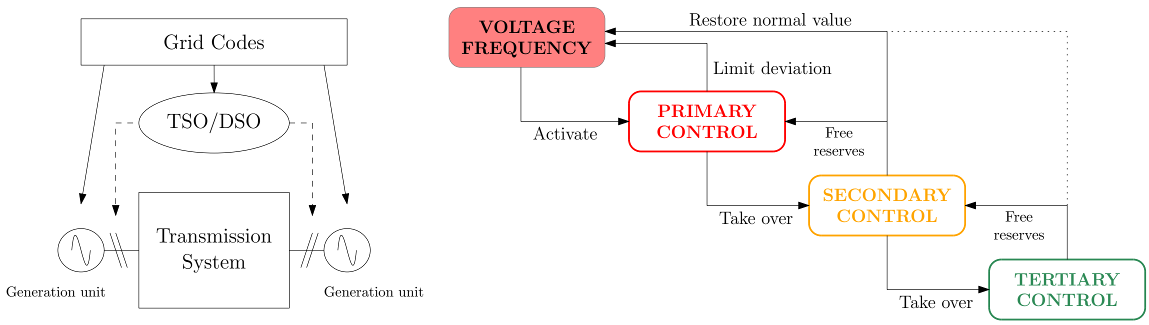

Figure 1: Grid Codes and Transmission system operation

Grid codes and regulations were and still are enhanced with technology advances (renewables, HVDC, etc.), new operating constraints, etc. One of the main and basic regulations, based on three levels of control, aims to maintain the balance between production and consumption and therefore the frequency. First, a local automatic control modulates the output power of generation units according to the frequency deviation, which is called the Primary Control or Frequency Containment Reserves. It reacts in a short time, ranging from a few seconds to 5 minutes. The Secondary Control or Frequency Restoration Reserves are activated automatically or manually by the Transmission System Operator to restore the system frequency to the nominal value, and for synchronous areas, to restore the power balance to the scheduled value. Lastly, the Tertiary Control or Frequency Replacement reserves aims to restore the power reserves allocated to support Primary Control on a longer time basis. This '*control triple*' was designed and operated for 'vertical' power systems, in which large generation units were connected to the transmission system, and the energy transported to the customer through transmission, and distribution systems. With the increase of the renewables and the desire to decrease carbon-based power generation, a new concept appears - Smart Grid - which aims to manage new assets to provide new ancillary services with the help of updated grid codes. Because of the insertion of distributed generation, bi-directional power flows and stochastic production are still challenging the Transmission and Distribution System Operators. As further step to increase the renewable share in the Western energy mix and provide reliability to the power systems, the Micro-grid concept appears as a solution to produce locally the energy consumed locally and as a solution to blackout and major disturbances. For different reference publications [1–3], we can infer the following definition of a micro-grid.

A ***micro-grid*** *is an entity of the power system with clearly defined boundaries, that aims to integrate renewable energy sources and to produce locally the energy that is needed locally. To achieve this, the micro-grid must include energy storage devices, local monitoring and local control. This entity must have the ability to operate off grid in case of necessity (blackout, disaster, island).*

Micro-grid supervision and control is ensured by a replicate of the previous '*control triple*' (see Figure 2). The primary control is generally droop-based to mimic the behavior of large synchronous generators in traditional power systems. It is designed to stabilize the grid frequency and voltage by using only local measurements and local Distributed Energy Resources controllers. The secondary control of the micro-grid is an Energy Management System which yields the references of the primary control and is commonly achieved by optimization-based algorithms. The purpose of tertiary control is to manage the power flow between the micro-grid and the utility grid and coordinate, whenever appropriate, the operation of grid-connected micro-grids.

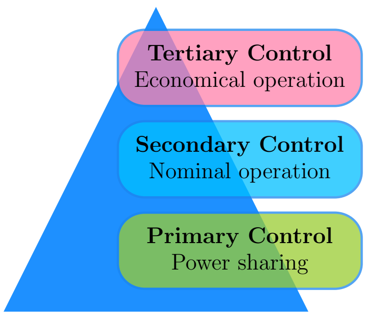

Figure 2: Micro-grid control structure

Towards a networked micro-grids based power system

Micro-grids introduce a local coordination of agents (DER's, storage systems, loads, etc.), and their development leads to imagine a *"Web of Micro-grids"* or *"Networked Micro-grids"* in which the large generation units would be replaced, at least partially, by micro-grids. Moreover, the concept of Networked Micro-grids is more probably to be developed in countries that do not have strong nor interconnected power systems and in which micro-grids are a solution to local rural electrification. Consequently and similarly to what has been developed in the early ages of power systems, this brings new challenges to coordinate and control a possibly huge and increasing amount of actors and units (cities, campuses, industrial parks etc.). However, large power systems are characterized by large reactances (ratio $\frac{X}{R} \geq 7$) and the control strategies are based on the resulting couplings and dynamics. In Micro-grids, and more generally in low voltage power systems, this ratio is close to the unity resulting in what we called a weak power system.

This thesis lies in the context of multiple weak low-voltage interconnected micro-grids. The nature of such a system makes think micro-grid control anew and the methods developed for strong distribution systems need to be modified. The objectives of this thesis are the following:

- the estimation of power flows capabilities and voltage and frequency support for micro-grids connected to weak power systems,
- the control of heterogeneous flexibilities to enforce a specified droop-like behavior at the PCC.

To attain these objectives a preliminary work shall focus on the optimal control of an islanded micro-grid. The resulting model and supervisor will serve as a basis for the development of this thesis.

Outline of this thesis

Chapter 1 presents the basics of power system control and the conventional control used from the early years of power systems. Then, a definition of weak power systems is introduced along with their challenges to highlight the need for novel control strategies. This chapter reviews the different architectures and control techniques used to build a micro-grid supervisor based on the conventional control triple. Finally, the methods and strategies applied to heterogeneous system in order to participate to the ancillary services and more precisely on the management strategies to control the interconnection between a micro-grids and a weak power system to form a so-called interactive micro-grid are presented.

As first step to study the interconnection and the ancillary services that a grid-interactive micro-grid is able to provide, **Chapter 2** presents the development of micro-grid supervisor based on Model Predictive Control technique which embeds different models and objectives (economical and physical) and coordinates the micro-grid components adequately. The interface between the economical perspective and the real-time physical supervision will be discussed and the performances compared.

The DERs and the distributed generations introduced new levers and flexibilities to control and support the network. **Chapter 3** reviews some of the recent methods proposed in the literature to aggregate these flexibilities at the Point of Common Coupling. The nature of weak low voltage micro-grids and its impact on these routines is highlighted and an extended version of a nonlinear optimal power flow is proposed to estimate accurately the capability of a micro-grid at the Point of Common Coupling. It results in a methodology to define feasible droop gains for a generic micro-grid.

Chapter 4 extends the MPC-based supervisor of Chapter 2 with an outer loop dedicated to the management of the Point of Common Coupling. This additional control enforces the micro-grid to provide a primary control similar to the conventional generation unit with a droop-like behavior. This chapter also presents a distributed method to define optimally DER primary controllers to enforce an automatic droop-like behavior at the Point of Common Coupling. The resulting control structure exhibits the following advantages and novelties:

- No external signal is required at the PCC to enforce a micro-grid primary controller.
- The primary control is optimally distributed among the flexibilities (DERs) considering their heterogeneity, constraints and limitations. The nonlinear primary control of the DERs requires only the PCC voltage and frequency signals, and is quite different from the conventional local droop architecture.
- The external operator (system operator or coordinator) only requires to know the capabilities and the behavior enforced at the PCC, preserving data and operating privacy.

The outline of this thesis can be represented by the following picture.

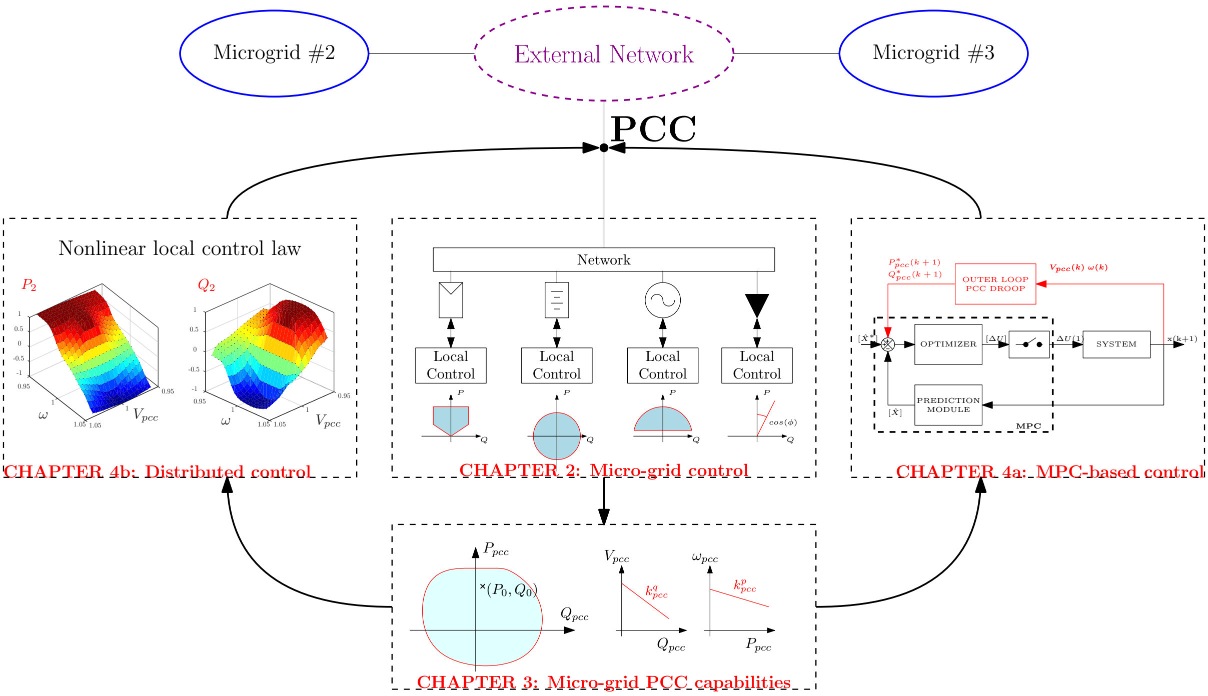

Figure 3: Micro-grid control structure

Chapter 1

Grid interactive micro-grids and ancillary services provision

Contents

1.1 General principle of power system control

1.1.1 Basics of power system

1.1.1.1 Fundamentals of system frequency

The frequency of a power system is the same in every point of a synchronous area and is determined by the angular speed of the alternators which are connected to it. Therefore, the system frequency dynamics depends on the dynamics of the angle of the alternators that is described by the swing equation:

$$\frac{2H}{\omega}\frac{d^2\delta}{dt^2} = P_m - P_e \tag{1.1}$$

where H is the inertia constant, ω the synchronous speed, P_m and P_e the mechanical and electrical powers.

The electrical power is imposed by the loads and generators connected to the network. Thus the system frequency depends on the balance between the mechanical power and the electrical load. The overall load-generator relationship is express by the swing differential equation:

$$\Delta P_m(t) - \Delta P_e(t) = 2H\frac{d\Delta f(t)}{dt} + D\Delta f(t), \tag{1.2}$$

with f the system frequency, D the frequency dependence of the loads and the operator $\Delta(\cdot)$ represents a deviation of the relevant characteristics. In the Laplace domain, the system can be represented by the block diagram in Figure 1.1.

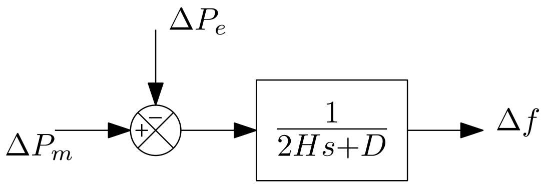

Figure 1.1: Block diagram representation of a generator-load model

Therefore, to maintain the system frequency within specified limitations, it is necessary to modulate and adjust the electrical load or the mechanical power. It is obvious that due to the high number of consumers connected to the power system it is not possible to control all the loads to maintain the system frequency, therefore alternators are equipped with a speed governor that controls the mechanical power. This local control is achieved with a simple linear feedback, a gain commonly named *droop*, and its normalized formulation is:

$$\Delta P^g_{k_{prim}} = -\frac{1}{fK_k}P^g_{k_{nom}}\Delta f \tag{1.3}$$

with $P^g_{k_{prim}}$ the change in the active power set point of unit k, $P^g_{k_{nom}}$ the nominal power of unit k, K_k the droop coefficient of the unit k and f is the system frequency (and we recall $\omega = 2\pi f$). Figure 1.2 shows an alternator with its speed governor and the relevant variables.

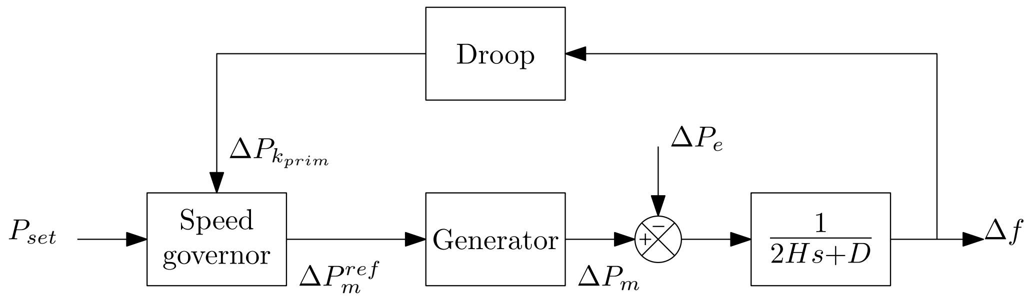

Figure 1.2: Simplified model of a generator with its speed governor and primary droop controller

Discarding the inertia and the frequency dependence of the loads, we can estimate the steady state frequency deviation due to a disturbance in either a production or a load change by defining ΔP as a power imbalance in the system (from any load or generation deviation). Suppose that the primary controllers are well designed and ensure the stability of the system. In addition, remark that the system power imbalance ΔP equals the sum of the primary control power $\Delta P^g_{k_{prim}}$. This leads to the following equations,

$$\begin{aligned} \Delta P = \sum_k \Delta P^g_{k_{prim}} &= \Delta P_m - \Delta P_e \\ -\frac{1}{f}\sum_k \frac{P^g_k}{K_k} &= \Delta P_m - \Delta P_e \\ \Delta f &= -\frac{\Delta P_m - \Delta P_e}{\frac{1}{f}\sum_k \frac{P^g_k}{K_k}} \end{aligned} \tag{1.4}$$

Including the frequency dependence of the load, the steady state frequency deviation can be expressed by,

$$\Delta f = -\frac{\Delta P_m - \Delta P_e}{DP_e + \frac{1}{f}\sum_k \frac{P^g_k}{K_k}} \tag{1.5}$$

Finally, the amplitude of the frequency deviation depends on the load changes, on the droop coefficients and on the ability of the generation units to modulate its prime mover references. If network operators require to limit the frequency deviations (commonly $\pm 5\%$), the droop gains have to be adjusted accordingly.

1.1.1.2 Fundamentals of system voltage

In order to illustrate the voltage control and the role of the reactive power, let's consider a dipole with a complex impedance (R_l and X_l). The terminal 1 produces active and reactive powers P_g and Q_g, to supply the load (P_2, Q_2) at terminal 2. Figure 1.3 depicts the dipole on the left part, and the equivalent Fresnel representation on the right.

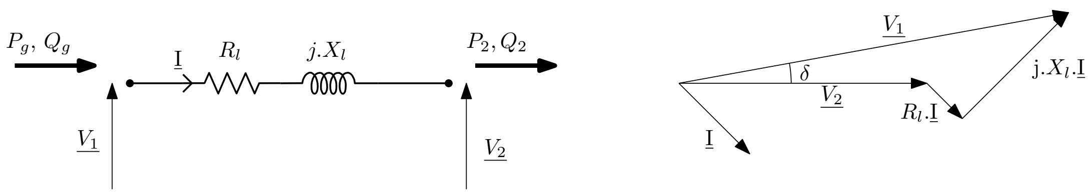

Figure 1.3: Representation of an electric line and its phasor diagram

From this figure, we can derive the following equation:

$$\underline{V_1} = \underline{V_2} + \underline{I}.(R_l + j.X_l) \tag{1.6}$$

Then, we recall that the apparent power S is

$$S = P + j.Q = V.I^* \tag{1.7}$$

and therefore,

$$I = \frac{P - j.Q}{V^*}. \tag{1.8}$$

Finally, the expression of the voltage is

$$\begin{aligned} \underline{V_1} &= \underline{V_2} + \underline{I}.(R_l + j.X_l) \\ \underline{V_1} &= \underline{V_2} + \frac{P_2 - j.Q_2}{\underline{V_1}^*}.(R_l + j.X_l) \\ \underline{V_1} &= \left[V_2 + \frac{R_l.P_2 + X_l.Q_2}{V_1}\right] + j.\left[\frac{X_l.P_2 - R_l.Q_2}{V_1}\right] \end{aligned} \tag{1.9}$$

In transmission systems, the lines are mainly inductive, and for a small angle, the expression of the voltage drop can be approximated by:

$$V_1 - V_2 = \frac{X_l.Q_2}{V_1} \tag{1.10}$$

Therefore, any change in the reactive power consumption at terminal 2 results in a voltage drop of $\underline{V_2}$ (with the assumption that $\underline{V_1}$ is controlled and constant). Controlling the consumption of the reactive power keeps the voltage in phase with the current at terminal 2 and as a consequence limits the reactive power consumed by the line.

However, this issue is relevant for transmission systems, for which the ratio $\frac{X}{R}$ is high. This relation becomes untrue for lower ratios and medium or low voltage networks - the term $R_l.P_2$ is not negligible anymore. Finally, this paragraph displays an important consideration about voltage control: contrary to the frequency, voltages are mainly sensitive to local changes and voltage management should therefore be local.

1.1.2 Ancillary services

In the previous section, the fundamentals of power systems were introduced. The role of the active and reactive power balance and their impact on the grid characteristics were presented. In this section, we detail the different controls which manage the imbalances and ensure the reliability of the power system.

1.1.2.1 Frequency Control

The European Network of Transmission System Operators for Electricity (ENTSO-E) defines the frequency control as *"the capability of a power generating module or HVDC system to adjust its active power output in response to a measured deviation of system frequency from a set-point, in order to maintain stable system frequency"*. The complete three-layer frequency control is structured as follows:

- **Primary Frequency Control**

  The primary control aims to maintain the power balance between production and consumption. This is an automatic regulation using speed governors of conventional generation units to modulate the active output power within 30 sec. This action is performed thanks to the Frequency Containment Reserve (or Primary Reserve). With the joint activation of all primary control within a synchronous area, the derivative of the frequency deviation ($\frac{\mathrm{d}\Delta f(t)}{\mathrm{d}t}$) converges to zero.

- **Secondary Frequency Control**

  The second control layer enforces new power references that remove the steady state offset induced by the primary control. This control is centralized in the way each controlled area restores the inter-area exchanges. This requires the activation of the Frequency Restoration Reserves (or Secondary Reserve), so that each controlled area adjusts its own generation (or load) to fit the local power mismatch. This reserve needs to last longer than 30 sec, up to 15 minutes. This means it can be a spinning reserve (a generation unit operating in derated mode) or a non-spinning reserve (that can be activated within 30 sec). In both cases, the activation can be automatic or manual.

- **Tertiary Frequency Control**

  The last layer is based on a centralized and manual change in the set-points of the generation units within a controlled area. This step restores an optimal dispatch of the load among the generators, and restores the secondary reserves. These changes activate the Replacement Reserves or tertiary reserves from several minutes up to hours.

The dynamics of each layer and the respective reserves are depicted in Figure 1.4. The ENTSO-E does not advise any amount of the reserves that are to be decided by TSOs. Figure 1.5 shows the activation and the estimated available reserves for the french TSO, RTE.

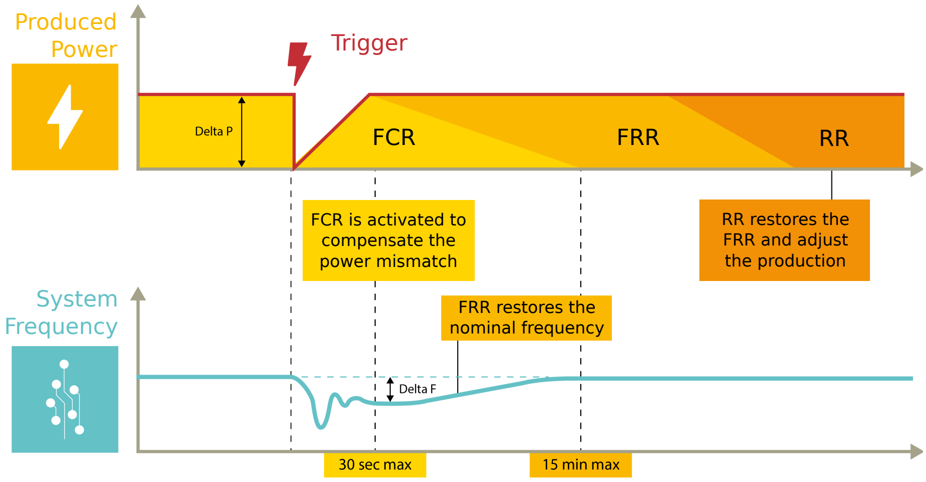

Figure 1.4: System frequency behavior and frequency controls activation [4]

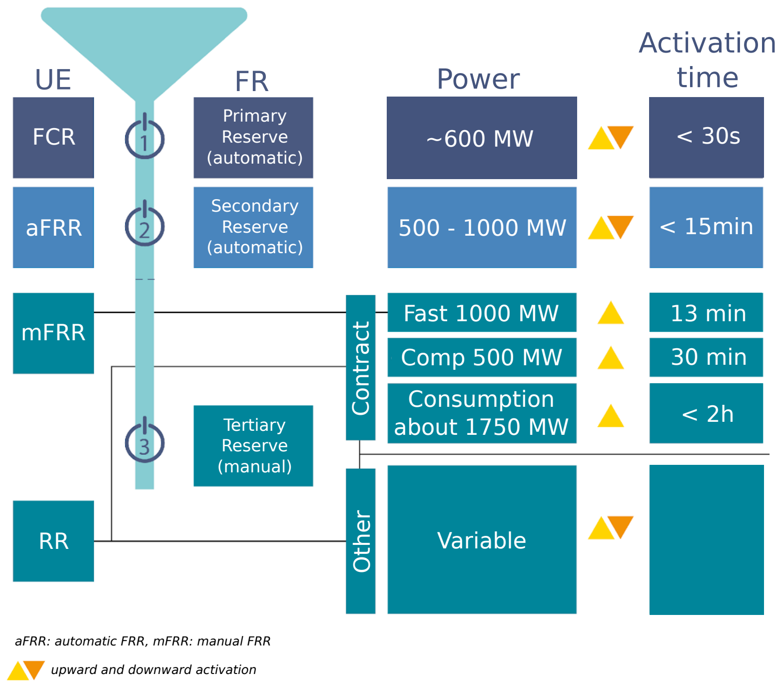

Figure 1.5: Adjustment mechanisms and reserves as defined by RTE [4]

1.1.2.2 Voltage Control

The voltage control relies on the same philosophy as for the frequency. The overall control includes three layers as follows:

- **Primary Voltage Control**

  As the voltage is a local characteristic, the primary voltage control aims to maintain the voltage at the connection point. To this end, automatic voltage regulators (AVR) react within few milliseconds, based on criteria such as the reactive power capability, the voltage drop, etc. The primary control can last up to few minutes.

- **Secondary Voltage Control**

  The secondary voltage control is a centralized coordination of reactive resources (capacitor banks, tap changer, etc.) to restore the voltage among the controlled area within boundaries. This control takes place after the primary control, up to several minutes.

- **Tertiary Voltage Control**

  The last layer acts on a longer time basis (30 min - 1 hour) and is dedicated to system-wide objectives such as losses minimization, security criterion, etc. It also frees secondary reserves and provides voltage and reactive power set points.

1.1.2.3 Other ancillary services

According to different TSOs, additional ancillary services can be required such as :

- **Black start capability**

  After (partial) shutdown of a power system, some of the generation units require auxiliary power to restart. The units able to restart on their own and to be reconnected to the system are said to have a black start capability.
  (Examples: Belgium, Italy, Denmark.)

- **Interruptible load service**

  This service is a demand-side management that is contracted between TSOs and big consumers that agree to decrease their consumption to help balance the system. This service is limited in time and in number of activations per period.
  (Examples: Belgium, Italy, Norway.)

- **Grid loss compensation**

  In this case, the TSOs purchase electricity to compensate the losses due to the transmission system.
  (Examples: Belgium, Austria.)

The conventional ancillary services presented in this section are those applied in high voltage transmission systems. They have been developed with respect to the physics as recall in the first section. Yet, micro-grids are limited to low (230/400 V) or medium voltage (about 1/10 kV). The relation and mainly the characteristics of the network change and question these ancillary services. The power system has developed an index to characterize the power system which is the stiffness of a network.

1.1.3 Stiffness of a networked micro-grid

A weak AC power system is defined, according to static and dynamic performances by the Standard IEEE 1204 [5]:

- AC system impedance may be high relative to AC power at the point of connection, i.e. short-circuit power at the point of connection may be low.

- AC system mechanical inertia may be inadequate relative to the AC power infeed.

The first item specifically expresses the capability of a power system to resist voltage deviations caused by load or generation. Generally, this characteristic is defined by the Short Circuit Ratio (SCR). This metrics is used when connecting a new equipment (load or generation) to an external system. SCR is the ratio of the short circuit power at the Point of Common Coupling (PCC), without the device, over the nominal power of the device:

$$SCR = \frac{S_{sc}}{S_{nom}}, \tag{1.11}$$

with S_{sc} the short circuit power at the PCC and S_{nom} nominal power.

Other SCR-based metrics have been proposed, as in [6], to consider multiple nearby converter-based generators:

$$WSCR = \frac{\sum_i^N S_{sc}.S_{nom}^i}{\sum_i^N S_{nom}^i} \tag{1.12}$$

As example, Table 1.1 displays the short circuit apparent power as a function of the voltage for the design of a power transformer.

Table 1.1: Short circuit apparent power for transformer design

Voltage for the equipment [kV]	**European practice [MVA]**	**North American practice [MVA]**
7 - 24	500	500
36	1000	1500
300	30000	30000
765	83500	82500

Another point which allows to evaluate the 'static' stiffness of a network is related to the ratio of the resistance over the reactance of the equivalent line connecting the external system to the DER or microgrid. This indicator is particularly relevant for the short circuit current, and its propagation through transmission lines. This ratio impacts the peak value of the short circuit current and the protection relay strategy.

Table 1.2: Typical line parameters

Voltage [kV]	**R** [Ω/km]	**X** [Ω/km]	**Ratio** $\frac{R}{X}$
Low Voltage	0.642	0.083	7.7
Medium Voltage	0.161	0.190	0.85
High Voltage	0.06	0.191	0.31

Despite these metrics, it is difficult to define a precise limit between weak and strong power systems. IEEE standard 1204-1997 proposes in [5] to define a low SCR AC/DC system by a stiffness between 2 and 3, and a very low SCR below 2. In [7], a weak grid is characterized by a SCR below 10.

The second item characterises the dynamic performances of a weak power system. One of the characteristics of these systems is the lack or low inertia provided by DERs and small conventional generators. The total inertia of such systems impacts their Rate Of Change Of Frequency (ROCOF).

$$ROCOF = \frac{\partial \Delta f}{\partial t} = \frac{f^0 \Delta P}{2 \sum_n H_n S_n} \tag{1.13}$$

with Δf the frequency deviation, f^0 the initial frequency, ΔP the active power deviation, H_n and S_n the inertial constant and nominal power of the synchronous machine n. Therefore, a low inertia system frequency is highly sensitive to active power deviations.

A weak grid is of major concern as the Distributed Energy Resources (DER) and their internal controls will largely impact the PCC behavior, and possibly results in an unstable operation of the DERs. The effects of the penetration of DERs on the stability of such power systems have been addressed in the literature. Power generators that rely on intermittent primary resources, such as renewables, may cause voltage instabilities [8, 9]. Furthermore, a low SCR and a high ratio $\frac{R}{X}$ limit the maximum transmitted active power and increase the need for reactive power capability [10]. Last, the control loops of weak power systems may interact and lead to instabilities.

From the definition of a weak grid, and when studying these system, the grid impedance and the PCC strength are significant and have to be taken into account in order to have valid conclusions. This point is particularly relevant when studying the integration of DER or small power system such as micro-grids to an external weak network. Throughout this thesis, the emphasis and the developments will focus on methodologies and algorithms which consider weak power systems and fluctuating voltages and frequency.

1.2 Control techniques for islanded micro-grid supervision

A ***micro-grid*** *is an entity of the power system with clearly defined boundaries, that aims to integrate renewable energy sources and to produce locally the energy that is needed locally. To achieve this, the micro-grid must include energy storage devices, local monitoring and local control. This entity must have the ability to operate off grid in case of necessity (blackout, disaster, island).*

From the definition of a micro-grid, controlling a micro-grid represents a first challenge, mainly in islanded mode, when it is not connected to a larger power system. In this section we introduce the conventional islanded micro-grid control architecture and some of the related control techniques. Last, when the micro-grid or more generally a hybrid power source is interconnected, a specific design of the controllers may allow such system to provide ancillary services. The end of this section will review the proposed control method for load aggregation, Virtual Power Plant (VPP) and finally grid-interactive micro-grids.

1.2.1 Islanded micro-grid hierarchical control

The ancillary services presented in the previous section were developed for conventional power systems and the micro-grid concept has converged to a similar architecture. Even though some differences exist regarding the control techniques or in the objectives, the micro-grid community mainly proposes three-layer supervisors [11–13].

Among the three control layers, the primary control layer is the only one for which a consensus is reached in the literature. It encompasses distributed solution commonly called 'droop control'. It mimics the local control of a conventional generation unit that modulates the output active power with respect to the measured frequency of the micro-grid. This relation is mainly linear, even if more advanced relations may exist, and generally aims to share the load among the DERs (see [14] for a deeper review of the droop-control methods proposed in the literature).

The scopes of the second and third layers are not well defined and the boundaries between both may slightly vary according to the literature (in term of time constants, objectives, scopes, etc.). Still, they address the main objectives that are the restoration of the nominal state of the micro-grid for the secondary layer and the update of optimal and economic operation point and power exchange with a possible external system for the third one. A comparison between the IEC/OSA 62264 standard and the layers commonly found in micro-grids management is detailed in [12], and is refined in Figure 1.6. Regarding secondary and tertiary layers in micro-grids, the proposed control techniques vary and are more detailed in the next section.

For sake of clarity, in the later, we denote as *micro-grid supervisor* (see the orange rectangle in Figure 1.6), the combination of the secondary and tertiary control layers irrespective of the architecture or control technique.

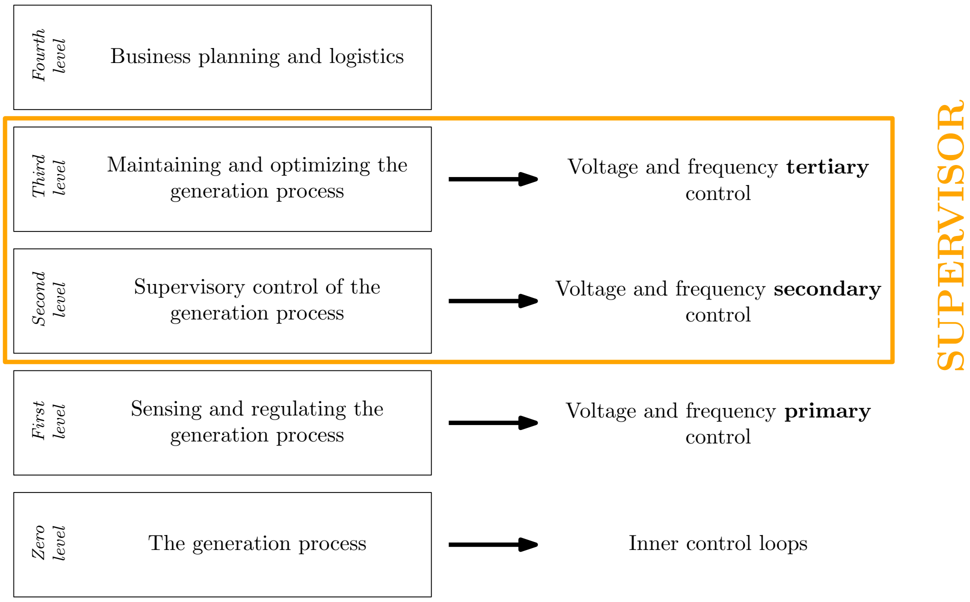

Figure 1.6: Control layers (IEC/OSA 62264 standard) and their application to micro-grids supervision

1.2.2 Micro-grid supervision techniques

Four typical architectures can be found in the literature [15]. The centralized architecture gathers information and measurements so that the references are computed and sent to the different levers. In the hierarchical control architecture, there is an intermediate layer that receives the data and that will send references to local controllers. This additional layer, for a hierarchical structure, is mainly dedicated to manage the interfaces between the subsystems, while the local controllers manage their own area. Finally, there are architectures without centralized control, so that the local controllers are independent. However, the difference between a fully decentralized and a distributed control is that in the distributed structure, the local controls may exchange information. It can be a peer to peer communication, a ring communication or a neighborhood communication. These architectures are depicted in Figure 1.7.

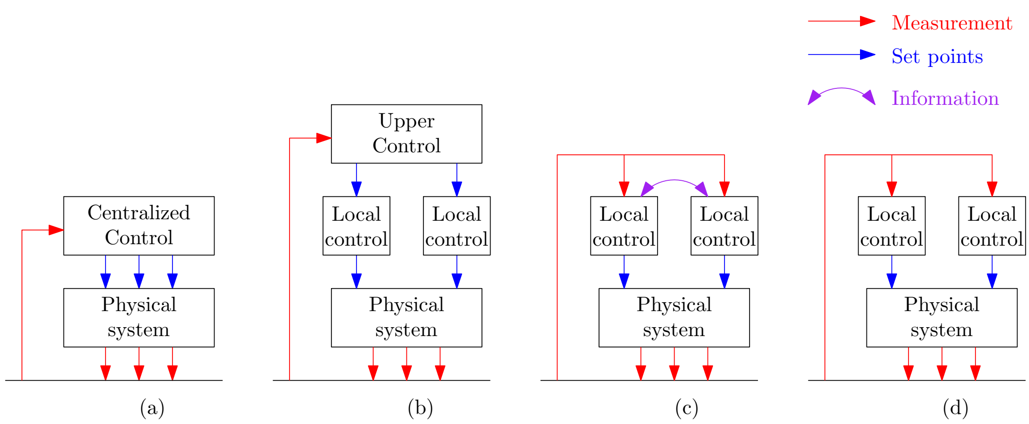

Figure 1.7: Generic control architectures – (a) Centralized structure. (b) Hierarchical structure. (c) Distributed structure. (d) Decentralized structure.

The micro-grid community mainly developed, for the specific case of an islanded micro-grid, centralized or distributed supervisors. A centralized architecture can be divided into two main categories:

- Optimization-based: Optimal Power Flow (OPF), Model Predictive Control (MPC), etc.
- Rule-based: Expert systems, Fuzzy Logic, Artificial Neural Networks, etc.

The first category of centralized architectures is based on a cost function that is to be minimized, subject to constraints related to the power system, the dynamics of the equipment, etc. The second one relies on a set of rules that are evaluated based on the system states measurements and objectives. The latter does not rely on any detailed physical model but on the knowledge of the system operator to infer rules or decision tables to operate.

A fuzzy logic supervisor for hybrid energy sources systems has been proposed in [16]. The concept is based on three main steps to determine a decision table. Once the objectives and the possible operating modes are defined, the input variables/measurements are transformed into fuzzy variables. According to the membership functions and the different operating modes, the output of the supervisor is inferred and transformed into references for the levers. Figure 1.8 displays the generic scheme of a fuzzy-based supervisor [17].

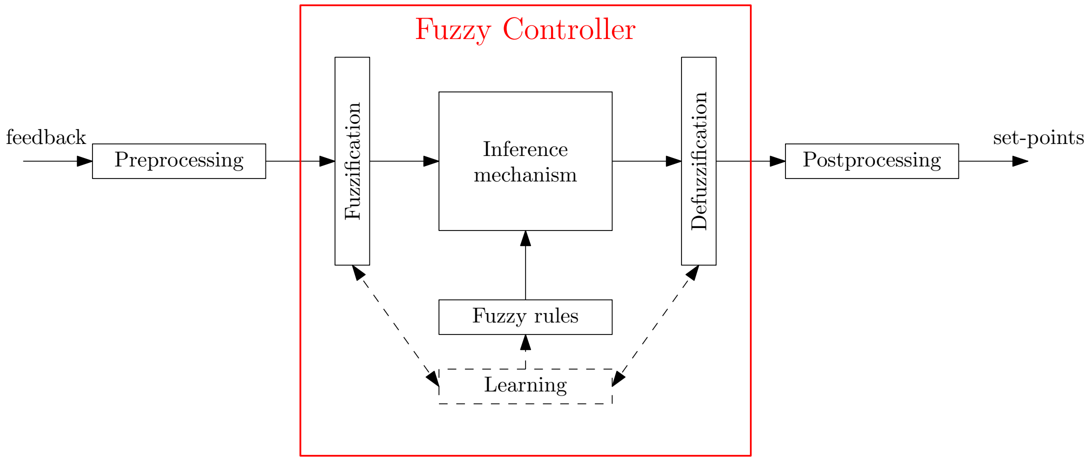

Figure 1.8: General scheme of a fuzzy-logic based supervisor [17]

This problem is also known as the economic dispatch of a power system. Other techniques have been proposed to solve the economic dispatch problem, based on a one-step robust or stochastic optimization problems. The proposed methods may include heuristics, such as genetic algorithms [18], swarm optimizers [19], or advanced optimization routines.

Another centralized technique relies on the well-know Model Predictive Control algorithm. This optimal controller yields a control sequence which is computed from the minimization of an objective function over a finite number of future time steps. To predict the future behavior of the system, the MPC controller embeds a detailed model. The principle consists to solve the optimization problem at each new time step, and apply the first control sequence. This technique is further described in Chapter 2, and will be used

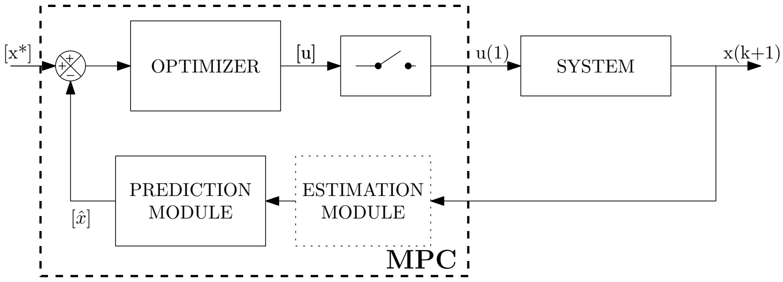

Figure 1.9: Basic structure of Model Predictive Control

to build our supervisor. An economic MPC has been proposed in [20, 21], in which the micro-grid equipment are modelled and the objective function minimizes the generation cost, while ensuring the power balance of the system. The same economic MPC principle has been extended to stochastic optimization in [22], taking into account the uncertain generation of DERs.

A complete decentralized architecture is hardly implementable. Therefore, at least some communication network is required to transmit data and measurements to the different micro-grid elements. This architecture can be applied with both techniques (optimization- or rule-based) and is sometimes called agent-based architecture. Its main challenge is to consider several sub-entities that have a limited knowledge of the whole system and to enforce a suitable operating point thanks to local control laws. There exists an important literature on distributed and hierarchical techniques [23–25]. These techniques are quite interesting when there are different actors or a restricted access to information.

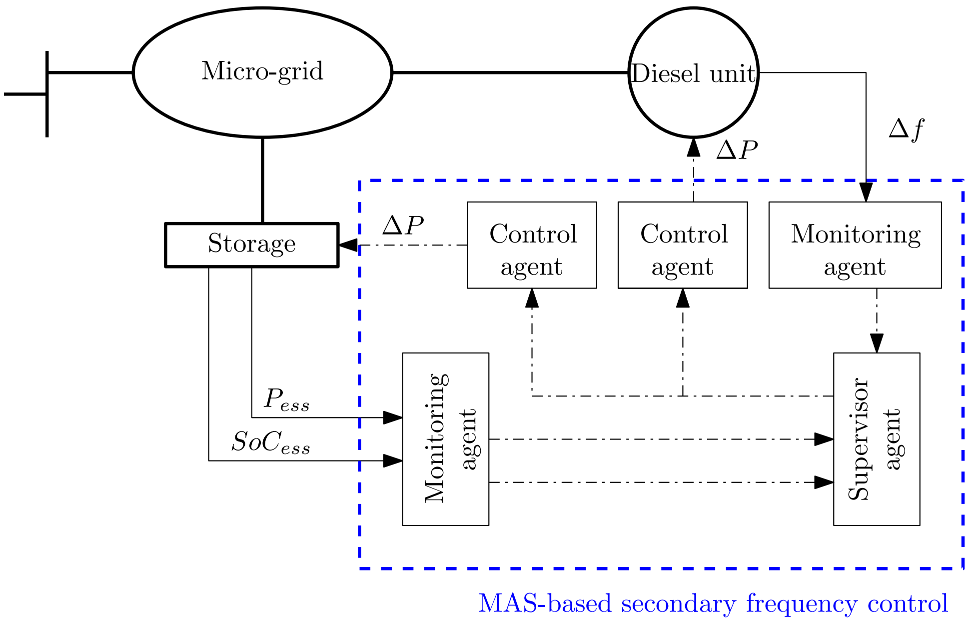

Figure 1.10: General scheme of MAS based supervisor [17]

In [26], the authors used a distributed MPC to coordinate storage systems to reduce the supply cost of the load. In [27], the authors proposed a multi-agent MPC-based supervision for voltage control and optimal power flow of a power system. Different agents were designed to control a limited portion of the system thanks to a linear model. For example, Figure 1.10 displays a multi agent system scheme proposed in [17] for secondary frequency control. It proposes three different types of agents: control, monitoring and supervisor, with a limited access to information through the communication network. The topology of the physical system as well as the communication network are of major importance in multi-agent systems. This topic is addressed in [28], in which the authors compared different network architectures, and finally proposed a systematic method to design the agent control laws.

Last, Table 1.3 proposes a comparison of the different control techniques and some of their advantages and drawbacks.

Table 1.3: Comparison of control techniques for micro-grid applications

Architecture	Control technique	Advantages	Drawbacks
Centralized	Rule-based	• Easy to implement	• Requires knowledge on the system • Flexibility
	Optimization-based	• Global optimality guaranteed • Strict respect of the constraints	• Requires a model of the system • Possibly large computational burden
Non-centralized	Optimization-based	• Computational burden (vs centralized optimization-based)	• Requires model of the interaction and coupling between sub-systems • Communication network
	Multi-agent Systems	• Flexibility • Plug and play	• Possibly sub-optimal solutions • Convergence of the solution • Complex local controller design

1.2.3 Network interconnection management strategies

The challenge of weak power systems have been highlighted in the previous section. Therefore, considering networked micro-grids, there is a need to coordinate the different assets in order to maximize the provision of ancillary services. Unlike conventional large power networks based on large synchronous machines, the generation units that form a micro-grid present much lower capabilities to ensure and maintain the stability of the complete network. However, micro-grids and aggregation of small generation or storage devices can, as single entities, provide ancillary services and more precisely primary response. This section presents the solutions to coordinate and control micro-grids such that they provide these ancillary services.

First, it is important to mention that for years until now, the literature focused on the control of a single DER (inverter-based, synchronous machine, etc.) to provide voltage and frequency primary responses. Table 1.4 presents the main capabilities of DERs to provide ancillary services [29].

Table 1.4: Technical capabilities of DER units to provide ancillary services

	PV	WTG		Hydro		Storage	
Power/Frequency Control	+	+		+		++	
Power/Voltage Control	++	Inv	++	Inv	++	Inv	++
		SG	++	SG	++	SG	++
		IG	-	IG	-	IG	-
		DFIG	+				

Legend: Inv: inverter-based - SG: synchronous generator - IG: induction generator - DFIG: doubly fed induction generator.
'+' designates a good capability in modulating active or reactive power production, '++' designates a very good capability, and '-' designates a bad capability or incapability.

When integrating multiple DERs or loads, the capabilities differ and can be combined to provide more or different services. The remainder of this section is dedicated to a review of the commonly used techniques for such heterogeneous systems and their corresponding capabilities and services.

1.2.3.1 Load control and Demand Side Management

The direct control of load or Demand Side Management (DSM) technique to alleviate power system is not new. It was first viewed as an emergency procedure to react to a large loss of production. With the increase of renewable generation, it appears to be a suitable option to handle fluctuating productions, and avoid the reinforcement of distribution systems [30]. The solution proposed in the literature are based on two main observations.

Peak load is one of the main challenges for TSOs/DSOs, which led to the development of load shifting or load shedding techniques. A large panel of control techniques exists, which is even more interesting with continuous integration of Electric Vehicle (EV) in the distribution systems. The second observation is that the voltage and the frequency of the whole system are more volatile due to renewables. Therefore, a large part of the literature focuses on the design of a local control of the load, or on load aggregation in order to provide a primary response to frequency deviations. In [31], the authors suggested that controlling the load could lead to a synchronous generator-like behavior of the loads. To this end, not only ON/OFF signals are sent according to the frequency deviation, but the local control also depends on the successive derivatives of the frequency. The advantage of the proposed control is that it does not require any communication, but only measurements of the frequency. The main drawback is that local controllers require a specific tuning of the parameters and no systematic methodology has been proposed. In [32], a complete industrial process is involved in the provision of a static and dynamic frequency response. In [33] and [34], a particularly interesting feature of the proposed control techniques lies in the droop-like response that aggregated HVACs exhibit to frequency variations. Based on the temperature measurements and forecasts, a central optimizer designs the local controllers with different frequency triggers and ON/OFF signals. Similar ideas have been further developed in [35], in which the dynamics and constraints of the devices have been taken into account.

The specific case of EV has been a prolific source for decentralized or distributed control techniques with the objective to provide primary frequency response. This kind of load presents significant advantages, mainly the ability to modulate its power, absorption, but also production, contrary to an ON/OFF mode. The evaluation of the EV in the primary reserves has been done in [36]. Last, it can be noticed that the literature focuses on the provision of a frequency response, neglecting the impact of the load or EV on the voltage profile of the feeders. The lack of voltage and reactive power compensation allows the authors of the previous publications to discard the impact of the line, and to avoid to provide a detailed model of the power system. Still, some papers address the problem of voltage management through a modulation of the charge of EV with respect to the local voltage [37]. In [38], a model of the distribution network is included in the primary frequency control so that it addresses the issues of line and transformer congestion and line losses.

1.2.3.2 Virtual Power Plant

A VPP is an aggregation of dispersed DERs, dispatchable loads and storage elements which aims to relieve the power system by providing ancillary services or by bidding on the energy market. A VPP does not have the ability to operate in islanded mode, contrary to a micro-grid, but relies on a similar multi-layer hierarchical control. Figure 1.11 displays a comparison between micro-grid and VPP control architecture and the objective of each layer [12].

Two designs of VPP coexist among the power system community [39]. First, the Commercial VPP or CVPP intends to aggregate flexibilities to sell the production capability into the energy markets avoiding, in real time, the penalties for the unserved energy. The second design, called the Technical VPP (TVPP), focuses on the interaction of DERs and flexible loads within the network. At first, the works on TVPP focused on the use of flexible loads and storage systems to manage the fluctuating output power of renewables, as in [40, 41]. The optimization based methods such as MPC are widely used to coordinate VPP. For instance, in [42], the VPP is committed in a load frequency problem. However, its hierarchical MPC controller requires to know or estimate the power system parameters (inertia and droop). The congestion management is one of the issues addressed by the VPP controller, as in [43], in which the authors proposed to quantify the cost of congestion to infer the sensible node and to minimize the cost. Last, the VPPs are also proposed as tools for system frequency regulation, as in [41] or [44].

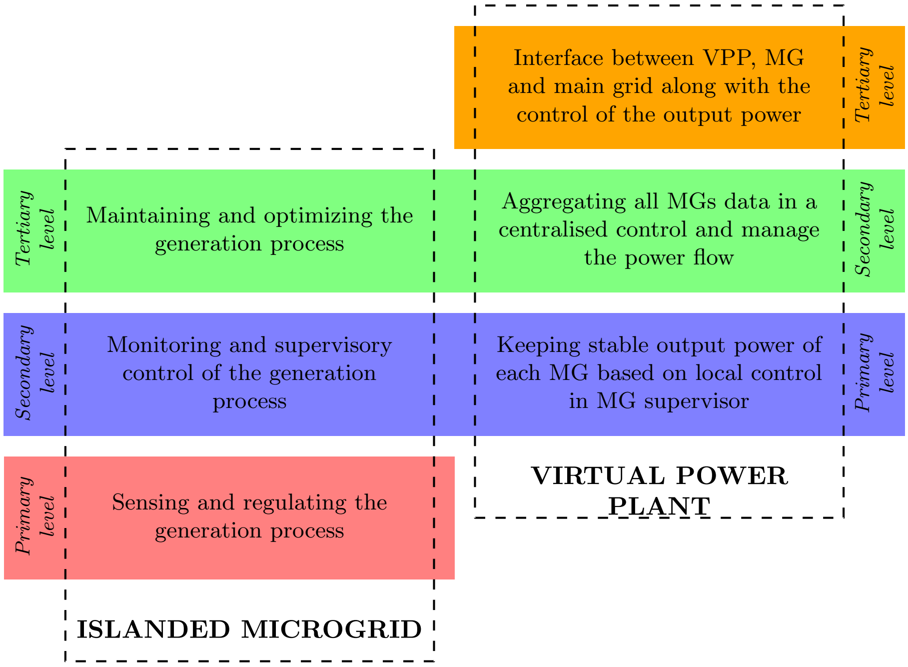

Figure 1.11: Comparison of Micro-grid and VPP control layers

1.2.3.3 Grid interactive micro-grids

The concept of micro-grid relies on a coordinated control of distributed flexibilities within a local network. Therefore it represents a great opportunity for such sub-part of the power system to provide ancillary services. Two main concepts can be found in the literature:

- a micro-grid controller that supervises the PCC, and defines appropriate references to DERs,
- a interlinking back-to-back converter which interfaces the micro-grid with the distribution or transmission network.

The first concept is closely linked to the TVPP previously presented. The premise of extending conventional supervisors for islanded mode has been proposed in the framework of the MICROGRID project through MAS-based system, as in [45], in which the authors propose to use MAS to manage the energy exchange between the different production units and the main grid. A dedicated agent regulates the interface between the distribution system and the micro-grid. Any optimization-based, as in [46], and rule-based, as in [47], supervisor may be updated to include the management of the interface in its design. Yet, this aspect has been mainly used for energy exchange, and to regulate the contractual power exchange.

The second concept is based on a additional back-to-back converter that interconnects the micro-grid network with the external system. At first, it aimed to replace conventional power transformers interfacing two subparts of the power system (LV/MV, MV/HV networks, etc.). Benefiting of the power electronics flexibility, it appears as an ideal lever for providing ancillary services [48]. Each side of the smart transformer has a specific purpose. On the low voltage side, the control loops provide and regulate the voltage waveform. Basically, this means that the smart transformer behaves as a slack node for the LV system. The embedded controller in the LV side may also use the distributed local droop controllers, and adapt the voltage waveform. The grid-side controller regulates the current absorbed by the micro-grid and the DC bus voltage. Combining these two features allows the smart transformer to control voltage-dependent loads, as proposed in [49]. Yet, it does not considers reverse power flows, and the provision of 'positive' ancillary services from the DER on the LV-side.

1.3 Positioning and contributions of the work

The increase in renewable production and distributed generators has lead to the aggregation of flexibilities to create VPP, micro-grids and load aggregators. Concurrently, the resilience and stability of the power systems decrease and require new contributions from DERs and distributed resources to provide ancillary services. The aggregated and heterogeneous systems exhibit interesting features and there exist solutions that mainly focused on the regulation of contracted energy. Some recent developments dealt with the provision of ancillary services and primary voltage and frequency control for complex heterogeneous systems. Although there exist solutions with power electronics-based 'smart transformers', the main advantage of the conventional primary response lies in its distributed nature.

In addition, the continuous increase in power-electronics interfaced, small and distributed generators challenges the conventional centralized control techniques and architectures. Therefore, the base line of this thesis is to study and propose novel control strategies using the new flexibilities to enforce a grid-interactive micro-grid to behave as a conventional primary droop control at the PCC without the need of any additional component. Last, this work differs from the VPP concept as it shall also consider the internal constraints of the micro-grid network, and the classical objectives of a micro-grids operator (economical operation, reliability, etc.).

The main contributions of this thesis are the following.

- First, the control of a islanded micro-grid remains a challenge to ensure stable and optimal operation. The proposed MPC-based supervisor embeds two layers which answer with these objectives by defining an economical trajectory at an upper layer, and a lower layer designed to ensure stable operation while minimizing the error on this trajectory.

- Second, the networked micro-grids form a weak power system which requires novel tools and control methodologies. This thesis proposed a algorithm to estimate the flexibility of a micro-grid which considers fluctuating PCC voltage.

- Third, an extension of the micro-grid supervisor is proposed to optimally adapt and coordinate the flexibilities in order to provide frequency and voltage support to the external network. Contrary to the supervisors in the literature, the proposed one focuses on the interaction in real time between the micro-grid and the external system to provide the required active and reactive powers.

- Finally, to respect the distributed nature of the primary control, the last contributions of this thesis aims to define new local controllers that ensure a droop-like behavior at the micro-grid PCC.

Chapter 2

Multi-layer MPC-based micro-grid supervision

Contents

The supervision of an islanded micro-grid is a real challenge to ensure stable and optimal operation. As detailed in the previous chapter, hierarchical control has become the standard to design a micro-grid supervisor that combines the secondary and tertiary layers, with both different objectives and models.

This chapter presents the MPC-based supervisor of an islanded micro-grid. It first presents the MPC technique and its state space formulation. Second, the micro-grid network and its main components are detailed to obtain the embedded model. This supervisor aims to achieve the secondary control as described in chapter 1. To that end an simple optimization routine has been developed based on simple and deterministic forecasts to serve as a tertiary layer. Finally, the main features of the proposed supervisor is to interface a long term, economical tertiary control, with a physical, faster time scale. This rises a last challenge to define the objective function, and a suitable interface which will be detailed in the third section. Lastly, to evaluate the effectiveness and the performances of the supervisor this chapter also presents the simulations for a Low Voltage (LV) benchmark micro-grid composed of several DERs.

2.1 Model Predictive Control and multi-layer Supervision

2.1.1 Model Predictive Control description

Among the different control techniques described in chapter 1, the MPC is a promising one. It has been developed in the 70s for petrochemical processes for Multi-Input Multi-Output (MIMO) and possibly delayed petrochemical systems [50] and improved since then, providing strong industrial application results. The following section will first present the basic principles of MPC and the main advantages are highlighted. For further formulations and theory (Nonlinear MPC, Robust MPC, Stochastic MPC, etc.) we refer to the reference books [51–53].

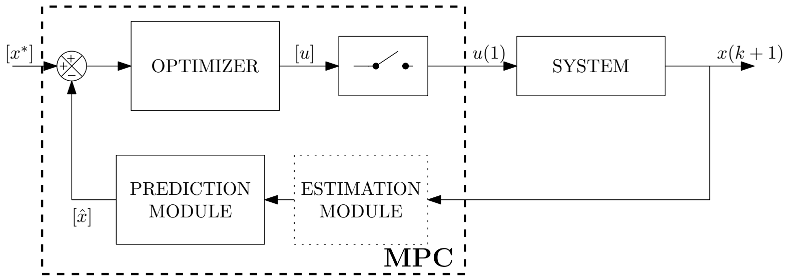

Figure 2.1: Basic structure of Model Predictive Control

Figure 2.1 presents the general synoptic of a discrete MPC. It is based on two main modules that are the *Prediction module* - and possibly an estimation module - and an *Optimizer module* to optimally define the control law.

The Model Predictive Control family is characterized by three main points. First, based on a model, measurements and estimation routines such as Kalman filters, the future behavior of the system is predicted over a specified time window called a horizon. Second, based on these predictions, a set of future control laws is determined by minimizing a (multi-)objective function. Finally, the standard procedure is to apply only the first element (one step ahead) of the set of controls and then shift the process to the next time step. This strategy, commonly foreseen as receding horizon control induces a closed loop nature of the MPC and ensures that over an infinite horizon, there exists an optimal control sequence for which the system remains stable. Obviously, it is not feasible to apply an infinite horizon, therefore, the choice of its length is a key issue that determines the stability of the system and the evolution of the cost function. Figure 2.2 shows the principle of the receding horizon control with the computation of an optimal control sequence, and the corresponding predicted behavior (left). Then only the first control sequence is applied to the system (center), and finally, the process is shifted with a new computation of an optimal control sequence, with an update of the state of the system (right).
Lastly, MPC has the following advantages:

- optimality, with the minimization of a multi-objective function,
- multi-input/multi-output models,
- multi-dynamics system models,

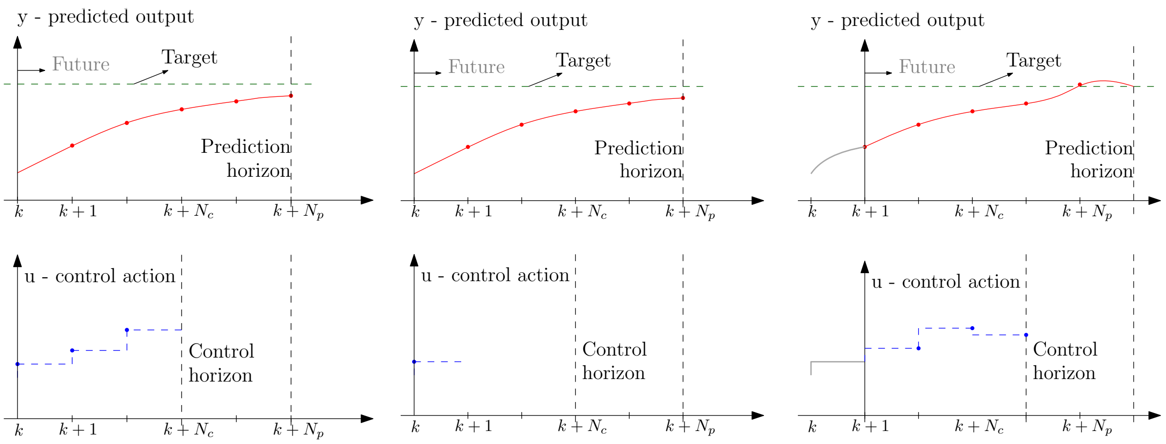

Figure 2.2: Receding multi-timestep MPC principle

- ability to deal with complex and various constraints,
- robustness against known disturbances and any aspect that requires anticipation such as time delays.

Still, the technique also presents drawbacks:

- convergence is hard to prove for nonlinear models or with complicated constraints, e.g. in case of nonlinear behavior with quantized inputs.
- control synthesis is not done explicitly but rests on the choice of the objective function (except if tight bounds are specified).

Nonetheless, MPC proves to be quite performing for smooth and large scale systems for which control synthesis is difficult.

2.1.2 State space formulation

MPC could be applied to linear and nonlinear systems and therefore the prediction module may be one or the other. For real-time micro-grid supervision, we are restricted to provide the control sequence fast enough to obtain the real time solution within a reasonable time (about a minute). Therefore, a commonplace solution is to linearize the system model so that the resolution of the optimization problem is faster. Finally, we choose to model the micro-grid system as a Linear Time Invariant State Space Model (LTI-SSM).

Let assume that the system to be controlled can be modeled by the following discrete Linear Time Invariant State Space Model:

$$\begin{aligned} x(k+1) &= \mathbf{A}x(k) + \mathbf{B}u(k) + \mathbf{D}\hat{d}(k) \\ y(k) &= \mathbf{C}x(k) \end{aligned} \tag{2.1}$$

and let us denote the internal state of the system, the inputs, the disturbances and the measured outputs of the system at the time step k by $x(k) \in \mathbb{R}^{n_x}$,$u(k) \in \mathbb{R}^{n_u}$, $d(k) \in \mathbb{R}^{n_d}$, and $y(k) \in \mathbb{R}^{n_y}$, and the state matrix, the input matrix, the disturbance matrix and the output matrix by $\mathbf{A} \in \mathbb{R}^{n_x \times n_x}$, $\mathbf{B} \in \mathbb{R}^{n_u \times n_x}$, $\mathbf{D} \in \mathbb{R}^{n_d \times n_x}$, $\mathbf{C} \in \mathbb{R}^{n_y \times n_x}$.

We desire to control the system under the following constraints on its states and inputs.

$$\begin{aligned} g(x) &\leq 0 \\ h(x) &= 0 \\ k(u) &\leq 0 \\ l(u) &= 0 \end{aligned} \tag{2.2}$$

where $g(x)$, $h(x)$ are the constraint functions on the states of the system, and $k(u)$, $l(u)$ are the constraint functions on the input of the system. Then, the control law is obtained by formulating and solving the following objective function subject to the model (2.1) and the constraint functions $g(x)$, $h(x)$, $k(u)$, $l(u)$.

$$\mathcal{C}(k) = \sum_{j=1}^{N_p} \lambda_y [\hat{y}\,(k+j|k) - y^*(k+j)]^2 + \sum_{j=1}^{N_c} \lambda_u [u(k+j-1)]^2 \tag{2.3}$$

where $\hat{y}\,(k+j|k)$ is the predicted value of the output at the instant $(k+j)$, calculated at the time step k, $y^*(k+j)$ is the output reference, $u(k+j-1)$ is the control signal at the instant $(k+j-1)$. λ_y and λ_u are the weighting factors of the state and input respectively and N_p and N_c are the prediction and control horizon that may differ. In the case the states of the system are directly measurable and tractable, we can reformulate the objective function as:

$$\mathcal{C}\left([u(0), ..., u(N_c-1)]\right) = \sum_{j=1}^{N_p} \|\hat{x}(k+j|k) - x^*(k+j)\|^2_{\lambda_x} + \sum_{j=1}^{N_c} \|u(k+j-1)\|^2_{\lambda_u} \tag{2.4}$$

where λ_x and λ_u are weighting matrices for the states and inputs and $\|\mathbf{v}\|^2_Q = \mathbf{v}^T Q \mathbf{v}$.

As previously explained, the secondary control aims to refresh the references of the actuators so that the system returns to its nominal state. Furthermore, one of the decision variables is directly the change of references that must be explicit in the prediction model. Thus, from now on, we will change the formulation of the model to use an incremental state space model that includes the dynamics of the references depicted by $\Delta \mathrm{u}(k) = u(k) - u(k-1)$. Finally, (2.1) becomes:

$$\begin{bmatrix} \hat{x}(k+1) \\ u(k) \end{bmatrix} = \begin{bmatrix} \mathbf{A} & \mathbf{B} \\ 0 & \mathbf{I} \end{bmatrix} \begin{bmatrix} x(k) \\ u(k-1) \end{bmatrix} + \begin{bmatrix} \mathbf{B} \\ \mathbf{I} \end{bmatrix} \Delta u(k) + \begin{bmatrix} \mathbf{D} \\ 0 \end{bmatrix} \hat{d}(k) \tag{2.5}$$

After some mathematical reformulations and with the assumption that the control horizon equals the prediction horizon (see Fig. 2.2), the predicted states for the whole control horizon are obtained and obey the following equation.

$$
\left[\begin{array}{c}
\hat{\mathbf{X}}(k+1) \\
\hat{\mathbf{X}}(k+2) \\
\vdots \\
\hat{\mathbf{X}}(k+N_c) \\
\hline
\mathbf{U}(k) \\
\mathbf{U}(k+1) \\
\vdots \\
\mathbf{U}(k+N_c-1)
\end{array}\right]
= \hat{\mathbf{A}}
\left[\begin{array}{c}
\mathbf{X}(k) \\
\hat{\mathbf{X}}(k+1) \\
\vdots \\
\hat{\mathbf{X}}(k+N_c-2) \\
\hline
\mathbf{U}(k-1) \\
\mathbf{U}(k) \\
\vdots \\
\mathbf{U}(k+N_c-1)
\end{array}\right]
+ \hat{\mathbf{B}}
\left[\begin{array}{c}
\Delta\mathbf{U}(k) \\
\Delta\mathbf{U}(k+1) \\
\vdots \\
\Delta\mathbf{U}(k+N_c-1)
\end{array}\right]
+ \hat{\mathbf{D}}
\left[\begin{array}{c}
\Delta\hat{\mathbf{d}}(k) \\
\Delta\hat{\mathbf{d}}(k+1) \\
\vdots \\
\Delta\hat{\mathbf{d}}(k+N_c-1)
\end{array}\right]
\tag{2.6}
$$

with

$$
\hat{\mathbf{A}} = \left[\begin{array}{cccccccc}
\mathbf{A} & 0 & \cdots & 0 & \mathbf{B} & 0 & \cdots & 0 \\
\mathbf{A}^2 & 0 & & 0 & \mathbf{AB} & \mathbf{B} & & 0 \\
\vdots & \vdots & \ddots & \vdots & \vdots & \vdots & \ddots & \vdots \\
\mathbf{A}^{N_c} & 0 & \cdots & 0 & \mathbf{A}^{N_c-1}\mathbf{B} & \mathbf{A}^{N_c-2}\mathbf{B} & \cdots & \mathbf{B} \\
\hline
0 & \cdots & \cdots & 0 & 1 & 0 & \cdots & 0 \\
\vdots & \ddots & & \vdots & 0 & 1 & & 0 \\
\vdots & & \ddots & \vdots & \vdots & & \ddots & \vdots \\
0 & \cdots & \cdots & 0 & 0 & 0 & \cdots & 1
\end{array}\right]
$$

and,

$$
\hat{\mathbf{B}} = \left[\begin{array}{cccc}
\mathbf{B} & 0 & 0 & 0 \\
\mathbf{AB} & \mathbf{B} & & 0 \\
\vdots & & \ddots & 0 \\
\mathbf{A}^{N_c-1}\mathbf{B} & \mathbf{A}^{N_c-2}\mathbf{B} & \cdots & \mathbf{B} \\
\hline
1 & 0 & \cdots & 0 \\
0 & 1 & & 0 \\
\vdots & & \ddots & \vdots \\
0 & 0 & \cdots & 1
\end{array}\right]
\qquad
\hat{\mathbf{D}} = \left[\begin{array}{cccc}
\mathbf{D} & 0 & \cdots & 0 \\
\mathbf{AD} & \mathbf{D} & & \vdots \\
\vdots & & \ddots & \vdots \\
\mathbf{A}^{N_c-1}\mathbf{D} & \mathbf{A}^{N_c-2}\mathbf{D} & \cdots & \mathbf{D} \\
\hline
0 & \cdots & \cdots & 0 \\
\vdots & \ddots & & \vdots \\
\vdots & & \ddots & \vdots \\
0 & \cdots & \cdots & 0
\end{array}\right]
$$

2.1.3 Multi-layer supervisor

The problem of the consistency of multi-layer supervisors with MPC has been discussed in [54]. It has been handled by a two-layer MPC with an intermediate module that computes reachable states, constraints and targets for the lower layer based on an economical criterion. The authors of [55] proposed a formulation of a two layer MPC and addressed the problem by determining a subset of control actions feasible at the higher level. Then, the lower layer solves each of the tracking problems for each feasible control action and regulates the actuators. For micro-grid applications, the main focus is motivated by providing a solution to stochastic and uncertain forecasts, as explained in [56,57]. The first is a survey on three methods to deal with the uncertainties of the renewable energy by using stochastic MPC. In [57], it is proposed to consider such stochastic optimization within the lower level and a deterministic layer at the higher level. However, the models and objective functions remain the same in each layer, that is to say based on the power balance of the micro-grid and a minimization of the operating costs. In [58] and [59], the authors suggested to use a multi-layer structure so that each layer includes different model dynamics and objectives. There are globally three main architectures that emerged (see Figure 2.3 (a)-(c)):

(a) a burdensome nonlinear Real Time Optimization (RTO) that defines references for local controllers,

(b) a Steady State RTO that determines repeatedly an objective which is tracked by an MPC to correct fast disturbances,

(c) a Dynamic RTO that only considers the slow dynamics to determine an objective which is tracked by a MPC module.

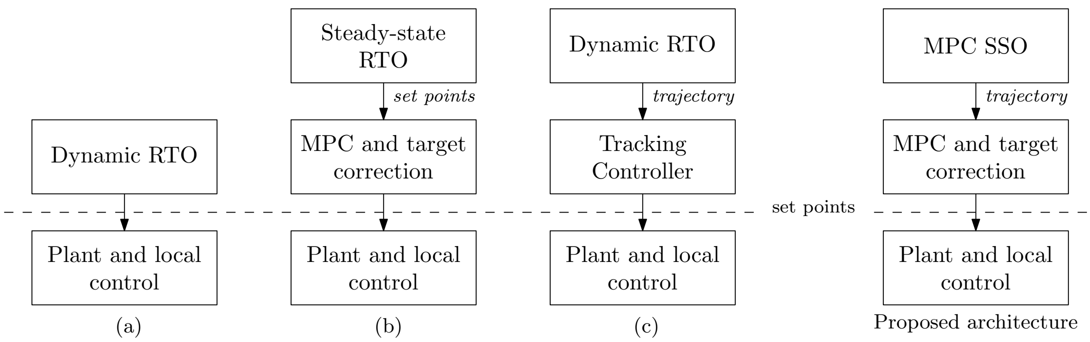

Figure 2.3: Multi-layer architectures proposed in [59] ((a) to (c)) – Proposed architecture

The supervisor we propose in this section combines the advantages of a receding Model Predictive Control State Space Optimization (MPC SSO), later on called *'Energy Management System' (EMS)*, that, based on a static model defines a trajectory with a faster MPC-based tracking controller, the *'Power Management System' (PMS)*, that embeds a refined model (Figure 2.3). Finally, the challenge in defining a suitable trajectory is to project a long time economical reference into a faster horizon. The proposed architecture is depicted in Figure 2.4. In this section, we will introduce and compare two methods to realize this interface layer. The last two will focus on the formulation of the EMS and the PMS.

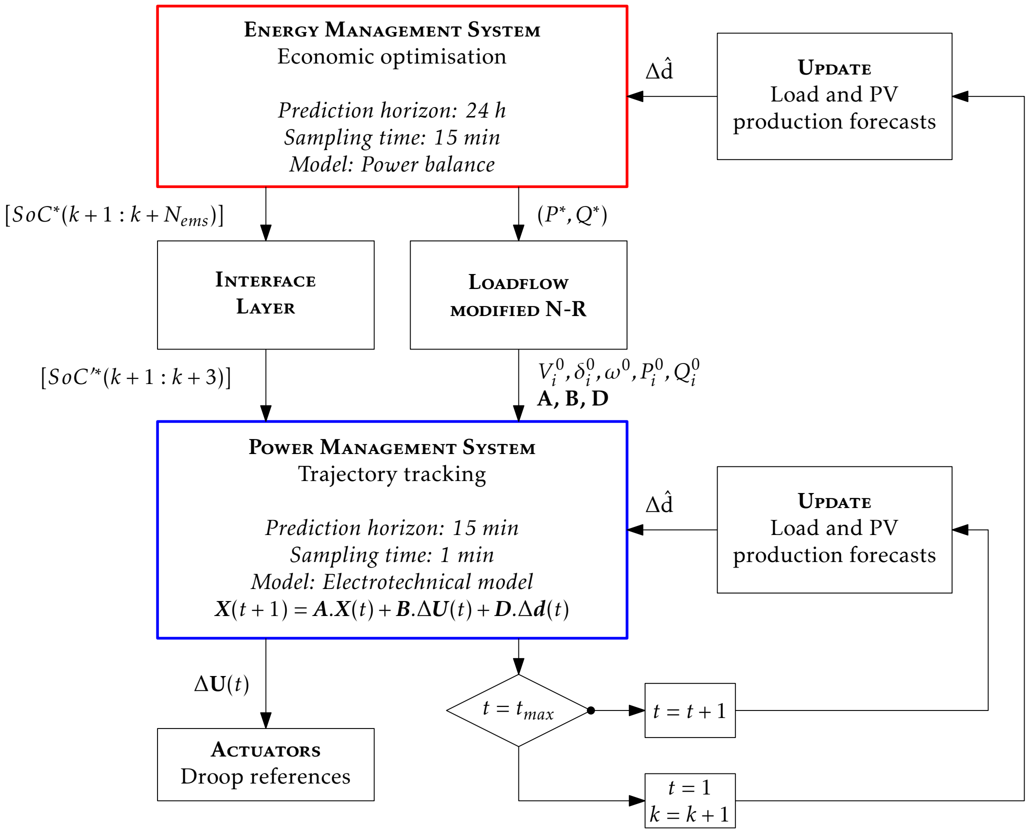

Figure 2.4: Receding horizon and asynchronism

2.2 Objective function formulation and Tertiary – Secondary Control interface

As presented in the introduction of this chapter, the MPC-based supervisor aims to embed the economical references into a secondary layer. Therefore, the formulation of the objective function of the lower layer is crucial to determine optimally the changes in the references. This section presents the methods used to project the economical references into the faster layer and their performances through simulations. We recall the generic formulation of (2.3) for an incremental model

$$\mathcal{C}(k) = \sum_{j=1}^{N_p} \lambda_y [\hat{y}\,(k+j|k) - y^*(k+j)]^2 + \sum_{j=1}^{N_c} \lambda_u [\Delta u(k+j-1)]^2 \tag{2.7}$$

2.2.1 Receding horizon based formulation of MPC problem

In this architecture, (2.7) directly applies and the difference between the predicted states and the interpolated references is minimized over a constant rolling horizon. However, using a receding horizon for secondary control requires to project the references from the secondary control into a faster horizon. To that end, one can simply use a linear interpolation, or use a stair-based approach [60] and assume the references constant for the time steps considered. With the former approach it is possible to induce different speeds of convergence by using different weighting factors according to the length of the horizon.

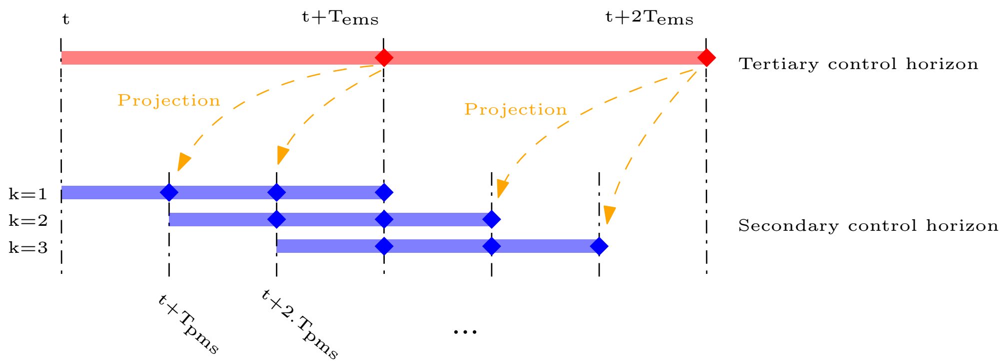

Figure 2.5: Receding horizon and asynchronism

2.2.2 Shrinking horizon based formulation of MPC problem

The basic idea of using a shrinking horizon is to deal with the economical reference as a *terminal* reference. In that sens, the horizon of the MPC reduces as time goes, until there is a synchronism between the secondary and tertiary time steps (see Figure 2.6). This means that contrary to the generic formulation of the MPC and of the objective function (2.7), we do not consider a fixed rolling control horizon N_p. Instead, we define a reducing horizon $(N_p - k)$ with an objective function that only penalizes the state at the end of the horizon.

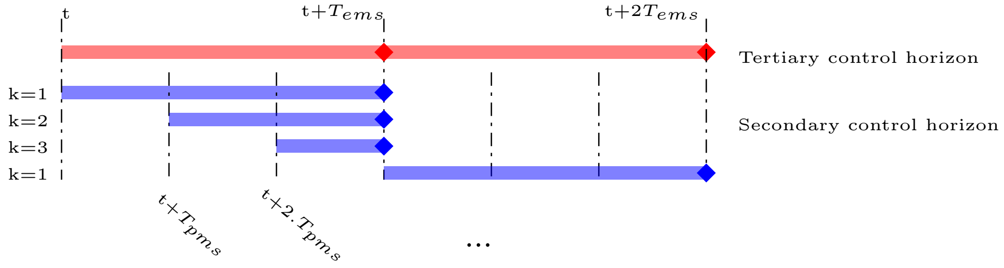

Figure 2.6: Shrinking horizon and synchronism

As a simple example, displayed in Figure 2.4, we set that the Power Management System (PMS) is defined for a control horizon N_p of three time-steps ($k \in [1, 2, 3]$). At the time $k = t = 1$, the PMS must achieve the optimal SoC determined by the Energy Management System (EMS) for the time step $t + T_{ems}$ and represented by the first red square (see Fig. 2.6). The optimal predicted State of Charge achieved by the PMS is represented by the blue square. Hence, based on a minimization of the error between the prediction model and the optimal value and of the control effort, the routine determines a sequence of three control inputs. Then, at time step $k = 2$, the objective function is updated to include two control steps to be penalized, and the routine determines a new sequence of two control inputs. The procedure continues until we reach the synchronism at the time step $t + T_{ems}$, when the references thus are updated with the new trajectory, and the procedure restarts. Finally, the generic cost function can be expressed as:

$$\mathcal{C}_1(k) = \lambda_y[\hat{y}\,(k + N_p|k) - y^*(k + N_p)]^2 + \sum_{j=0}^{N_P-k} \lambda_u[\Delta U(k + j - 1)]^2 \tag{2.8}$$

with k the current time step.

2.3 Development of linear models for micro-grids

The following sub-sections will present the development of the LTI-SSM of the main devices of a microgrid in order to be embedded into the prediction module. It is basically composed of four items: the power network, the power electronic devices (DER and Energy Storage System (ESS) - power dynamics), the storage devices (ESS - energy dynamics) and the conventional generators.

2.3.1 Power network model

In order to model the microgrid network, Figure 2.7 recalls the nodal power balance. Tellegen's theorem states that the sum of the energy at the node i must be zero:

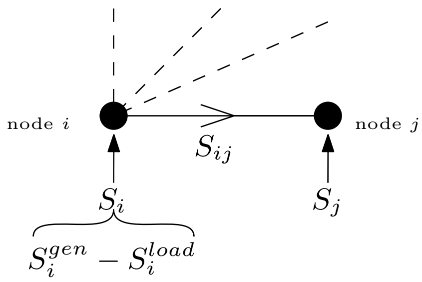

Figure 2.7: Nodal power balance

Thus, by decomposition of the apparent power into active and reactive power, the powers balance states:

$$\begin{cases} P_i^{gen} = P_i + P_i^{load} \\ Q_i^{gen} = Q_i + Q_i^{load} \end{cases} \tag{2.9}$$

where S_i^{gen} is the complex power flowing into the node i,
S_i^{load} is the complex power flowing out of the node i to the connected load,
S_i is the complex power flowing out of the node i to the adjacent nodes,

and P_i^{gen} and Q_i^{gen} are the active and reactive power flowing into of the node from the connected generator,
P_i^{load} and Q_i^{load} are the active and reactive power flowing out of the node to the connected load,
P_i and Q_i are the active and reactive power flowing out of the node to the adjacent nodes.

We can develop the transmitted power from the node i to m adjacent nodes and extend it to the active and reactive power formulation:

$$S_i = \sum_{j=1}^{m} S_{ij} = \sum_{\substack{j=1 \\ j \neq i}}^{m} (P_{ij} + jQ_{ij}) \tag{2.10}$$

where S_{ij} is the complex power from node i to node j,
P_{ij} and Q_{ij} are the active and reactive power from node i to node j.

If we consider the complex current in a transmission line as

$$I_{ij} = y_{ij}\left(E_i - E_j\right) + y_i^{sh} E_i \tag{2.11}$$

where E_i is the complex voltage at node i, defined as $E_i = V_i e^{j\delta_i}$, and V_i, δ_i are the voltage magnitude and the phase angle of node i,
y_i^{sh} is the shunt admittance of node i,
y_{ij} is the serie admittance of the transmission line, and $y_{ij} = g_{ij} + j\dot{b}_{ij}$,
with g_{ij} and b_{ij} the real and imaginary part of the admittance matrix.

Thus, we can develop the complex power from node i to node j as:

$$S_{ij} = E_i I_{ij}^* = y_{ij}^* E_i (E_i^* - E_j^*) - jb_i^{sh} E_i E_i^* \tag{2.12}$$

where I_{ij}^* is the complex conjugate of the current flowing though the line ij.

Then, we can develop the expression of P_{ij} and Q_{ij}

$$\begin{aligned} P_{ij} &= g_{ij}V_i^2 - V_iV_jg_{ij}cos\left(\delta_i - \delta_j\right) - V_iV_jb_{ij}sin\left(\delta_i - \delta_j\right) \\ Q_{ij} &= -\left(b_{ij} + b_i^{sh}\right)V_i^2 + V_iV_jb_{ij}cos\left(\delta_i - \delta_j\right) - V_iV_jg_{ij}sin\left(\delta_i - \delta_j\right) \end{aligned} \tag{2.13}$$

In the latter, we will assume that the shunt component of the nodes is negligible. Furthermore, we introduce the notation $\mathcal{N}$ as the set of adjacent nodes and define the admittance matrix as $\mathbf{Y} = \mathbf{G} + j\mathbf{B}$, and the elements of the matrix are defined by:

$$\begin{aligned} Y_{ij} &= -y_{ij} = -\left(g_{ij} + jb_{ij}\right), \forall i \neq j \\ Y_{ii} &= \sum_{j\in N} y_{ij} = \sum_{j\in N}\left(g_{ij} + jb_{ij}\right) \end{aligned} \tag{2.14}$$

Finally, we can formulate (2.13) as to express the active and reactive power injection for the node i by

$$\begin{aligned} P_i &= V_i \sum_{j\in N} V_j(G_{ij}\cos(\delta_i - \delta_j) + B_{ij}\sin(\delta_i - \delta_j)) \\ Q_i &= V_i \sum_{j\in N} V_j(G_{ij}\sin(\delta_i - \delta_j) - B_{ij}\cos(\delta_i - \delta_j)) \end{aligned} \tag{2.15}$$

Equations (2.15) are the usual equations for the power flow model. They assume that the components of the network, series resistances and reactances, are constant. This is a weak hypothesis for distribution and transmission systems where the frequency is kept almost constant. However, in islanded micro-grids, the frequency may vary. In addition, to build a micro-grid supervisor, we should be able to track the frequency of the system and thus this characteristic must appear in the model. For that purpose, we will mathematically modify the expression of the power injection, using the equation of the frequency dependent impedance (2.16) and define the absolute value of the impedance $|Y_{ij}|$ and the angle of the transmission line θ_{ij} in (2.17).

$$Z_{ij} = R_{ij} + jX_{ij} = R_{ij} + jL_{ij}\omega \tag{2.16}$$

with ω the pulsation.

$$\begin{aligned} Y_{ij} &= \frac{1}{\sqrt{R_{ij}^2 + \omega^2 L_{ij}^2}} \\ \theta_{ij} &= \tan^{-1}\left(\frac{\omega L_{ij}}{R_{ij}}\right) \end{aligned} \tag{2.17}$$

We finally formulate the so called Bus Injection Model (BIM) of a network by (2.18).

$$\begin{aligned} P_i &= V_i \sum_{j\in N} V_j \left|Y_{ij}\right| \cos(\delta_i - \delta_j - \theta_{ij}) \\ Q_i &= V_i \sum_{j\in N} V_j \left|Y_{ij}\right| \sin(\delta_i - \delta_j - \theta_{ij}) \end{aligned} \tag{2.18}$$

These equations are non-linear, and, to solve the power flow and to build a linear model of the micro-grid system, we need to use the Newton Raphson technique applied to this set of equations. First, we recall that according to (2.18), the active and reactive power injections are dependent on the voltage magnitudes and phase angles of all the nodes of the system plus the system frequency and can be rewritten as:

$$\begin{cases} P_i\left(\delta_1,..,\delta_n,V_1,..,V_n,\omega\right) = V_i \sum_{j\in\mathcal{N}} V_j \left|Y_{ij}\right| \cos(\delta_i - \delta_j - \theta_{ij}) \\ Q_i\left(\delta_1,..,\delta_n,V_1,..,V_n,\omega\right) = V_i \sum_{j\in\mathcal{N}} V_j \left|Y_{ij}\right| \sin(\delta_i - \delta_j - \theta_{ij}) \end{cases} \tag{2.19}$$

Then we denote the active and reactive power set point defined by an Energy Management System by P_i^{ref} and Q_i^{ref} and by $\mathbf{X}^0 = [\delta_1^0,..,\delta_i^0,V_1^0,..,V_i^0,\ \omega^0]^T$ the initial state of the system. The solution of the non-linear system is denoted by the superscript $\tilde{X}$, and (2.20) holds.

$$\begin{aligned} \forall i \in N,\ P_i\left(\tilde{\delta}_1,..,\tilde{\delta}_n,\tilde{V}_1,..,\tilde{V}_i,\tilde{\omega}\right) &= P_i^{ref} \\ Q_i\left(\tilde{\delta}_1,..,\tilde{\delta}_n,\tilde{V}_1,..,\tilde{V}_i,\tilde{\omega}\right) &= Q_i^{ref} \end{aligned} \tag{2.20}$$

Suppose now that the system is initiated with the vector $\mathbf{X}^0$, and that we define the corrections needed to satisfy (2.20) by $\mathbf{\Delta X} = [\Delta\delta_1,..,\Delta\delta_i,\Delta V_1,..,\Delta V_i,\Delta\omega]^T$, thus,

$$\begin{aligned} \forall i \in N,\ P_i\left(\mathbf{X^0}{+}\Delta\mathbf{X}\right) &= P_i\left(\tilde{\delta}_1,..,\tilde{\delta}_n,\tilde{V}_1,..,\tilde{V}_i,\tilde{\omega}\right) = P_i^{ref} \\ Q_i\left(\mathbf{X^0}{+}\Delta\mathbf{X}\right) &= Q_i\left(\tilde{\delta}_1,..,\tilde{\delta}_n,\tilde{V}_1,..,\tilde{V}_i,\tilde{\omega}\right) = Q_i^{ref} \end{aligned} \tag{2.21}$$

It is then possible to develop (2.21) with the Taylor's expansion formula to obtain:

$$\begin{aligned} P_i^{ref} = P_i\left(\mathbf{X_0} + \Delta\mathbf{X}\right) = P_i\left(\mathbf{X_0}\right) &+ \sum_{j=1}^{n}\left(\frac{\partial P_i\left(\delta_1,..,\delta_n,V_1,..,V_n,\omega\right)}{\partial\delta_j}\Delta\delta_j\right) \\ &+ \sum_{k=1}^{n}\left(\frac{\partial P_i\left(\delta_1,..,\delta_n,V_1,..,V_n,\omega\right)}{\partial V_k}\Delta V_k\right) \\ &+ \frac{\partial P_i\left(\delta_1,..,\delta_n,V_1,..,V_n,\omega\right)}{\partial\omega}\Delta\omega \end{aligned} \tag{2.22}$$

The same holds for the reactive power injection, and we can reformulate the set of equations in a matrix form:

$$\begin{bmatrix} P_1^{ref} - P_1\left(\delta_1^0, .., \delta_1^0, V_1^0, .., V_1^0, \omega^0\right) \\ \vdots \\ P_i^{ref} - P_i\left(\delta_1^0, .., \delta_1^0, V_1^0, .., V_1^0, \omega^0\right) \\ Q_1^{ref} - Q_1\left(\delta_1^0, .., \delta_1^0, V_1^0, .., V_1^0, \omega^0\right) \\ \vdots \\ Q_i^{ref} - Q_i\left(\delta_1^0, .., \delta_1^0, V_1^0, .., V_1^0, \omega^0\right) \end{bmatrix} = \mathbf{J} \begin{bmatrix} \Delta\delta_1 \\ \vdots \\ \Delta\delta_i \\ \Delta V_1 \\ \vdots \\ \Delta V_i \\ \Delta\omega \end{bmatrix} \tag{2.23}$$

with the Jacobian matrix $\mathbf{J}$ defined by:

$$\mathbf{J} = \begin{bmatrix} \mathbf{J_{PV}} & \mathbf{J_{P\delta}} & \mathbf{J_{P\omega}} \\ \mathbf{J_{QV}} & \mathbf{J_{Q\delta}} & \mathbf{J_{Q\omega}} \end{bmatrix} \tag{2.24}$$

and

$$\mathbf{J_{PV}} = \begin{bmatrix} \left.\frac{\partial P_1}{dV_1}\right|_{\mathbf{X^0}} & \cdots & \left.\frac{\partial P_1}{dV_i}\right|_{\mathbf{X^0}} \\ \vdots & & \vdots \\ \left.\frac{\partial P_i}{dV_1}\right|_{\mathbf{X^0}} & \cdots & \left.\frac{\partial P_i}{dV_i}\right|_{\mathbf{X^0}} \end{bmatrix} \quad \mathbf{J_{P\delta}} = \begin{bmatrix} \left.\frac{\partial P_1}{d\delta_1}\right|_{\mathbf{X^0}} & \cdots & \left.\frac{\partial P_1}{d\delta_i}\right|_{\mathbf{X^0}} \\ \vdots & & \vdots \\ \left.\frac{\partial P_i}{d\delta_1}\right|_{\mathbf{X^0}} & \cdots & \left.\frac{\partial P_i}{d\delta_i}\right|_{\mathbf{X^0}} \end{bmatrix} \quad \mathbf{J_{P\omega}} = \begin{bmatrix} \left.\frac{\partial P_1}{d\omega}\right|_{\mathbf{X^0}} \\ \vdots \\ \left.\frac{\partial P_i}{d\omega}\right|_{\mathbf{X^0}} \end{bmatrix}$$

$$\mathbf{J_{QV}} = \begin{bmatrix} \left.\frac{\partial Q_1}{dV_1}\right|_{\mathbf{X^0}} & \cdots & \left.\frac{\partial Q_1}{dV_i}\right|_{\mathbf{X^0}} \\ \vdots & & \vdots \\ \left.\frac{\partial Q_i}{dV_1}\right|_{\mathbf{X^0}} & \cdots & \left.\frac{\partial Q_i}{dV_i}\right|_{\mathbf{X^0}} \end{bmatrix} \quad \mathbf{J_{Q\delta}} = \begin{bmatrix} \left.\frac{\partial Q_1}{d\delta_1}\right|_{\mathbf{X^0}} & \cdots & \left.\frac{\partial Q_1}{d\delta_i}\right|_{\mathbf{X^0}} \\ \vdots & & \vdots \\ \left.\frac{\partial Q_i}{d\delta_1}\right|_{\mathbf{X^0}} & \cdots & \left.\frac{\partial Q_i}{d\delta_i}\right|_{\mathbf{X^0}} \end{bmatrix} \quad \mathbf{J_{Q\omega}} = \begin{bmatrix} \left.\frac{\partial Q_1}{d\omega}\right|_{\mathbf{X^0}} \\ \vdots \\ \left.\frac{\partial Q_i}{d\omega}\right|_{\mathbf{X^0}} \end{bmatrix}$$

The development of the partial Jacobian matrices is detailed in Appendix A. After solving the linear system (2.23), it is possible to determine an updated value of $\mathbf{X^0}$, denoted $\mathbf{X^1}$.

$$\mathbf{X^1} = \mathbf{X^0} + \Delta\mathbf{X} \tag{2.25}$$

If for all $i \in \mathcal{N}$, $\max\left(P_i^{ref} - P_i\left(\delta_1, .., \delta_i, V_1, .., V_i, \omega\right)\right)$ is greater than a prescribed tolerance, then the process is repeated by replacing the value $\mathbf{X^0}$ by $\mathbf{X^1}$, and with the new Jacobian matrix. Finally, once a stable state is reached, we determined the power flow and the state of the micro-grid. We also computed the Jacobian matrix that determines the sensitivity of the system according to its parameter matrix $\mathbf{X}$.

The model obtained for the power flow is static. In order to embed a prediction model into the supervisor, we have to determine the evolution of the state for the complete micro-grid network. Based on the considered time-scale (1-minute) and with the hypothesis that the disturbances will be relatively small, so that the system does not largely deviate from the nominal operation point, we can extend the static linearised power flow equations into a Quasi Steady State model. Therefore, we neglect the transients and high order dynamics of the micro-grid. To this end, we will use the Jacobian matrix, and (2.25) that is discretized to the following equation:

$$\mathbf{X}\left(k+1\right) = \mathbf{X}\left(k\right) + \Delta\mathbf{X}\left(k+1\right) \tag{2.26}$$

We recall that from (2.23), the vector $\Delta\mathbf{X} = \mathbf{J}^{-1}\left[\Delta P_1, \dots \Delta P_i,\ \Delta Q_1,\ ..,\ \Delta Q_i\right]^T$ denotes a small variation around an equilibrium, and we define ΔP_i and ΔQ_i as the deviations of the injected active and reactive power according to their references.

At this stage, it is worth mentioning that each of the nodes is treated independently of its nature (production of absorption), except that the references may be positive (for generators), negative (for loads) or null. To complete the model, we modify the Quasi Steady State model, to incorporate the levers and the states of the different equipments connected. To this end, the nodes are split into the generators and the loads, assuming without loss of generality that either a generator or a load is connected. The generator nodes are also considered as controlled nodes and thus will represent the levers, while the loads will be considered as a disturbance in the model (uncontrolled nodes). In the following, we define $\mathbf{\Delta U}$ as the vector that contains the active and reactive power reference changes provided by the secondary controller, and the disturbance by $\Delta\hat{\mathbf{d}}$. It is worth noting that for the remainder of this work, the renewable production such as that of PVs or wind turbines are considered as a positive power disturbance. Finally, the micro-grid network may be represented by an incremental state space form as follows:

$$\mathbf{X}\left(k+1\right) = \mathbf{A}\mathbf{X}\left(k\right) + \mathbf{B}\mathbf{\Delta U}\left(k\right) + \mathbf{C}\Delta\hat{\mathbf{d}}\left(\mathbf{k}\right) \tag{2.27}$$

with the following notations:

$$\begin{aligned}
\mathbf{A} &= \mathbf{I}_{n\times n}\\
\mathbf{B} &= \mathbf{J}^{-1}\left(\left[1,\cdots d\right],\left[1,\cdots d\right]\right), d\in\mathcal{N}_d\\
\mathbf{C} &= \mathbf{J}^{-1}\\
\Delta\mathbf{U}\left(k\right) &= \left[\Delta\mathbf{P}_l\left(k\right),\cdots,\Delta\mathbf{P}_d\left(k\right)\right]^T, d\in\mathcal{N}_d\\
\Delta\hat{\mathbf{d}}\left(\mathbf{k}\right) &= \left[\Delta\mathbf{P}_1^{load}\left(k\right),\cdots,\Delta\mathbf{P}_i^{load}\left(k\right)\right]^T, i\in\mathcal{N}
\end{aligned}$$

and with $\mathcal{N}_d$ the set of piloted nodes.

From the previous section, we considered the micro-grid network model as a network of nodes and of power injections. From now on, we will detail in the next sections the model of each asset connected to the nodes that participate to these power injections. First, we will review the droop-controlled inverters that interface most of the assets. Then, we will detail the storage devices and finally, the non-controllable assets.

2.3.2 Power electronics devices model

The micro-grid supervisor will operate at a sampling time of one minute. In that sense, it is only relevant to capture the dynamics of the droop control. The conventional double loop control (see [61] for a detailed description) is neglected, and we refer to [62] for a complete review of the droop techniques. The main discrete dynamics of the droop technique are recalled in (2.28). We refer the set of droop-controlled nodes by $\mathcal{N}_d$, and for $i\in\mathcal{N}_d$,

$$\begin{cases} P_i^{gen}(k+1) - P_i^{ref}(k+1) = -k_i^p.(\omega(k+1)-\omega^*)\\ Q_i^{gen}(k+1) - Q_i^{ref}(k+1) = -k_i^q.(V_i(k+1)-V_i^*)\end{cases} \tag{2.28}$$

Equation (2.28) directly introduces the levers of the droop-controlled power electronic devices, that are the active and reactive power references denoted by P_i^{ref} and Q_i^{ref} , respectively. Although we could also use the voltage magnitude and the system frequency as levers, we neglected them in the remainder. The frequency reference will be stated at 1 p.u and the voltage magnitude results of the power flow routine that determines the initial state of the micro-grid. From the time scale considered, we suppose that the transient of the frequency is neglected and thus the frequency is globally the same. Finally, as for each lever, we can formulate these references in incremental form as

$$\begin{cases} P_i^{ref}(k+1) = P_i^{ref}(k) + \Delta P_i^{ref}(k) \\ Q_i^{ref}(k+1) = Q_i^{ref}(k) + \Delta Q_i^{ref}(k) \end{cases} \tag{2.29}$$

where ΔP_i^{ref} and ΔQ_i^{ref} refer to the change of active and reactive power references. By using (2.29), it is possible to rephrase (2.28) into

$$\begin{cases} P_i^{gen}(k+1) = P_i^{ref}(k) + \Delta P_i^{ref}(k) - k_i^p(\omega(k+1) - \omega^*) \\ Q_i^{gen}(k+1) = Q_i^{ref}(k) + \Delta Q_i^{ref}(k) - k_i^q(V_i(k+1) - V_i^*) \end{cases} \tag{2.30}$$

At this stage, (2.30) allows to model the active and reactive power produced by the droop controlled inverters. However, it requires to add four states to the model, that are $P_i^{gen}(k)$, $P_i^{ref}(k)$, and $Q_i^{gen}(k)$, $Q_i^{ref}(k)$, which are the active power generation, the active power reference, the reactive power generation, and the reactive power reference respectively. It is worth insisting that these states are not based on the nodal power balance, but on the output of each generator. In addition, the frequency and voltage references will be considered as parameters of this model, based on the optimal power flow that also determines the power references. At last, we assume that the droop coefficients k_i^p and k_i^q are constant and deduced from the N-1 criterion and that the stability is ensured. From (2.30), it can be observed that the evolution of the injected active and reactive powers $P_i^{gen}(k)$, and $Q_i^{gen}(k)$, are related to the evolution of the frequency and the voltage, both are states already included in the QSS model (2.27). Therefore, the Jacobian matrix previously computed must be updated to include the gains k_i^p and k_i^q. (See Appendix A for indepth development).

Furthermore, both powers depend on the voltage and frequency at the time step $k+1$. It is required that the system only depends on states at time step k so that it is possible to define optimally the input while anticipating the system behavior. In that sense, with (2.27), and by injecting (2.23), it is possible to determine $\omega(k+1)$ and $V_i(k+1)$ as a function of $V_i(k)$, $\mathbf{B}$, $\mathbf{C}$, $\Delta\mathbf{U}(k)$ and $\Delta\mathbf{d}(k)$.
At last, the state vector is augmented to
$\mathbf{X}(k) = \Big[V_1(k), \cdots, V_i(k), \delta_1, \cdots, \delta_i, \omega(k), P_1^{gen}(k), \cdots, P_d^{gen}(k), Q_1^{gen}(k), \cdots, Q_d^{gen}(k), P_1^{ref}(k), \cdots, P_d^{ref}(k), Q_1^{ref}(k), \cdots, Q_d^{ref}(k)\Big]$.

Finally, technical constraints apply to the active and reactive power injections:

$$\begin{gathered} 1 \geq P_i^{gen}(k) \geq -1 \\ (P_i^{gen}(k))^2 + (Q_i^{gen}(k))^2 \leq 1 \end{gathered} \tag{2.31}$$

2.3.3 Synchronous generators model

A conventional generator, mainly gas or diesel can be considered as a specific droop control converter with a null droop coefficient, and as for droop-controlled inverters, the fast dynamics of the controller (excitation system and governor) are neglected. Therefore, the model of conventional generators is a piloted active and reactive power production, and can be formulated as:

$$\begin{cases} P_i^{gen}(k+1) = P_i^{ref}(k) + \Delta P_i^{ref}(k) \\ Q_i^{gen}(k+1) = Q_i^{ref}(k) + \Delta Q_i^{ref}(k) \end{cases} \tag{2.32}$$

In addition, active and apparent power limitations apply:

$$\begin{gathered} 1 \geq P_i^{gen}(k) \geq 0 \\ (P_i^{gen}(k))^2 + (Q_i^{gen}(k))^2 \leq 1 \end{gathered} \tag{2.33}$$

2.3.4 Storage model

The last variable we must supervise is related to the State of Charge of the storage devices. The behavior of the storages, mainly batteries of different technologies (Li-ion, Pb, etc.) is nonlinear [63, 64]. In order to build a linear model of the micro-grid, we assume that the main non-linearity, that is in the time scale considered the efficiency, is constant.

This results in the model of the storage devices as follows:

$$\begin{cases} SoC(k) - \eta_{ch} \dfrac{P_b(k+1)T_s}{60}, & \text{if } P_b(k+1) \leq 0 \\ SoC(k) - \eta_{disch} \dfrac{P_b(k+1)T_s}{60}, & \text{if } P_b(k+1) \geq 0 \end{cases} \tag{2.34}$$

with $SoC(k)$ the State of Charge of the devices at time step k, η_{ch} and η_{disch} the charge and discharge efficiency, $P_b(k)$ the output power of the storage devices and T_s the sampling time (one minute). In the latter, we assume that the charge and discharge efficiency are similar so that we can reduce the storage devices model to:

$$\begin{cases} SoC(k) - \eta \dfrac{P_b(k+1)T_s}{60}, & \text{if } P_b(k+1) \leq 0 \\ SoC(k) - \dfrac{1}{\eta} \dfrac{P_b(k+1)T_s}{60}, & \text{if } P_b(k+1) \geq 0 \end{cases} \tag{2.35}$$

It is worth mentioning that the output power of the storage P_b refers to the output powerof a droop-controlled inverter, and therefore is constrained by (2.31). In addition, the State of Charge of the storage is constrained :

$$\begin{cases} \overline{SoC} \geq SoC(k+1) \geq \underline{SoC} \\ \overline{P} \geq P(k+1) \geq \underline{P} \end{cases} \tag{2.36}$$

2.3.5 Renewable energies and loads model

The last elements of the model embedded in the MPC refer to the loads and renewable productions. We assume in the latter that an additional module predicts the loads and renewable production for the whole horizon considered. Therefore, loads and renewables will be included as a known disturbance of the system.

2.3.6 Complete model of the micro-grid

Finally, with the development in subsection 2.3.1 to 2.3.5, the micro-grid can be modeled as a linear system:

$$\begin{bmatrix} \mathbf{X}(k+1) \\ \mathbf{X}(k+2) \\ \vdots \\ \mathbf{X}(k+N_c+1) \\ \hline \mathbf{U}(k) \\ \mathbf{U}(k+1) \\ \vdots \\ \mathbf{U}(k+N_c) \end{bmatrix} = \hat{\mathbf{A}} \begin{bmatrix} \mathbf{X}(k) \\ \mathbf{X}(k+1) \\ \vdots \\ \mathbf{X}(k+N_c) \\ \hline \mathbf{U}(k-1) \\ \mathbf{U}(k) \\ \vdots \\ \mathbf{U}(k+N_c-1) \end{bmatrix} + \hat{\mathbf{B}} \begin{bmatrix} \Delta\mathbf{U}(k) \\ \Delta\mathbf{U}(k+1) \\ \vdots \\ \Delta\mathbf{U}(k+N_c-1) \end{bmatrix} + \hat{\mathbf{D}} \begin{bmatrix} \Delta\hat{\mathbf{d}}(k) \\ \Delta\hat{\mathbf{d}}(k+1) \\ \vdots \\ \Delta\hat{\mathbf{d}}(k+N_c-1) \end{bmatrix} \tag{2.37}$$

with

$$\mathbf{X}(k) = [\mathbf{V}_i(k), \delta_i(k), \omega(k), \mathbf{P}_j^{ref}(k), \mathbf{Q}_j^{ref}(k), \mathbf{P}_i(k), \mathbf{Q}_i(k)]^T, \ i \in \mathcal{N}, \ j \in \mathcal{N}_d$$

and

$$\begin{aligned} \mathbf{\Delta}\mathbf{U}(k) &= [\mathbf{\Delta}\mathbf{P}_j^{gen}(k), \mathbf{\Delta}\mathbf{Q}_j^{gen}(k)], \ j \in \mathcal{N}_d \\ \mathbf{\Delta}\hat{\mathbf{d}}(k) &= [\mathbf{\Delta}\mathbf{P}_i^{load}(k), \mathbf{\Delta}\mathbf{Q}_i^{load}(k), \mathbf{\Delta}\mathbf{P}_i^{DER}(k), \mathbf{\Delta}\mathbf{Q}_i^{DER}(k)], \ i \in \mathcal{N} \end{aligned}$$

and, finally, the constraints on the states and inputs changes apply :

$$\begin{aligned} \underline{\mathbf{\Delta}\mathbf{U}} \leq \mathbf{\Delta}\mathbf{U}(k) \leq \overline{\mathbf{\Delta}\mathbf{U}} \\ \underline{\mathbf{X}} \leq \mathbf{X}(k+1) \leq \overline{\mathbf{X}} \end{aligned}$$

With a complete linear model of the micro-grid, designing the objective function remains the last challenge. Formulating a linear -or more generally a convex- objective function ensures a fast convergence to a global solution thanks to Mixed Integer Linear Programming (MILP) or Mixed Integer Quadratic Programming (MIQP) solvers.

2.4 Comparison and performances of shrinking and receding horizon based MPC

This section aims to compare both methods to project the economical reference into the faster layer and compare the system behavior and lever effort in each case. To this end, we briefly review the computation of economical references based on the minimization of the diesel generator operating cost to define the input of the micro-grid supervisor. Then this section presents two simulations to compare the receding and shrinking horizon-based supervisor with a generic LV test benchmark model.

2.4.1 Tertiary Control formulation and unit commitment

The formalization of a generic Unit Commitment problem (UC) for micro-grid systems is presented. It basically corresponds to the Energy Management System. Figure 2.8 recalls the inputs/outputs and the parameters we consider for this module. We only consider a deterministic system for which the disturbances are known. The formulation we present in this subsection is valid for one step, but as detailed for the MPC supervisor, we use a receding MPC to compute the SoC references for 24 hours ahead, on a time basis of 15 minutes.

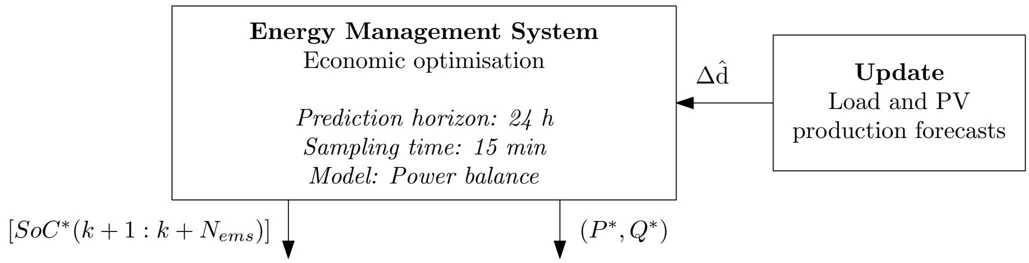

Figure 2.8: Energy Management System inputs/outputs

Within the time scale considered, each element is modeled by its static behavior. We refer to [65] and the references therein for an extensive review of deterministic and uncertain large scale unit commitment problems. For these simulations, we will consider three main components for determining the cost function of the UC problem:

- a diesel generator,
- a short term storage,
- a long term storage.

While the first item is clear, the difference between long term and short term storages consists of the way to address efficiently intra-day or seasonal fluctuations. For the remainder of this section, we focus on the design of the cost function and constraints related to these three items to formulate an optimization problem. Last, we only consider the electrical aspect of the UC problem, and neglect the '*multi-fluid*' aspect (diesel refueling, cogeneration, etc.).

Diesel generator

Diesel, and more generally thermal generation units are one of the most costly and polluting components of a micro-grid. Therefore, they play an important role in the EMS formulation and on the economical and emissions optimal operation of the system. The operating cost of these systems can be modeled, for both fuel cost and pollutant emissions, by quadratic functions [66–68]. Therefore, the objective function $\mathcal{C}_i$ for a thermal generation unit is

$$\mathcal{C}_i = \sum_{i \in \mathcal{N}_{dg}} d_i \left(\alpha_i + \beta_i P_i + \gamma_i P_i^2 \right) \tag{2.38}$$

with α_i, β_i, γ_i the cost coefficients, and d_i an integer which represents the state (on/off) of the unit. The system is constrained by its maximum and minimum active power generation, and on the time basis considered, we neglect the ramp up and dynamics of the thermal units. In addition, it is sometimes recommended to avoid under-loading of the generator set to increase its life span and reduce maintenance costs. Finally, for a multiple time step horizon control, the generator set is usually constrained to remain on a fixed ON or OFF position for a specific time duration, mainly for cooling and heating efficiency purposes. The constraints are then:

$$d_i \underline{P_i} \leq P_i \leq d_i \overline{P}_i \tag{2.39}$$

in addition to the conditional constraints:

$$\begin{cases} \text{if } \uparrow d_i(t) & \text{then } d_i(t : t+k) := 1 \\ \text{if } \downarrow d_i(t) & \text{then } d_i(t : t+k) := 0 \end{cases} \tag{2.40}$$

with $d_i(t)$, a binary which represents the state of the generator set at the time step t and the operators $\uparrow$ or $\downarrow$ which represent the decision to start or stop the generator unit. The resulting model is a MIQP which has a computational complexity which grows exponentially with the number of binary variable.

Short and long term storage

The model of storage dynamics and limits are the same as previously detailed in (2.35) and (2.36):

$$\begin{cases} SoC(k) - \eta \dfrac{P_b(k+1)T_s}{60}, & \text{if } P_b(k+1) \leq 0 \\ SoC(k) - \dfrac{1}{\eta}\dfrac{P_b(k+1)T_s}{60}, & \text{if } P_b(k+1) \geq 0 \end{cases} \tag{2.41}$$

$$\begin{cases} \overline{SoC} \geq SoC(k+1) \geq \underline{SoC} \\ \overline{P} \geq P(k+1) \geq \underline{P} \end{cases} \tag{2.42}$$

The difference between long term (hydrogen, compressed air, etc.) and short term (batteries – Lithium-ion, lead-acid, etc.) storage systems is mainly due to the internal capability and performances [69]:

Table 2.1: Storage characteristics

Type	**Efficiency** [%]	**Self discharge** [% per day]	**Depth of discharge** [p.u]	**Response time** [s]
Lithium-ion	80-85	0.1-0.3	0.8	0.005
Lead acid	70-75	0.1-0.4	0.8	0.005
Hydrogen	35-40	0.003-0.03	1.0	600

Therefore, most of the micro-grid supervisors are based on a priori rules for a better use of low efficiency and time delayed storage devices. Along with long enough control horizon, these characteristics may be used to address long term fluctuations – daily, monthly or seasonal variation of DER production.

Power balance

The last constraint is related to the power balance equation which ensures that the load power is produced by any relevant generator:

$$\sum_{i\in\mathcal{N}_{dg}} P_i + \sum_{j\in\mathcal{N}_{st}} P_j + \sum_{k\in\mathcal{N}_{lt}} P_k = \sum P_{load} - \sum_{d\in\mathcal{N}_{der}} P_d \tag{2.43}$$

Unit Commitment problem

Finally, the UC problem is formulated for the complete prediction horizon considered as:

$$\begin{array}{ll} \text{minimize} & \mathcal{C}_i \ (2.38) \\ \text{subject to} & \text{Equations (2.39) to (2.43)} \end{array} \tag{2.44}$$

2.4.2 Simulation results and comparison

2.4.2.1 Micro-grid testbench

The simulations are based on the European Low Voltage Distribution benchmark network proposed by the CIGRE Task Force C6.04.02 in [70] for residential 400 V systems. The micro-grid topology is depicted in Figure 2.9, and the characteristics of the lines in Tables 2.2 and 2.3. It is based on two different storage devices. A hydrogen-based storage is committed to meet the daily forecast load demand (node 6), and a lithium-ion based device with a conventional droop mechanism (node 2) copes with the fluctuating power generation of DERs. Last, a diesel generator (node 15) supplies the base load. The ratings and characteristics of the devices are summarized in Table 2.4.

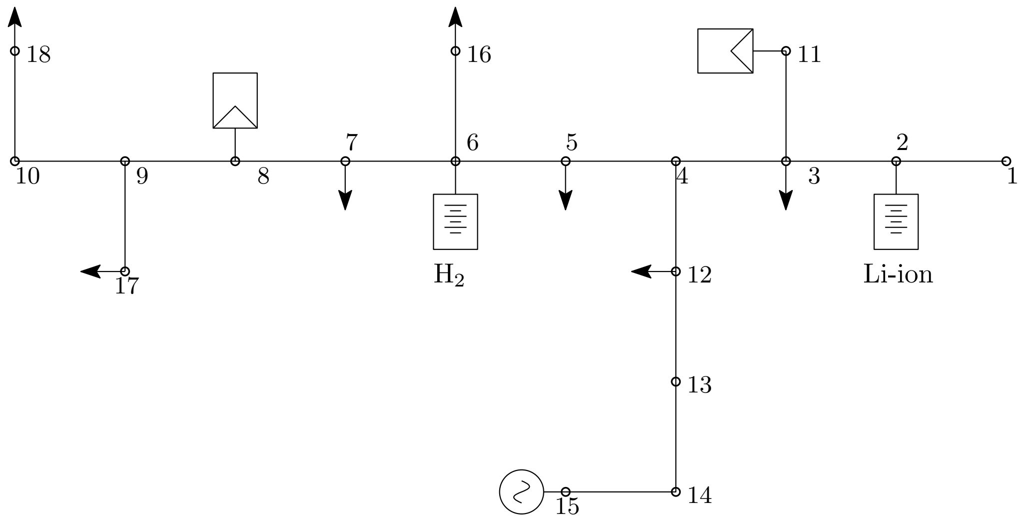

Figure 2.9: Microgrid network topology and DERs positions

Table 2.2: Line parameters

Type	**R [Ohm]**	**X [Ohm]**
1	0.170	0.087
2	0.280	0.087
3	0.353	0.091

Table 2.3: Line characteristics

Line		**Type**	**Length [m]**
From	**To**		
1	2	1	45
2	3	1	90
3	4	1	70
4	5	1	90
5	6	1	75
6	7	2	85
7	8	2	45
8	9	2	95
9	10	3	35
3	11	2	30
4	12	3	20
12	13	2	25
13	14	2	100
14	15	2	85
6	16	2	125
10	18	3	45
17	9	3	50

3264

Table 2.4: DER parameters

Type	**Node**	P_{nom} **[kW]**	SoC_{nom} **[kWh]**
Battery 1	2	100	200
Battery 2	6	100	500
Genset	15	100	-
PV1	8	100	-
PV2	11	50	-

2.4.2.2 Modeling system and numerical solvers

To formulate the problem previously stated, different modeling tools exist together with external solvers. Regardless the nature of the optimization problem, one can cite the following modeling software:

- Matlab,
- General Algebraic Modeling System (GAMS)[1],
- YALMIP [71],
- CVX[2].

Among them, YALMIP presents several advantages that explain our choice. First, it is an open source software that is fully developed as a toolbox for MATLAB. It uses the formalism of MATLAB and can easily be integrated into MATLAB scripts. Secondly, as for GAMS, it is able to handle Linear Programming (LP) and Non Linear Programming (NLP) , and MILP and Mixed Integer Non Linear Programming (MINLP) thanks to its interface with several relevant solvers. In opposition, CVX is mainly designed to Convex problems.

For the remainder, the supervisor will use YALMIP. It can be interfaced with the following solvers:

- CPLEX[3] - external, commercial software for MILP, Quadratic Programming (QP), MIQP, Second Order Cone Programming,
- GUROBI[4] - external, commercial software for MILP, QP, MIQP, Second Order Cone Programming,
- FMINCON[5] - MATLAB native solver for general NLP (Interior point method, sequential quadratic programming, etc.),
- BMIBNB[6] - YALMIP internal solver for general NLP.

[1] https://www.gams.com/
[2] http://cvxr.com/cvx/
[3] https://www.ibm.com/analytics/cplex-optimizer
[4] http://www.gurobi.com/
[5] https://www.mathworks.com/help/optim/ug/fmincon.html
[6] https://yalmip.github.io/solver/bmibnb/

2.4.2.3 Shrinking horizon

The first simulation is based on the shrinking horizon objective function. For this simulation, the weighting factors of (2.8) over the horizon are identical, and no convergence speed is considered. The results are depicted in the Figures 2.10 to 2.12 and 2.14. Figure 2.10 presents the power profile of the system, with the economical reference, plus the PMS corrections. We refer the Li-ion storage by Battery 1, and the hydrogen-based by Battery 2.

It can be seen that according to the design criteria, the Battery 1 actually handles the daily fluctuation, while the second one maintains the power balance through the droop control mechanism (see for example between 12 and 17 hour the fluctuations of the photovoltaic production and its compensation from Battery 2). It is to be noticed that the forecast energy for the considered period is the same for the secondary and tertiary layers, therefore there are no large power deviations, nor large changes in the references for any storage devices. Still, as both layers consider different time scales of moving average forecast, the real time power flow differs from a layer to another. These results in the frequency profile of the micro-grids are displayed in Figure 2.11 and the corresponding frequency variations, particularly during the variable PV production. In addition, the supervisor does not act on the voltage profile, and therefore the node voltages fluctuate with the active power injections only (see Figure 2.12). As a result, despite the error on the forecast, the micro-grid remains within its frequency and voltage boundaries.

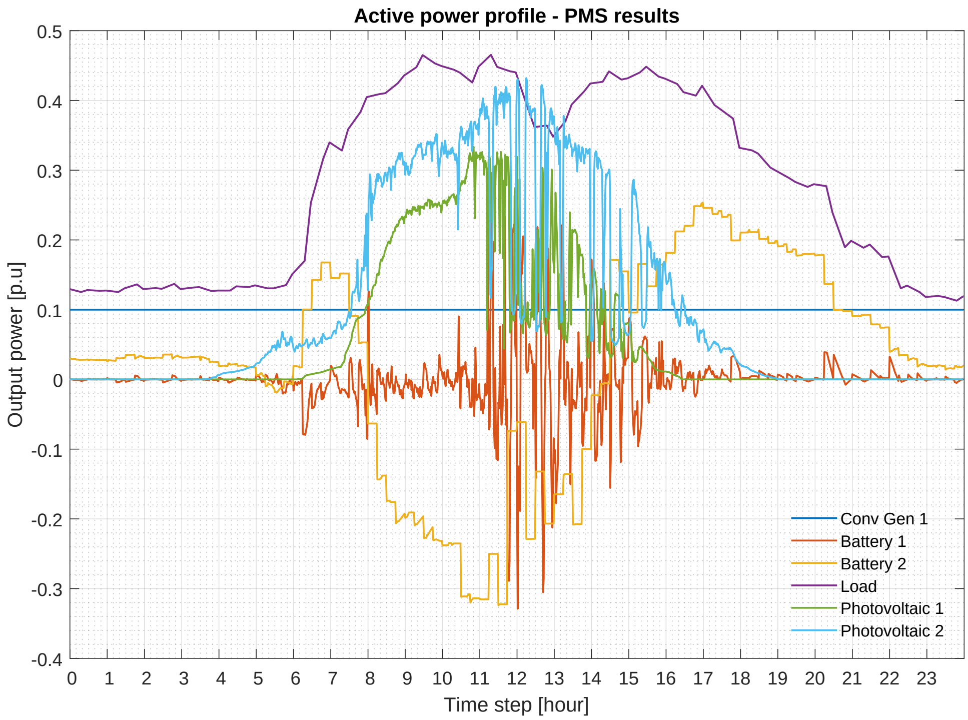

Figure 2.10: Active power profile – Shrinking horizon supervisor

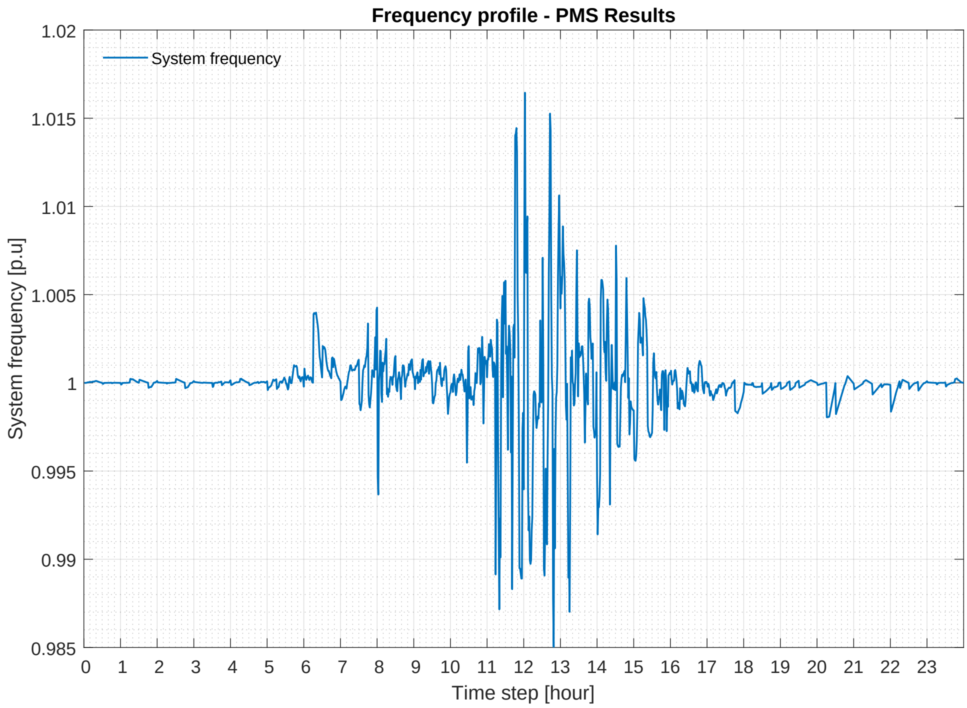

Figure 2.11: System frequency – Shrinking horizon supervisor

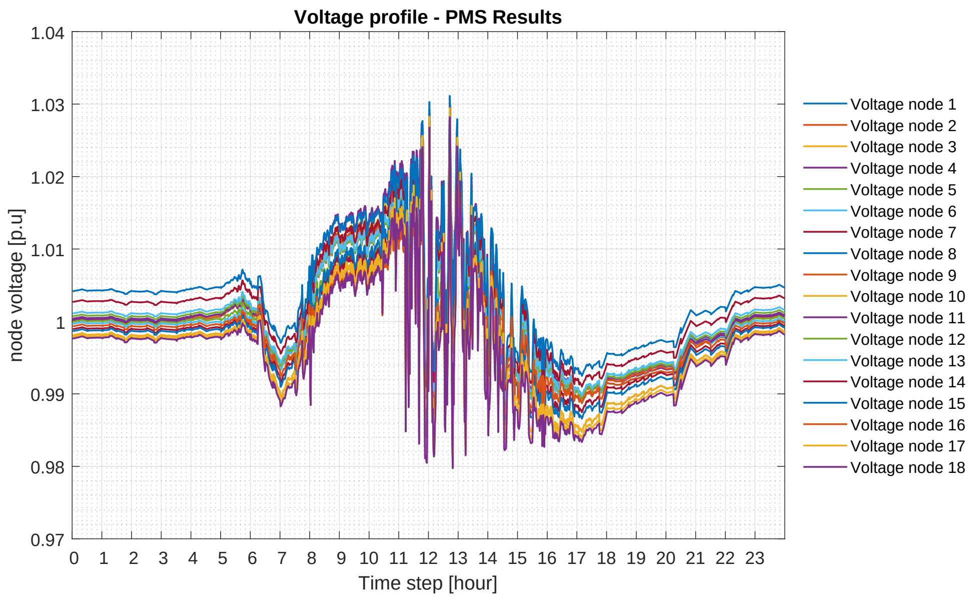

Figure 2.12: Node voltages – Shrinking horizon supervisor

At last, we recall that the secondary layer inputs are the SoC references, calculated from the economical model. Figure 2.13 presents the economical trajectory. The red dots represent the resulting trajectory from the tertiary layer during the first time step. The blue ones represent the receding trajectory that serves as a reference for the secondary layer. Considering a 15-min average forecast, the tertiary layer plans to supply the micro-grids thanks to the hydrogen-based storage (the figure at the bottom). However, the secondary layer, and real time operation engages the first storage, resulting in a deviation on the forecast SoC and a temporary correction of the trajectory (see the difference between the blue and red curve in Figure 2.13 (top) and its impact on the second storage). However, while the second storage succeeded to reach the same objective at the end of the day, the first one reached a State of Charge lower than expected, mainly due to the line losses. Finally, the performances of the secondary layer are presented in Figure 2.14 and it can be observed that the supervisor is able to closely reach the references.

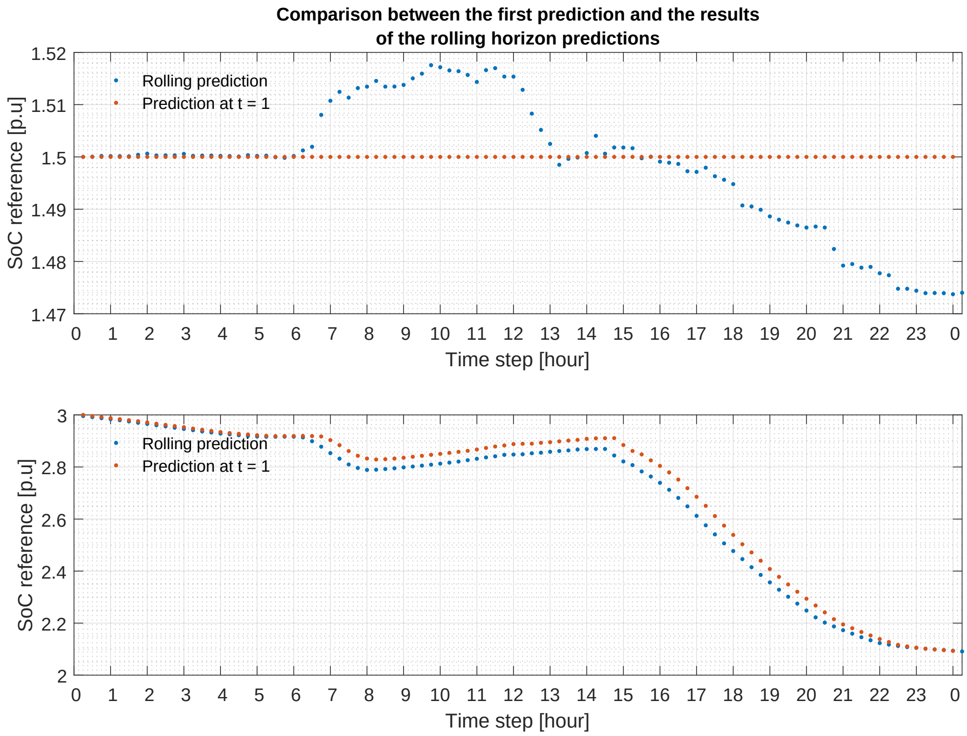

Figure 2.13: SoC trajectory – Shrinking horizon supervisor

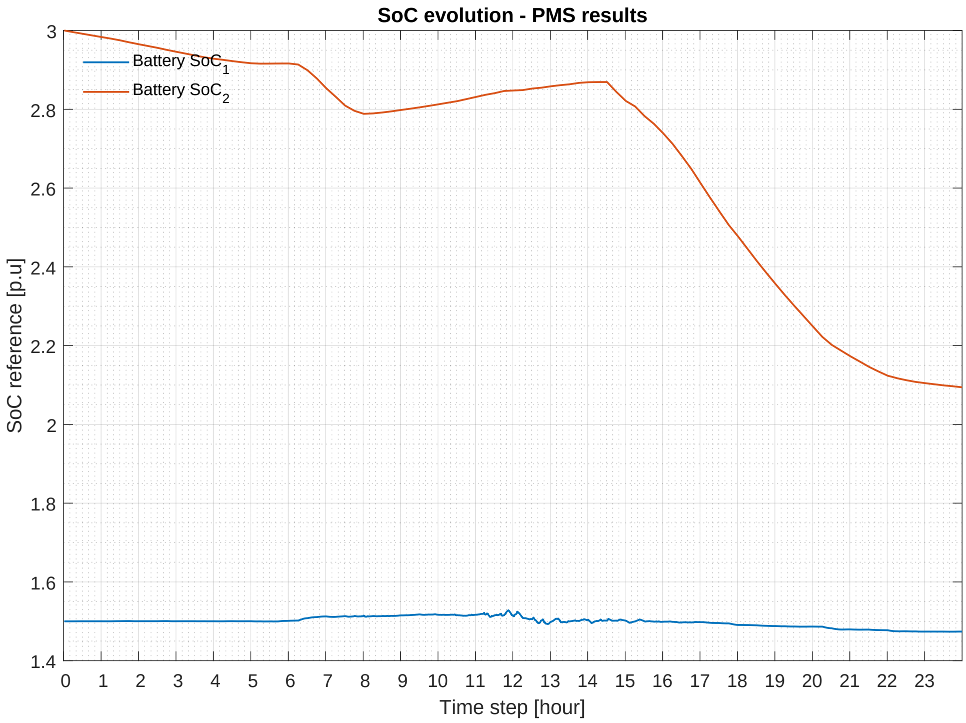

Figure 2.14: PMS State of Charge performances – Shrinking horizon supervisor

2.4.2.4 Receding horizon

The results of the receding horizon supervisor are depicted in the Figures 2.15 to 2.18. Once again, the weighting factors (2.7) over the horizon are the same, and no convergence speed is considered. Figure 2.15 presents the power profile of the system, with the economical reference, plus the PMS corrections. The same remarks hold for the droop mechanism that maintain the power balance, and its impact on the node voltages and the system frequency. Overall, the system presents a similar response to the load and PV profile, and the provision of the mismatch power through droop mechanism of Battery 2. The frequency and voltage profiles (Figures 2.16 and 2.17) are similar and mainly depends on the PV production. The major difference lies in the power profile of Battery 1. It can be observed that for some period, the PMS adjusts the references at the end of the 15-minutes period (see for example between 8 and 12h). This difference is a result of an anticipation of large changes in the tertiary layer reference, that the lower layer is not aware of, and the fast fluctuation of the PV forecast. It is confirmed by comparing the period between 0 and 5h for which there is not change in the power profile.

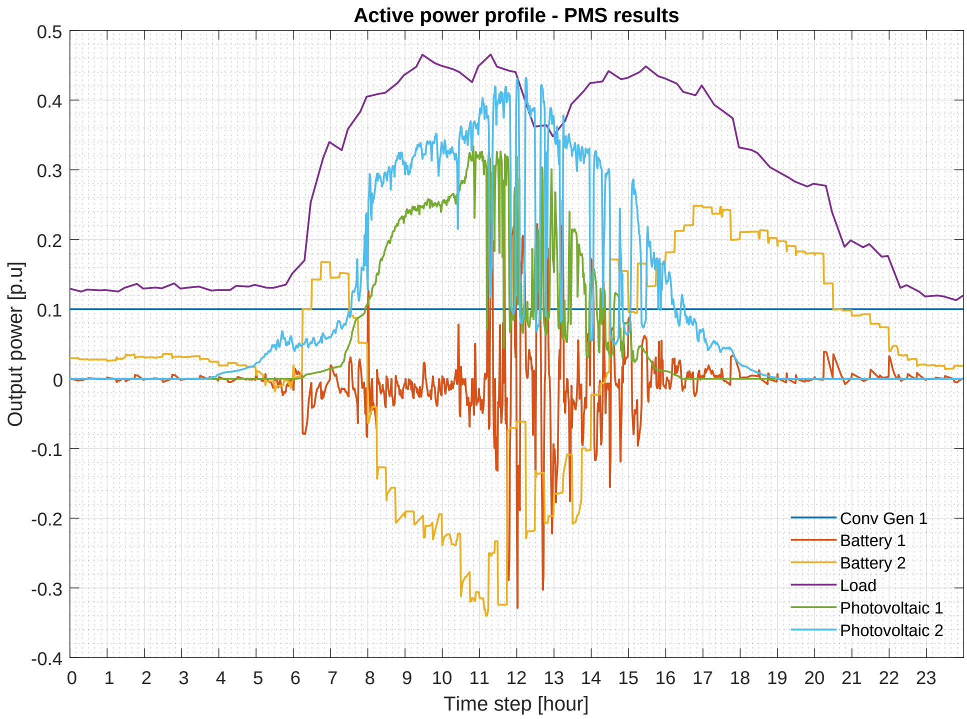

Figure 2.15: Active power profile – Receding horizon supervisor

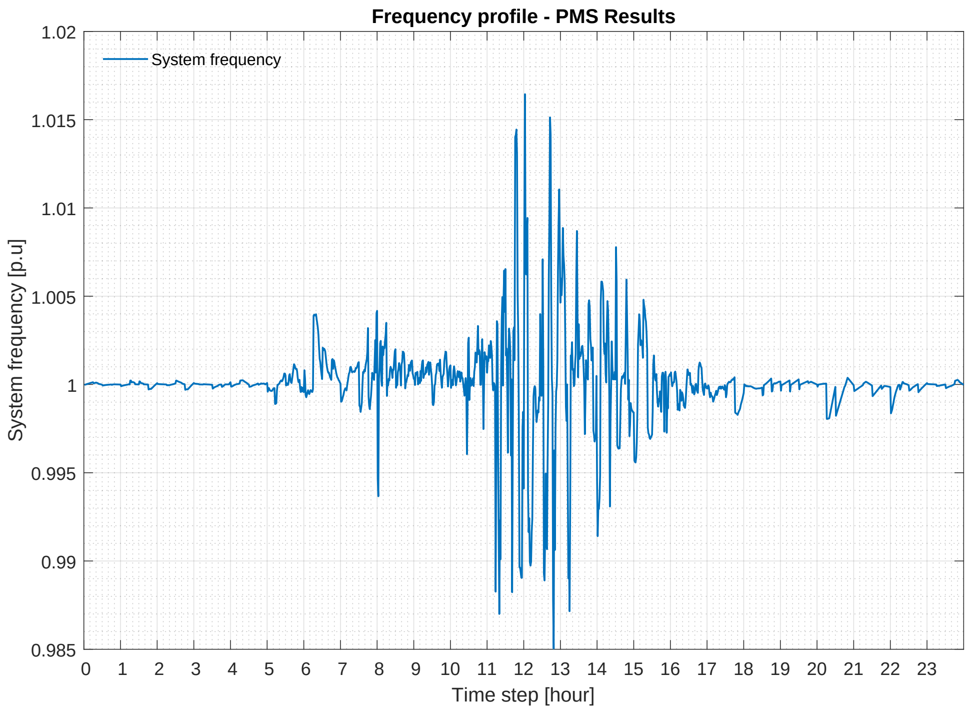

Figure 2.16: System frequency – Receding horizon supervisor

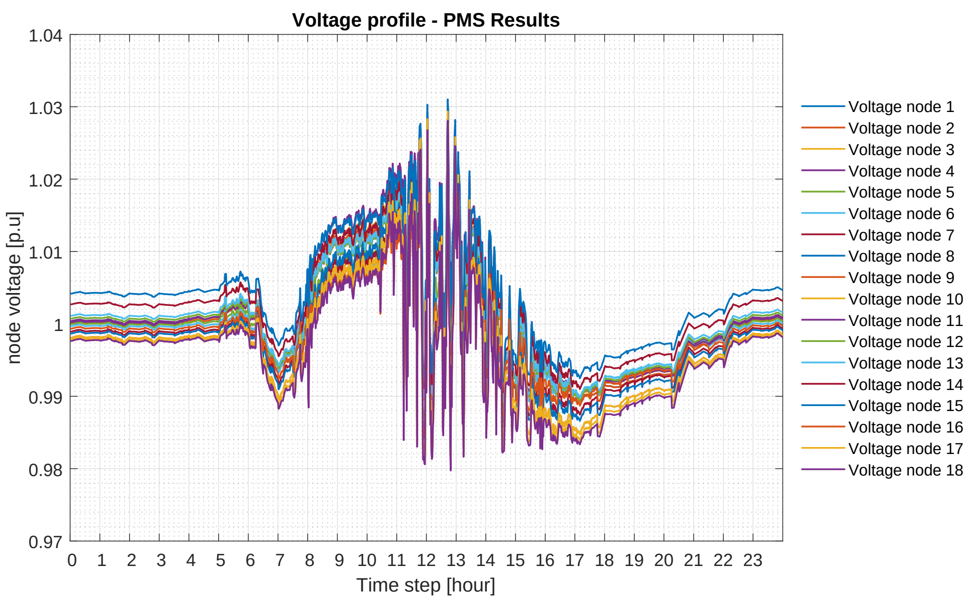

Figure 2.17: Node voltages – Receding horizon supervisor

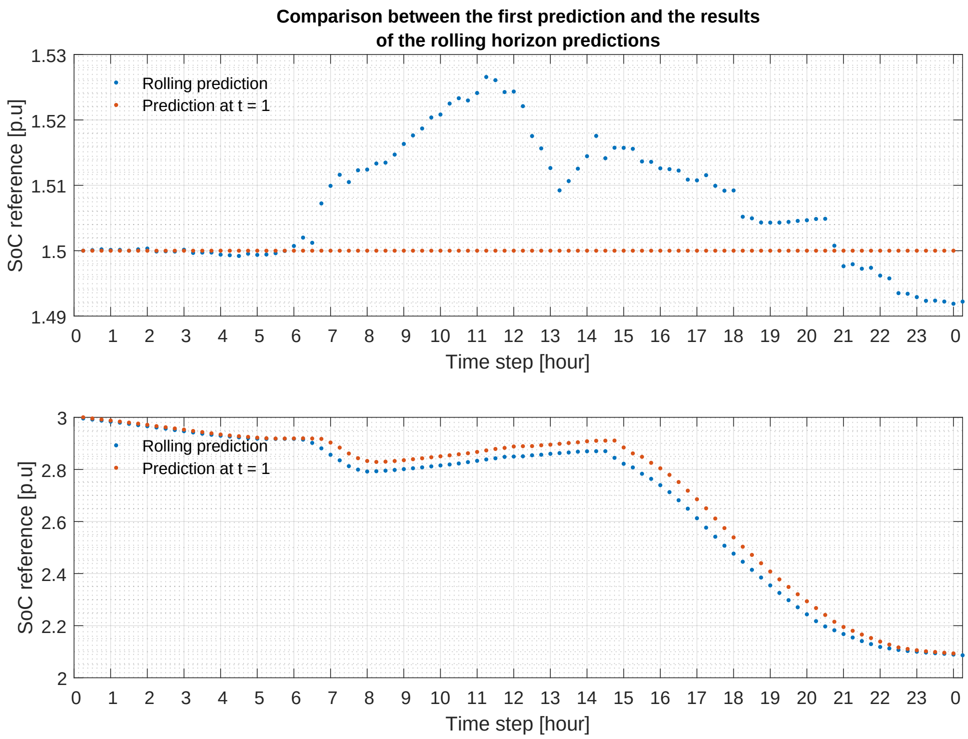

Figure 2.18: SoC trajectory – Receding horizon supervisor

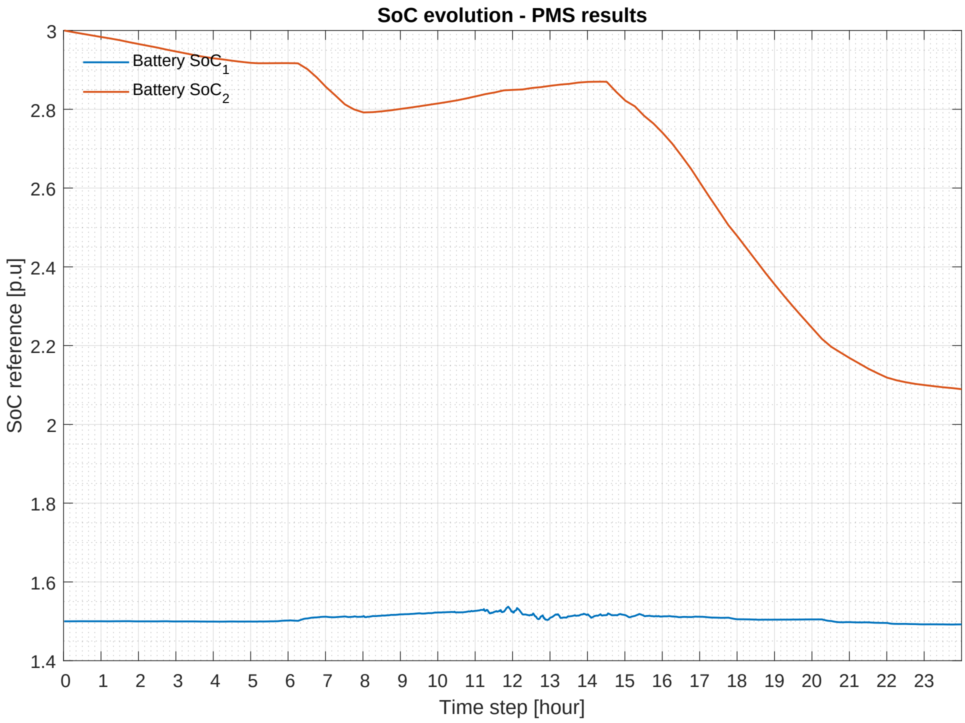

Figure 2.19: PMS State of Charge Performances – Receding horizon supervisor

2.4.2.5 Comparison of Tertiary-Secondary layer interface methods

There are two main indicators which allow to compare the performances of both supervisors. The first and main one is the State of Charge profile. Figure 2.20 presents the evolution of the SoC for the receding (the solid lines) and the shrinking (dot lines) supervisor. The performances are very similar, even if the battery 2, used to mitigate the intra-day fluctuations, has a lower SoC for the shrinking horizon (1.474 p.u versus 1.492 p.u).

Table 2.5 presents the initial references, and compares the adjusted references and achieved performances for both supervisors. It can be seen that the tertiary layer optimization changed the references due to the mismatch power between fluctuating real time DERs production and its forecast powers. This starts at 9h when the production begins.

Table 2.5: Economical trajectory comparison

		Receding horizon		Shrinking horizon	
	Initial reference	Dynamic reference	Performance	Dynamic reference	Performance
Battery 1	1.500	1.492	1.492	1.474	1.474
Battery 2	2.093	2.093	2.094	2.093	2.094

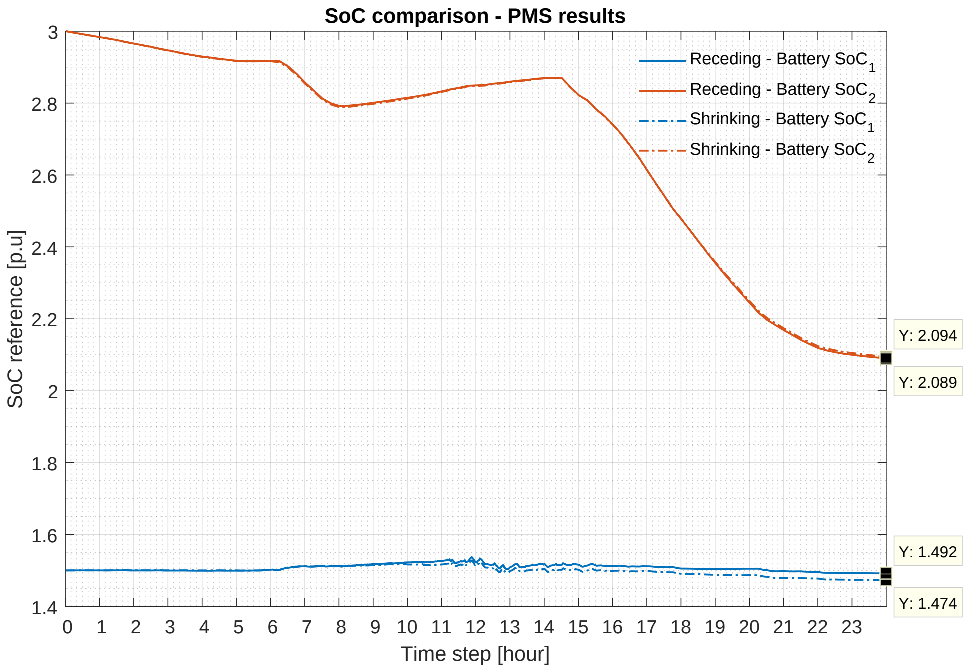

Figure 2.20: Comparison of State of Charge performances

Second, the computation time for both methods is similar, and the complete day is simulated in less than 10 minutes (2 sec to solve the secondary layer optimization problem). It is therefore suitable to be applied in real time, even for larger systems, with multiple DERs, storage and diesel generators.

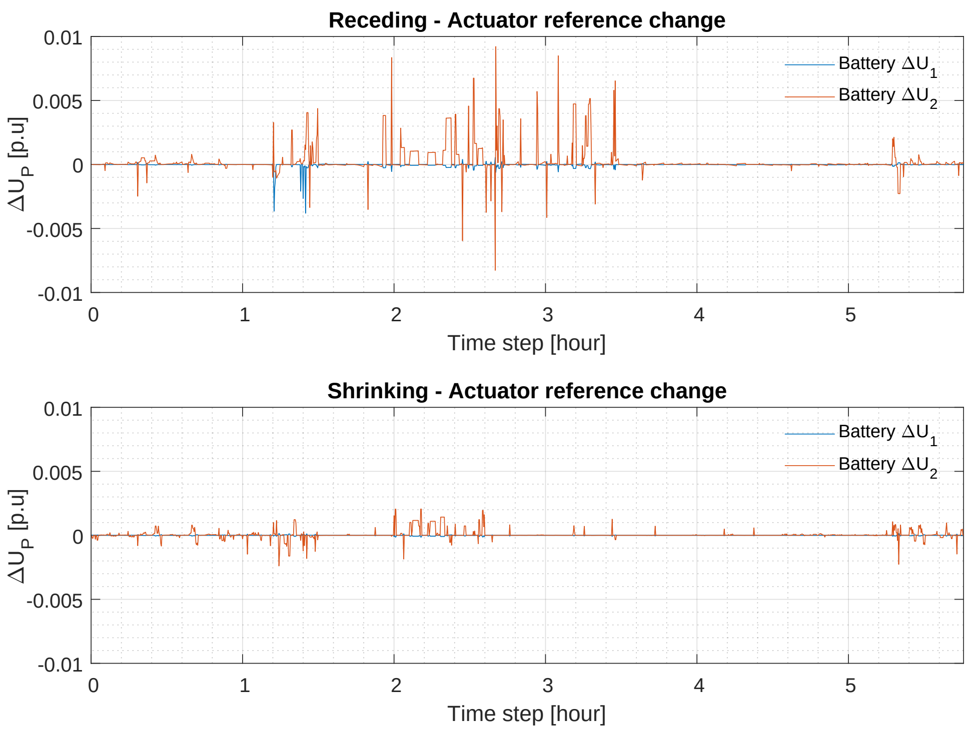

Figure 2.21: Comparison of actuator references changes

To complete the comparison, it is important to analyze the changes of active power references decided at the secondary level. Figure 2.21 displays the corresponding adjustments of the power references. It can be observed that the levers are more called for by the receding horizon, due to the anticipation over the rolling horizon as previously stated. Regarding the shrinking horizon-based supervisor, the decisions of the secondary layer are below 0.005 p.u, and could be considered as null.

2.5 Conclusion on Multi-layer MPC-based micro-grid supervision

To control the micro-grid, the Chapter 2 introduced the Model Predictive Control technique, and more precisely its linear time invariant incremental formulation. Based on the literature, a novel architecture has been proposed, based on two layers that computes a receding real time economical optimization, and a refined short term supervision of the micro-grid. The interface between tertiary and secondary layer objectives and models rises challenges, which are addressed by the generation of an economical trajectory for each of the storage devices that will be used as references for the faster layer. Two methods have been discussed and simulated to generate this trajectory: a shrinking and a receding horizon. The simulations showed that in low stressed system, both methods display satisfactory results.

The resulting supervisor has been applied to the tertiary-secondary control of a micro-grid system to supervise the power injections, and as consequences, the node voltage and system frequency. The use of a linear model to obtain a MIQP allows the supervisor to determine quickly the optimal control sequence and its application to real time systems. Still, when additional objectives are embedded in the faster layer, the supervisor may lead the system to a sub-optimal state, and more in-depth studies are needed to refine the weighting factors.

Chapter 3

Flexibility aggregation and micro-grid capability diagram

Contents

P-Q planes are well-known tools used in power system studies. At first, they were used to illustrate the reactive power capability limits of synchronous machines, namely the armature current, the field current and heating limits [72]. The concept has been extended to machines and converters to map the capability of an asset to provide active and reactive power modulations. In order to determine the capability of a micro-grid to provide a service to the external network, the micro-grid must be able to quantify the reserves it has in a similar manner that for a single inverter through a capability diagram. Therefore, based on the unitary flexibility diagrams of the micro-grid elements, a preliminary routine aims to determine the aggregated capability at the PCC. This results in a 2D-polytope for a specific voltage at the PCC. The following sections present the literature review of commonplace aggregation techniques to build a capability diagram of a sub-part of a power system. The impact of the PCC voltage on the capability diagram is highlighted and showed to be nonlinear. A nonlinear routine is proposed to address the specific case of a micro-grid with a variable PCC voltage. The effectiveness of the proposed routine is illustrated by the aggregated diagram of a micro-grid network benchmark.

3.1 Unitary flexibility diagrams and distributed energy resources capabilities

A capability diagram - also named PQ-diagram or flexibility diagram – is a two-dimensional diagram that captures the feasible operating region of an equipment. The axes define the active and reactive power limits and the shape determines the maximal apparent power that can be delivered or absorbed. This diagram is built based on several considerations:

- Physical constraints. The design and the nature of the equipment induce inherent limitations (Primary resources of DERs, design of a converter, etc.).
- Regulation and grid codes. DSO and TSO prescribe local operating regulations to coordinate the different actors within the power system.
- Operation. The operation (voltages, status of the grid) imposes some constraints and determines the behavior of non-flexible devices.

The following subsections will detail the construction of such diagrams for the most common distributed generators in micro-grids, from a technical and regulatory point of view.

3.1.1 Type 1 – Energy storage systems

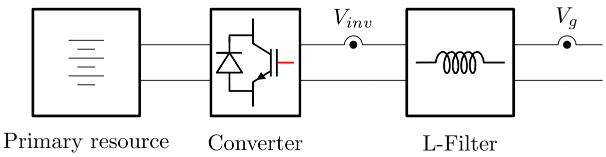

Figure 3.1: Energy storage system stages

Flexibility type 1 models the energy storage systems (ESS). These systems are composed of a storage unit (Battery, super-capacitors, etc.), a 4-quadrant inverter and a L/LC-filter (see Figure 3.1). Each stage of the storage system induces specific limitations of the active and reactive power injections. These three elements must be taken into account to estimate the capability of an ESS.

First, the storage unit is able to provide a DC power up to its nominal value. Let's assume that the DC voltage is correctly regulated and the system is sufficiently charged so that it can provide or absorb the maximum DC power. Then, the inverter, based on a proper control, is designed to provide apparent power up to the nominal value of the DC side.

$$P_{inv}^2 + Q_{inv}^2 \leq (S_{inv}^{max})^2 \tag{3.1}$$

with P_{inv} and Q_{inv} the active and reactive power respectively at the output of the converter, and (S_{inv}^{max}), the maximum apparent power.

This results in a first 4-quadrant PQ diagram centered at $c = (0, 0)$ and with a radius equal to the maximum apparent power (S_{inv}^{max}) (see the red circle in Figure 3.2). Finally the L/LC filter induces a reactive current at the output of the inverter and affects the output voltage. Let's denote the voltage at the output of a L filter by V_g. We can formulate the active and reactive power flow at this point by:

$$\begin{aligned} P_g &= 3V_g I_{inv}\cos(\delta) \\ Q_g &= 3V_g I_{inv}\sin(\delta) \end{aligned} \tag{3.2}$$

with δ the angle between the inverter voltage V_{inv} and the grid voltage V_g. We can reformulate to obtain the output powers of the inverter only depending on the voltages by:

$$\begin{aligned} P_{inv} &= \frac{3V_{inv}V_g}{X}\sin(\delta) \\ Q_{inv} + \frac{3V_g^2}{X} &= \frac{3V_{inv}V_g}{X}\cos(\delta) \end{aligned} \tag{3.3}$$

Finally, one has the expression of the apparent power

$$P_{inv}^2 + \left(Q_{inv} + \frac{3V_g^2}{X}\right)^2 = \left(3\frac{V_g V_{inv}}{X}\right)^2 \tag{3.4}$$

A voltage constraint appears on V_{inv} defined by a circle centered at $c_2 = (0, -\frac{3V_g^2}{X})$ and with a radius of $r_2 = 3\frac{V_g V_{inv}}{X}$ (see the blue circle in Figure 3.2). The resulting area (in green) is the intersection of two circles as depicted in Figure 3.2. For the remainder of this thesis and for the sake of simplicity, the effect of the output filters is neglected.

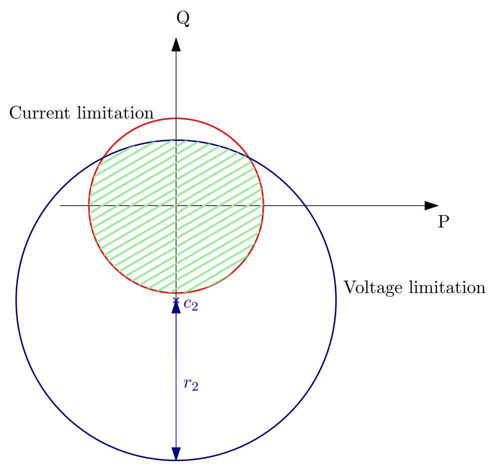

Figure 3.2: Flexibility diagram of an ESS

3.1.2 Type 2 – Renewable production connected through power electronic converters

Type 2 is used for two kinds of flexibilities of renewable resources depending on whether a fully-rated or a partially-rated converter is used to interface the primary resource to the grid. Technically, both have different capabilities. The first one is easily obtained by adding to the type 1 two active power limitations (see Figure 3.3 with $P \geq 0$ and $P \leq P_{primary}$). The second, mainly used for doubly-fed induction machine is more complex and dependent of the rotor-side converter to provide the reactive power consumed by the generator (Figure 3.4). The complete model and hypotheses of the partially-rated converter can be found in [73]. Note that the system described in [73] includes two coupling transformers (Y-Δ) to reduce the stator voltage and decrease the losses at low power.

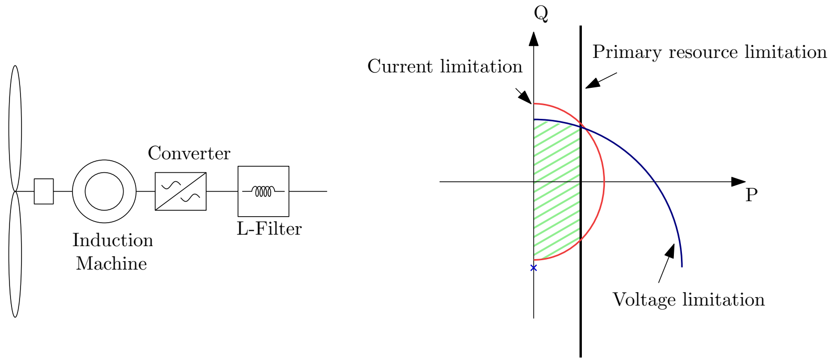

Figure 3.3: DERs with fully-rated converter

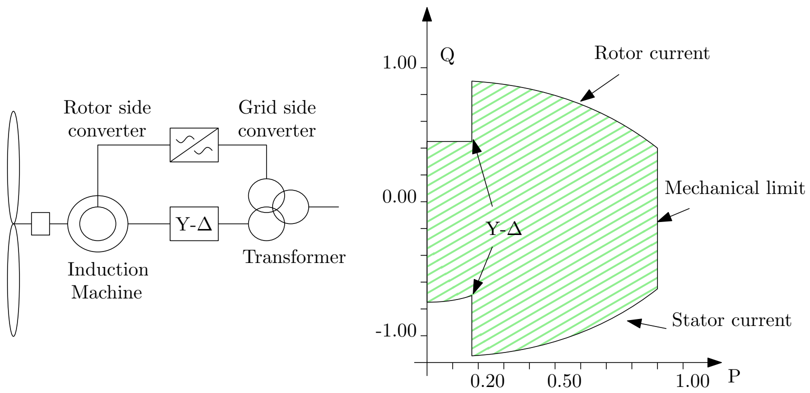

Figure 3.4: DERs with partially-rated converter

Even though it is technically possible to operate within the entire diagram, regulations and grid codes require less reactive power capabilities. The European framework [74] mentions two envelopes. First, an outer envelope defines the maximum Q/P_{max} range. DSOs cannot request DERs to operate outside of this envelope. Secondly, the inner envelope, that is the real operating $P - Q/P_{max}$-profile, shall be specified in coordination with the relevant system operator. Similarly, the European regulations specify outer and inner envelopes for a $U - Q/P_{max}$ profile within which the generation unit may be able to operate. Even though the reactive support is only mandatory for Type C power park modules (power electronics-interfaced generation units of 1 MW up to 49 MW). For the remainder of this thesis we will consider such requirements for lower nominal powers. The range and limits depend on the synchronous area considered (Continental, Nordic, Baltic, UK). For continental Europe, the Q/P_{max} range is 0.75, may be asymmetric and the maximum voltage range is 0.225 p.u. (See Figure 3.5 and Figure 3.6 for the European regulation, and its application by the French distribution system operator ENEDIS [75]).

Finally, without loss of generality, we will use the French regulations, and assume that the provision of the maximum reactive power is possible, no matter the output voltage, by limiting the voltage range to 5 %, resulting in the green hatched part of the diagram on Figure 3.5.

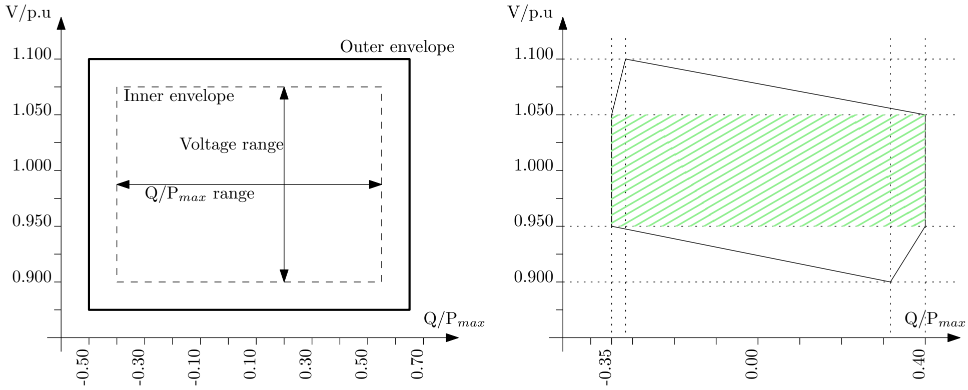

Figure 3.5: U-Q/Pmax-profile
Left: European framework – Right: French regulation diagram

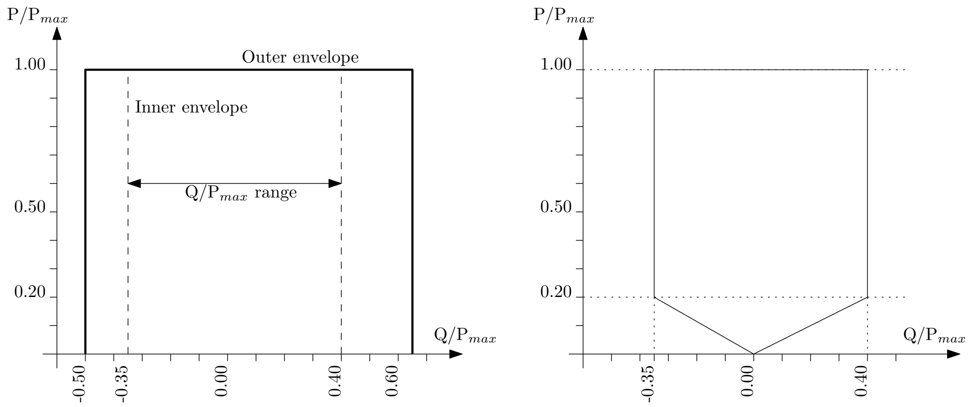

Figure 3.6: P-Q/Pmax-profile
Left: European framework – Right: French regulation diagram

3.1.3 Type 3 – Conventional generators

The third type of flexibility represents the conventional synchronous generators. Basically, the synchronous generator with a proper excitation system and governor is able to modulate both its active and reactive output power making it able to operate in two quadrants. The following limits apply to the synchronous machine:

- stator current limits the apparent power,
- rotor current limits the reactive power,
- the governor and prime mover limit the active power and finally,
- the excitation system limits the reactive power consumption.

This results in Figure 3.7 with these four limitations. An additional constraint apply that limits the minimum mechanical power of the prime mover, and therefore, the active power.

For the remainder, we will neglect the excitation constraint and will only consider the prime mover and stator current constraints.

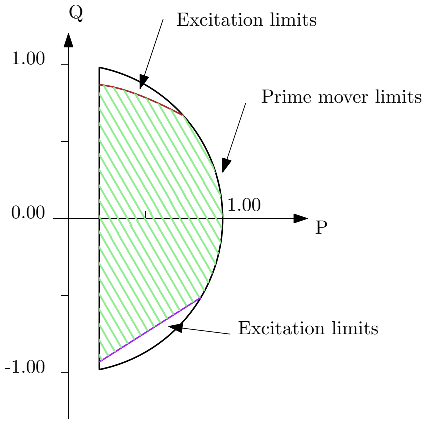

Figure 3.7: Flexibility diagram of a synchronous generator

3.2 Estimation of micro-grid capability and aggregation routines

Unlike VPP operator or load aggregators, for whom a geometric solution can estimate the capability of the system [76, 77], micro-grid systems include line impedances and non-linear behaviors. In these publications, the proposed routine consists in the addition of geometric diagrams by the Minkowski operator. However, this method does not directly apply to the PCC for a micro-grid. Fortunately, a number of recent papers have addressed this point when a sub-part of a grid is connected to a distribution grid with a nonlinear formulation of the power flow problem [78] or based on a linearization of the Optimal Power Flow (OPF) equations [79]. This section first reviews and compares these two formulations to finally extend it to a variable PCC voltage.

3.2.1 Aggregation routine based on a nonlinear micro-grid model

Most of the developments in this sub-section are related to the publications [78,80,81], developed in the scope of the European project EvolvDSO[1]. The different partners proposed methodologies and tools for System Operator (SO) to address the challenges raised by the increasing penetration of DERs and the changes in the role of the SO. Among them, one of the tools assesses the flexibility of distribution systems at the interface between different voltage levels. It is based on the nonlinear formulation of the distribution system, and a maximization of the active and reactive power injection deviations at the interface while maintaining classical power flow constraints and limits. However, in their publications, one of the aspects addressed is related to the economical valorization of the service. In the following, we will neglect this aspect, and focus on the physical and technical aspects of the routines.

The objective of the routine proposed in [78,80,81] is to maximize the apparent power at the interface, with either a specific reactive power or active power flow at the PCC. It results in a two step algorithm that first initializes the routine with several points and then iterates to explore the entire shape of the diagram.

Step 1 - Initialization

The first step consists in estimating the maximum active and reactive power at the PCC. To that end, the objective function is formulated as:

$$\mathcal{J}_1 = \alpha P_{pcc} + \beta Q_{pcc} \tag{3.5}$$

in which α and β are fixed ($\alpha = \pm 1,\ \beta = 0$) or ($\alpha = 0,\ \beta = \pm 1$).
The optimization is constrained by the power flow equations,

$$\begin{aligned} P_i &= V_i \sum_{j \in N} V_j (G_{ij} \cos(\delta_i - \delta_j) + B_{ij} \sin(\delta_i - \delta_j)) \\ Q_i &= V_i \sum_{j \in N} V_j (G_{ij} \sin(\delta_i - \delta_j) - B_{ij} \cos(\delta_i - \delta_j)) \end{aligned} \tag{3.6}$$

[1] https://cordis.europa.eu/project/rcn/109548_fr.html

the voltage and current limitations

$$
\begin{aligned}
V_{i,\,min} \leq V_i \leq V_{i,\max} \\
I_{ij} \leq I_{ij,\,max}
\end{aligned}
\tag{3.7}
$$

and the levers (generators, flexible loads, etc.) which are constrained by their respective limitations and capabilities as detailed in Section 3.1 that we simply reduce to:

$$
\begin{aligned}
P^g_{i\ min} \leq P^g_i \leq P^g_{i\ max} \\
Q^g_{i\ min} \leq Q^g_i \leq Q^g_{i\ max} \\
P^l_{i\ min} \leq P^l_i \leq P^l_{i\ max} \\
Q^l_{i\ min} \leq Q^l_i \leq Q^l_{i\ max}
\end{aligned}
\tag{3.8}
$$

where $(\cdot)^g_i$ and $(\cdot)^l_i$ denote the generator and load flexibilities respectively of node i.
Last, the nodal power balance constraints apply:

$$
\begin{aligned}
P_i = P^g_i - P^l_i,\ \forall i \in \mathcal{N} \\
Q_i = Q^g_i - Q^l_i,\ \forall i \in \mathcal{N}
\end{aligned}
\tag{3.9}
$$

The resulting optimization problem is a particularly nonlinear, non convex OPF. The non-convexity of the problem remains an issue and even if step 2 of the routine ensures to converge to a suitable solution, the initialization still may not converge or converge to an infeasible solution. Anyway, if the problem converges, it results in a mapping of four couples that will be used as a basis to explore the entire diagram.

Step 2 - Exploration

Step 2 of the aggregation routine splits the diagram in two areas. Upper and lower parts are defined by the intersection of the minimum and maximum reactive power determined in step 1 (see the red dashed line in Figure 3.8).
Let's denote by the superscript $^{(k)}$ the iteration number of the routine. By ordering the resulting points of the step 1 by their respective angle ($\theta = \arctan\left(\frac{Q}{P}\right)$) we obtain:

$$
\begin{aligned}
k = 1 \quad (P^{(k)}_{pcc},\ Q^{(k)}_{pcc}) = (P^{(1)},\ Q_{min}) \\
k = 2 \quad (P^{(k)}_{pcc},\ Q^{(k)}_{pcc}) = (P_{max},\ Q^{(1)}) \\
k = 3 \quad (P^{(k)}_{pcc},\ Q^{(k)}_{pcc}) = (P^{(2)},\ Q_{max}) \\
k = 4 \quad (P^{(k)}_{pcc},\ Q^{(k)}_{pcc}) = (P^{(2)},\ Q_{max})
\end{aligned}
\tag{3.10}
$$

Finally, step 2 of the routine consists in determining the couple of the iterate $k+1$, $(P^{(k+1)}_{pcc},\ Q^{(k+1)}_{pcc})$, from two successive couples with the following optimization problem:

$$
\begin{aligned}
\text{minimize} \quad & \mathcal{J}_2 = \sigma P^{(k+1)}_{pcc} \\
\text{subject to} \quad & V_1 = V_{pcc} = 1 \\
& \theta_{pcc} = 0 \\
& \text{Eqs. (3.6) to (3.9)} \\
& Q^{(k+1)}_{pcc} = 0.5 \times \left(Q^{(k)}_{pcc} - Q^{(k-1)}_{pcc}\right)
\end{aligned}
\tag{3.11}
$$

The upper and lower part of the diagram are explored by specifying σ equal to -1 or 1 respectively, and with the correct initial points. The additional constraint $Q_{pcc}^{i+1} = 0.5 \times \left(Q_{pcc}^{i} - Q_{pcc}^{i-1}\right)$ in (3.11) ensures the existence of a solution as we assume the PQ-plane to be compact. We reorder the previous points of the diagram with the resulting couple $(P_{pcc}^{i+1}, Q_{pcc}^{i+1})$. This last step is repeated until the difference of angle between two successive points is less that an prescribed tolerance ϵ. Figure 3.8 displays a basic example of the exploration of the upper part of a diagram.

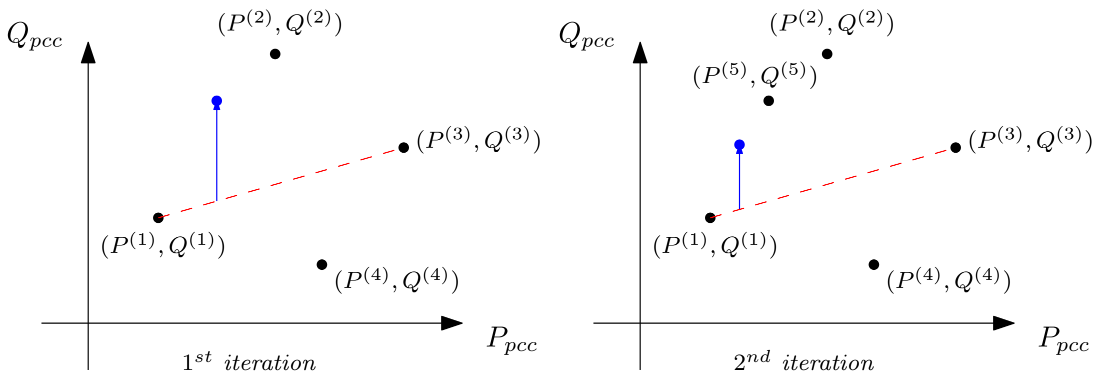

Figure 3.8: Step 2 - Exploration of the diagram

- The initialization step results in four couples of points on the PQ-plane, $((P^{(1)}, Q^{(1)})$, $(P^{(2)}, Q^{(2)})$, etc.) presented by the black points in the Figure 3.8.
- The first iteration of the exploration routine considers the two first couples $((P^{(1)}, Q^{(1)})$ and $(P^{(2)}, Q^{(2)}))$ to determine the average reactive power $Q^{(5)}$ and the optimization problem determines the maximum active power at the PCC for $\sigma = 1$ (resp. minimum with $\sigma = -1$), with the constraint $Q_{pcc} = Q^{(5)} = 0.5 \times \left(Q_{pcc}^{(4)} - Q_{pcc}^{(4-1)}\right)$.
- The second step considers two other successive couples $((P^{(1)}, Q^{(1)})$ and $(P^{(5)}, Q^{(5)})$ in Figure 3.8 and the process iterates until the distance between each two successive couples is below a specified tolerance.

3.2.2 Aggregation routine based on a linear micro-grid model

Due to the non-linearities of the power flow equations considered in the previous section, the numerical optimization is time consuming. To reduce the computational burden, it is commonplace to linearize the model and the constraints around an operating point. The conventional Newton Raphson (NR) power flow uses this linearization and exhibits fast convergence if the problem is correctly stated. The linearization of the power flow equations (3.6) results in (3.12) [72].

$$\begin{bmatrix} \Delta V_2(k+1) \\ \vdots \\ \Delta V_i(k+1) \\ \Delta\delta_2(k+1) \\ \vdots \\ \Delta\delta_i(k+1) \end{bmatrix} = \begin{bmatrix} \dfrac{\partial P_i}{dV} & \dfrac{\partial P_i}{d\delta} \\ \dfrac{\partial Q_i}{dV} & \dfrac{\partial Q_i}{d\delta} \end{bmatrix}^{-1} \begin{bmatrix} \Delta P_2^*(k) \\ \vdots \\ \Delta P_i{}^*(k) \\ \Delta Q_2{}^*(k) \\ \vdots \\ \Delta Q_i{}^*(k) \end{bmatrix} \tag{3.12}$$

The current limitation (3.7) can be rewritten as the quadratic constraint $P_{ij}^2 + Q_{ij}^2 \leq S_{ij\ max}^2$, and approximated by a set of linear constraints that defines a polytope [82]. The 4-quadrant and 2-quadrant flexibilities are linearized following the same approximations. It results in a set of n linear constraints:

$$\begin{cases} L_{ij}^k = \lambda_{ij}^k P_{ij} + \zeta_{ij}^k Q_{ij} + \gamma_{ij} = 0 \\ \gamma_{ij} \geq 0 \end{cases} \tag{3.13}$$

with k referring to the set of coefficients, depending on the angle $\theta = \arctan\left(\frac{Q_{ij}}{P_{ij}}\right)$. Figure 3.9 presents the linear approximation of a 4-quadrant diagram.

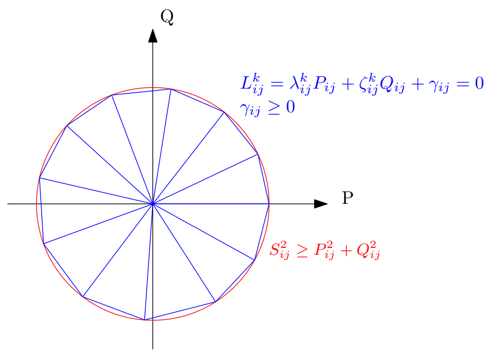

Figure 3.9: Linearization of a 4-Quadrant diagram

In [79] the linear OPF is formulated as follows:

$$\begin{aligned} \text{minimize} \quad & \mathcal{J}_3 = \alpha(P_{pcc} + \beta Q_{pcc}) \\ \text{subject to} \quad & V_1 = V_{pcc} = 1 \\ & \theta_{pcc} = 0 \\ & \text{Eqs. (3.8), (3.9), (3.12) and (3.13)} \end{aligned} \tag{3.14}$$

The algorithm starts with a similar step 1 as previously detailed with $\alpha = \pm 1$ and $\beta = \{0, \infty\}$ to estimate the maximum and minimum active and reactive powers at the PCC. The second step of the proposed algorithm relies on the convex nature of the solution space of the OPF induced by the linearization of equation (3.6). It is therefore possible to explore the diagram for different angles $\beta = \arctan\left(\frac{Q_{pcc}}{P_{pcc}}\right)$ with a linear programming method. The four couples of points determined in step 1 define four quadrants that can be explored by specifying the value of α and the sign of β:

Table 3.1: Optimization parameters

Quadrant	**Value of α**	**Sign of β**
1	$+1$	-
2	-1	$+$
3	$+1$	$+$
4	-1	-

Similarly to previously, the proposed routine enters a closed loop that determines for each quadrant the maximum apparent power. The same convergence criterion on the difference between two successive angles applies and the exploration can be performed in parallel, decreasing the computational time. Figure 3.10 presents the first iteration of the exploration routine, and for four values of β the resulting solution is displayed in blue.

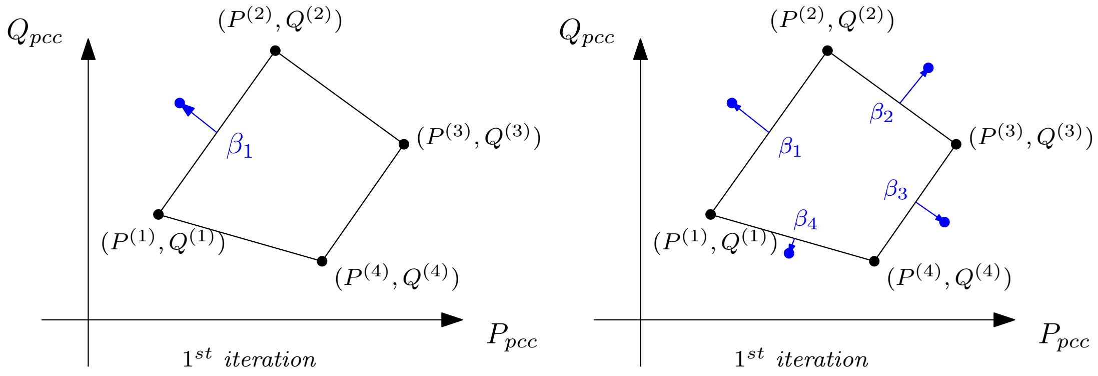

Figure 3.10: Exploration of the diagram based on the linear formulation

- Similarly to the exploration routine of the non-linear formulation, we start with four couples of points (the black dots in Figure 3.10), and explore the diagram with two successive couples.
- The first iteration of the exploration routine considers the two first couples ((1) and (2)) to determine β_1 and the optimization problem determines the resulting couple $(P^{(5)}, Q^{(5)})$ (in blue) with α and β chosen so that they correspond to the search direction.
- The process is repeated for each successive couples, and the resulting points are added to the exploration routine. It stops whenever the angle between each two successive couples is below a specified tolerance.

3.2.3 Comparison and results of the aggregation methods

3.2.3.1 Solver and algorithms

Linear programming: the Simplex method

To solve the linear optimization problem,

$$\begin{aligned} \min \quad & c^T.x \\ \text{s.t} \quad & A.x \leq b \\ & A_{eq}.x = b_{eq} \\ & lb \leq x \leq ub \end{aligned} \tag{3.15}$$

we use the well-known simplex algorithm [83–85]. This method is based on the fact that whenever it exists (see Theorem 13.3 [84]), the feasible region of the LP is a convex polytope. We denote any feasible solution of (3.15) as a *basic feasible solution* and remark that it corresponds to one of the vertices of the polytope (see Theorem 13.3 in [84]). Therefore, the *basic optimal solution* is the *basic feasible solution* that minimizes $c^T.x$. The algorithm basically consists in moving along the vertices to find the edge that minimizes the objective function.

The convex polytope and the maximum number of iterations only depends on the rank of A, A_{eq}, b and b_{eq}. Therefore, the dimension of the problem and the number of edges and vertex depend on the number of constraints and the number of iterations required to explore the entire diagram is bounded.
A direct observation is that the number of points that represent the flexibilities and, as a consequence, the number of linear constraints may increase the complexity and the computational burden. The impact of the linear approximation is highlighted by an additional test case in which the energy storage is modeled by a sixteen-sided polytope, and the conventional generator of node 2 by a nine-sided polytope (case 6b). To deal with inequalities constraints, the simplex method has been extended to the *big-M method* which adds additional artificial variables to classical simplex and pivot method.

Nonlinear programming: Sequential Quadratic Programming and Interior Point method

The AC-OPF is a nonlinear nonconvex problem, which is generally without any approximation, computationally intractable.

$$\begin{aligned} \text{minimize} \quad & f(x) \\ \text{subject to} \quad & c_{eq}(x) = 0 \\ & c(x) \leq 0 \end{aligned} \tag{3.16}$$

where f is the objective function, c_{eq} and c are the equality and inequalities constraints functions. The power flow equations are quadratic, and therefore generally nonconvex. This kind of problem can be either handled through convex relaxation [86] to obtain a guaranteed global solution, or solved using local algorithms using Interior Point method (IP) or Sequential Quadratic Programming method (SQP) methods with a good estimate of the initial point.
The idea of SQP is to model the nonlinear problem by an approximate quadratic subproblem, using the quadratic approximation of the Lagrangian function and a linearization of the constraints at each iteration. The solution of this subproblem is used in the next iteration as a new starting point and to reformulate a new subproblem [84, 87]. This results in a local convex relaxation of the problem.
IP, in turn, handles inequality constraints by logarithmic barrier function. The problem is reformulated as

$$\begin{aligned} \text{minimize} \quad & f(x) - \mu \sum_{i=1}^{m} \log s_i \\ \text{subject to} \quad & c_{eq}(x) = 0 \\ & c(x) - s = 0 \end{aligned} \tag{3.17}$$

with s_i a slack variable associated to the inequality i and m the number of constraints. And finally, the method successively solves this problem for μ converging to zero.

As we want to determine the extremum of the capability diagram we need an algorithm robust enough to deal with the numerical conditioning and able to work closely to the limits. SQP allows the optimization problem to outreach the limits, and is less subject to numerical conditioning problem than IP. For the remainder of this thesis, we observed that the SQP method provided better results - SQP provided a suitable solution of the step 1 of the nonlinear formulation, while IP did not converge.

3.2.3.2 Test cases description

The different test cases must illustrate the parameters that influence the shape of the aggregated diagram. Intuitively, these characteristics are the usual ones for OPF - voltage and current limitations, power flow, line impedances. In order to compare these two methods we compute different aggregated diagrams by successively enabling or changing some of the parameters of the flexibilities.

The test case is a 18-node power system based on a modified European LV residential distribution network benchmark [70]. The network includes two storage systems (type 1, see subsection 3.1), two DERs (type 2) and a conventional generator (type 3). DERs rating, line parameters and network topology are presented in the Appendix B. From now on, a positive power indicates a generation, while a load is labeled as negative. The external network is considered as a load at the PCC. The base power is 100 kW.

Initially, the micro-grid is powered by the PV at node 8 and 11, and the diesel generator at node 15 ($P_8 = 0.22$ p.u, $P_{11} = 0.42$ p.u, $P_{15} = 0.11$ p.u respectively). The total load supplied is about $P_{load} = 0.72$ p.u. There is no power injection at the PCC. For the sake of simplicity, we only consider one of the storage devices.

The different test cases (TC) are:

- TC 1 – a storage device is directly connected to the PCC,
- TC 2 – a storage device is connected far from the the PCC,
- TC 3 – a storage device and two DERs are connected, the DERs are fully controlled in active and reactive power,
- TC 4 – a storage device, two DERs and a diesel generator are connected and fully controlled,
- TC 5 – a storage device, two DERs and a diesel generator are connected and the DER reactive power output is controlled with a droop law.

Note that even if the diesel generator and the PV supply the micro-grid, they are not necessarily considered as flexibilities (see for example the first test case for which the diesel supplies 0.1 p.u of active power that cannot be modulated).
The 4-Quadrant ESS flexibility is linearized to obtain a 16-sided polytope as detailed in subsection 3.2.2. Similarly, the conventional generator (2-quadrant SG) is modeled by a 5-sided polytope.

3.2.3.3 Results and comparison of the linear and nonlinear aggregation methods

The results of both methods are summarized for the five test cases in Figure 3.11 and in Table 3.2. The results from the nonlinear optimisation are depicted by the blue points, and the linear optimization by the red ones. The error in the shape of the diagram is between 0.59 and 3.17 %. In addition, to assess the linear results, a Newton-Raphson based power flow showed that some of the results of the linear approximation converged to infeasible points. This is mainly due to the linearization of the power flow equations that results in the violation of the voltage constraints. As general observation, it can be observed that the computational burden increases with the number of flexibilities for the nonlinear formulation due to the increasing dimension of the gradient, while the time to solve the linear problem is quite constant for an increasing number of flexibilities.

From test case 1, it can be seen that the linear approximation of the type 1 flexibility leads to suitable results. However due to the low number of linear constraints to model the ESS, the surface of the diagram is truncated resulting in an difference of 9.3%. The impact of the position of the flexibility, and of the line impedances are highlighted by Figure 3.11(b). In Figure 3.11(c) and Figure 3.11(d), a diesel generator and two DERs are fully controlled. The derating of the DERs and the active power capability of the diesel increase the active power margins at the PCC. In addition, the voltage support from the full control of the reactive power output leads to the upper left and bottom right deformation of the diagram.

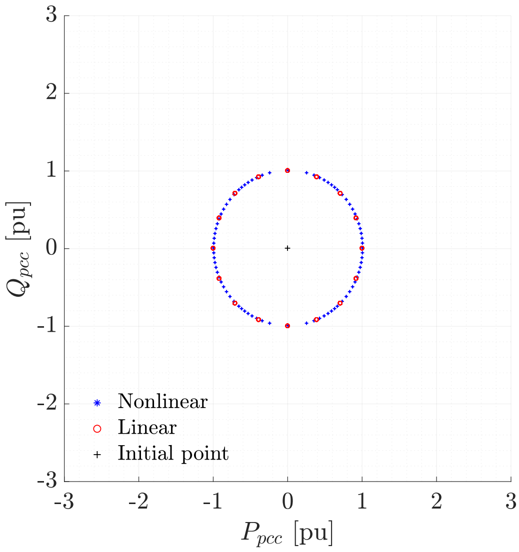

(a) Test case 1

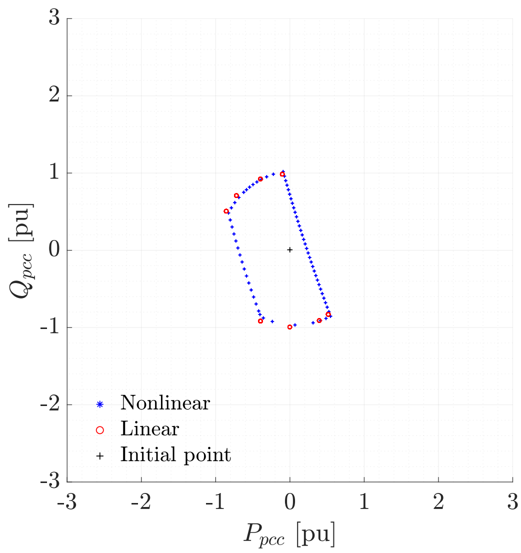

(b) Test case 2

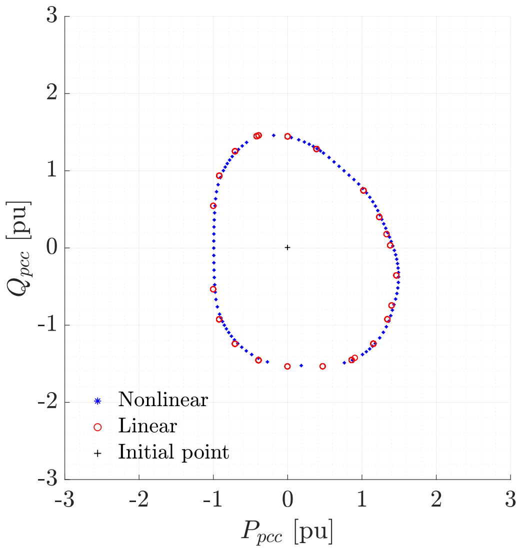

(c) Test case 3

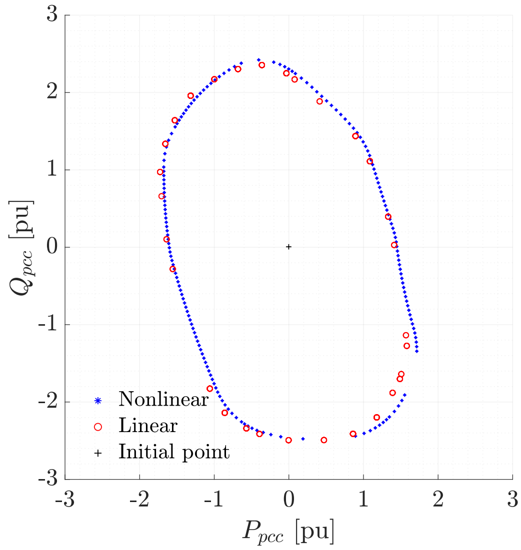

(d) Test case 4

Figure 3.11: Comparison of linear and nonlinear aggregation methods on a 18-node micro-grid system

It is interesting to discuss about the convexity of the resulting shapes. Nonlinear and conventional power flow formulation are, without any relaxation, generally non convex.

Therefore, the diagram could not be explored from such formulation for test cases 3, 4 and 5. Still, adding a constraint on the reactive power (or active power) at the PCC in step 2 of the nonlinear formulation allows the routine to converge even for the nonconvex parts of the diagram (see right part of Figure 3.11(d)). From these figures and the table, it can be concluded that the linear routine is generally less conservative and the possibly non-convex regions of the diagram are not captured by the linear routine.

Table 3.2: Test cases results and computational time

Test case	Nonlinear		Linear		Difference max
	Time [s]	**Surface** [p.u]	**Time** [s]	**Surface** [p.u]	**Surface** [%]
1	90	3.13	9.1	3.06	2.48
2	72	1.61	10.1	1.63	-1.12
3	162	5.93	10.7	5.89	0.59
4	303	12.36	9.9	12.11	2.02
5	207	10.02	8.3	9.70	3.17

Usually, in micro-grids or from grid code definitions, some of the DERs should embed a primary control (mainly droop-like, or $\tan(\phi)$ in distribution systems) that can be included without loss of generality in the aggregation routines as a set of (non)linear constraints. This last point is illustrated with the test case 5 which considers the DERs at node 8 and 11 as droop-controlled converters for voltage support. For this simulation, we set the droop coefficients k_q to 7.2 and 3.6 for node 8 and 11 respectively. These droop gains are commonly obtained by the ratio 'maximum reactive power' over 'allowed voltage deviation'. In our case, the maxima are 1 and 0.5 p.u respectively, for a voltage deviation of 0.05 p.u.

$$Q_i = Q_i^0 - k_q(V_i - 1) \tag{3.18}$$

This configuration leads to a maximum reactive power of 0.36 and 0.18 p.u respectively. Figure 3.12 compares test cases 4 and 5. One can see that the surface is reduced compared to a fully-controlled converter as the reactive power injections are less flexible. Contrary to TC4, the droop-controlled DERs limits the reactive power margin at the PCC and significantly change the shape of the diagram.

At last, the influence of the linear approximation is presented in Table 3.3 in which the ESS is linearized by either a 16-sided polygon (Case 5) or by a 8-sided polytope (case 5b). It can be seen that the error decreases, while the computation time slightly increases. A second element which allows to compare the impact of the granularity on the linear approximation is the number of iterations to find a solution for a specific objective function. The mean value for both cases is about 46 iterations. The limitations on the number of iterations can be explained in a similar way by the fact that the voltage constraints become preponderant in the optimization problem and limit the number of vertices of the LP. This also explains that the proposed linear routine exhibits a similar computational burden.

Table 3.3: Test cases results and computational time

Case	**Non linear**		**Linear**		**Error max**
	Time [s]	**Surface** [p.u]	**Time** [s]	**Surface** [p.u]	**Surface** [%]
5	-	-	10.15	10.87	2.07
5b	364	11.10	9.73	10.47	5.68

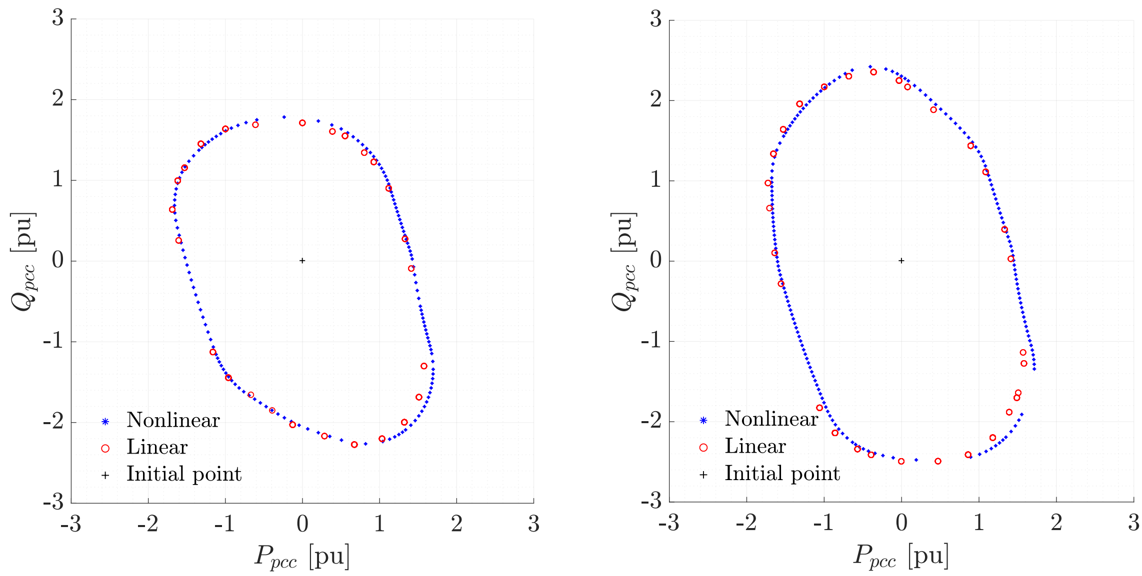

(a) Test case 5 with droop-controlled DER (b) Test case 5 with fully-controlled DER

Figure 3.12: Influence of droop-controlled DERs on capability diagram

3.3 Improved routine for variable PCC voltage estimation of micro-grid capability diagrams

The previous routines were developed for high and medium voltage power systems in which the point of common coupling is strong enough to keep the voltage close to its nominal value (1.0 p.u). To provide a primary response at the PCC, it is necessary to estimate the capability after voltage or frequency deviation and to identify the key parameters that affect the capability diagram. From the previous section, the type or the position of the flexibilities are one of the main parameters that influence the diagram. In Chapter 1 we introduced the definition and characteristics of stiffness and weak power systems. In such systems, the PCC voltages are highly fluctuating, and, in turn, any change in the power injections alters the PCC voltage due to the power sharing between the networked micro-grids. This section highlights the impact of the PCC voltage on the capability of a micro-grid and proposes a revised algorithm to accurately estimate the diagram for a wider voltage range.

3.3.1 Voltage influence on capability diagram and improved routine for variable PCC voltage

The following development is based on the nonlinear routine. Figure 3.13 illustrates this point and highlights the active constraints.

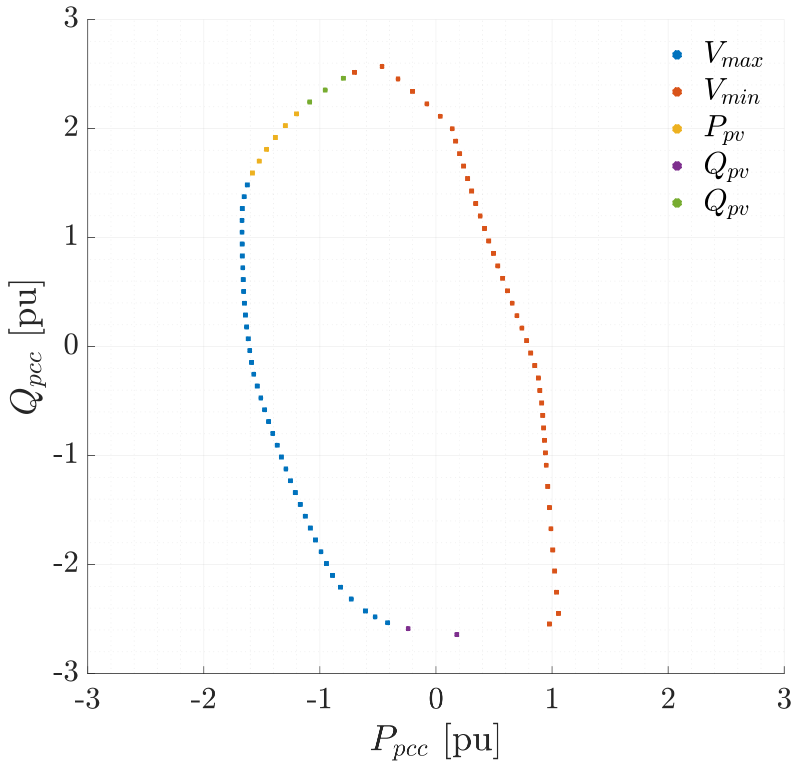

Figure 3.13: Active constraints of the optimization results for the test case 4

Let's recall that a constraint $g_i(x)$ is said to be active if for any x in the feasible region of the optimization problem, $g_i(x) = 0$. In addition, the solution of an optimization problem would possibly change if we remove that active constraint. Particularly, this means that the capability diagram is restrained by this constraint, and without its activation, the micro-grid diagram would possibly be larger. It is straightforward that for small systems, power limitations may be the active constraints. However, when considering larger systems and loosely coupled, the voltage constraint appears to be prominent. From Figure 3.13 it can be observed that the voltage constraints are the main active constraints and as consequence, the PCC voltage and the levers to control the voltage node are of great interest for networked micro-grids systems for which the voltage fluctuates. Therefore, we need to improve the previous aggregation routines to consider a wide voltage range. This task can easily be tackled by adding an outer loop to the nonlinear routine that iterates on the PCC voltage as shown in Figure 3.14. In order not to drastically increase the computational time, and based on the independence of the iterations, it is possible to parallelize the computation of the aggregated diagrams.

Finally, the proposed routine suffers from the same issues as for nonlinear OPF, that is the nonconvexity of the problem. However, the same hypotheses and solutions are used as for the nonlinear routine [78].

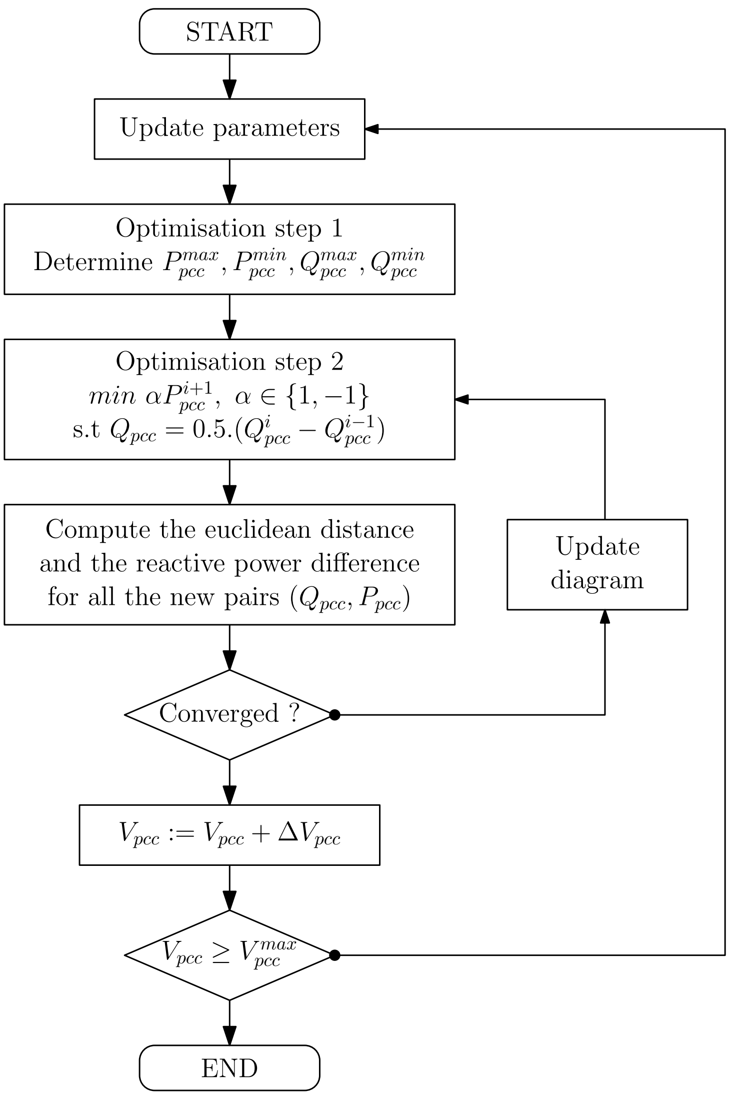

Figure 3.14: Flexibility aggregation routine for variable PCC voltage

3.3.2 Validation and results of the proposed aggregation routine for variable PCC voltage

The algorithm is validated with the same test cases 4 and 5 from the previous section. The results are depicted in Figure 3.15 for a PCC voltage of 0.96, 1 and 1.04 p.u. It can be observed that in the portion of the diagram for which the voltage constraints were the active constraints, the diagram is highly affected by the PCC voltage. In opposition, the 'hard' constraints resulting from the active and reactive power injections limitations do not change (see top left part of the diagram for example).

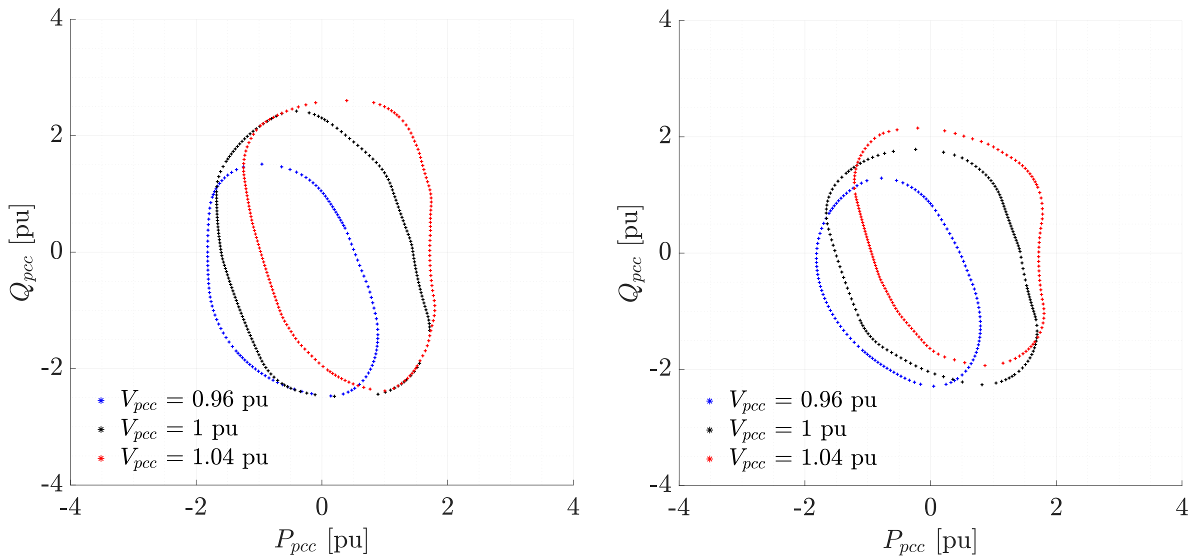

(a) Test case 4

(b) Test case 5

Figure 3.15: Influence of PCC voltage on he capability diagram for test cases TC4 and TC5

The shape of the diagram largely varies from a voltage to another, leading to variable active and reactive power reserves. Low (or high) PCC voltages greatly reduce the capability of a micro-grid to absorb or generate reactive power, as it would require to lower (or increase) the inner voltage nodes. The coupling between active power and voltage in micro-grids also constrains the active power transfer at the PCC for voltages constraints as well. These last two figures illustrate the high influence of the PCC voltage on the capability diagram. With the objective to provide primary reserves, this diagram must be estimated in real time, which in the case of the primary control means a basis of a few minutes to adjust the active and reactive power margins that the micro-grid is able to modulate. Another constraint on the capability of a micro-grid is related to the energy reserves and the duration of this capacity to provide active and reactive power modulations. This will not be further detailed, but some aspects such as stochastic forecasts, State of Charge estimation would be key issues for this point.

3.4 Conclusion on Flexibility aggregation and micro-grid capability diagram

This section introduced the aggregation of multiple flexibilities from distributed energy resources, energy storage systems and synchronous generators within a micro-grid. The need for aggregation routines based on the resolution of a linear or nonlinear optimal flow has been highlighted. Fortunately, some recent papers proposed aggregation routines for a sub-part of a power system. It has been shown that the PCC voltage has a large influence on the capability of a micro-grid through the active constraints. To solve this point, the nonlinear routine has been extended to consider a wider range of voltages. A micro-grid operator is thus able to quantify the active and reactive power reserves in order to provide a primary support at the PCC.

Based on these power reserves, the next chapter will propose and develop a centralized and a hierarchical control structure so that the micro-grid presents at the interface point a behavior that mimics the linear droop relations.

Chapter 4

PCC behavior of grid-interactive micro-grids

Contents

In the previous chapter we introduced a supervisor able to coordinate DERs and integrate local droop controller of storage devices to operate the micro-grid optimally. As reviewed in the Chapter 1, the idea of interconnecting several micro-grids or clusters of DERs gained the attention of the scientific community owing to multiple advantages that such systems exhibit. The idea developed in this Chapter 4 is to control specifically each micro-grid so that it can be seen in the time scale considered, as a droop controlled unit. This means that, for every micro-grid there exists a linear relation between the active and reactive powers and the PCC frequency and voltage respectively. Working this concept out requires novel control laws that could be based either on a centralized architecture, somewhat akin of the micro-grid supervisor or on a hierarchical control structure, as for a conventional droop mechanism. In this section, the main principle of droop-like behavior of the micro-grid PCC is presented. The required information, and control topology are discussed. Then, the centralized MPC-based supervisor built in Chapter 2 is extended to encompass the management of the PCC connection. Finally, a hierarchical structure is proposed that, based on the resolution of a specific OPF, defines nonlinear primary mappings for each DER. Both methods are validated through simulations of a realistic micro-grid.

4.1 Architecture and control objective for droop-like behavior of grid-interactive micro-grids

4.1.1 Droop-like behavior of micro-grid PCC

We recall that the droop mechanism is a linear relation between the active power and the system frequency, and the reactive power and the node voltage (4.1).

$$\begin{cases} P_i^{gen} - P_i^{ref} = -k_i^p.(\omega - \omega^*) \\ Q_i^{gen} - Q_i^{ref} = -k_i^q.(V_i - V_i^*) \end{cases} \tag{4.1}$$

The usual design of the primary control does not consider the micro-grid PCC nor the aggregation of multiple droop-controlled inverters. Figure 4.1 presents the behavior of a micro-grid as detailed in Appendix B and for which the DERs are controlled by conventional droop laws. These figures are obtained by incorporating the droop relations into the Jacobian matrix, as proposed in [88], and by using the PCC voltage (considered as a slack bus) or the frequency as parameters. The OPF is then solved using Newton-Raphson's method.

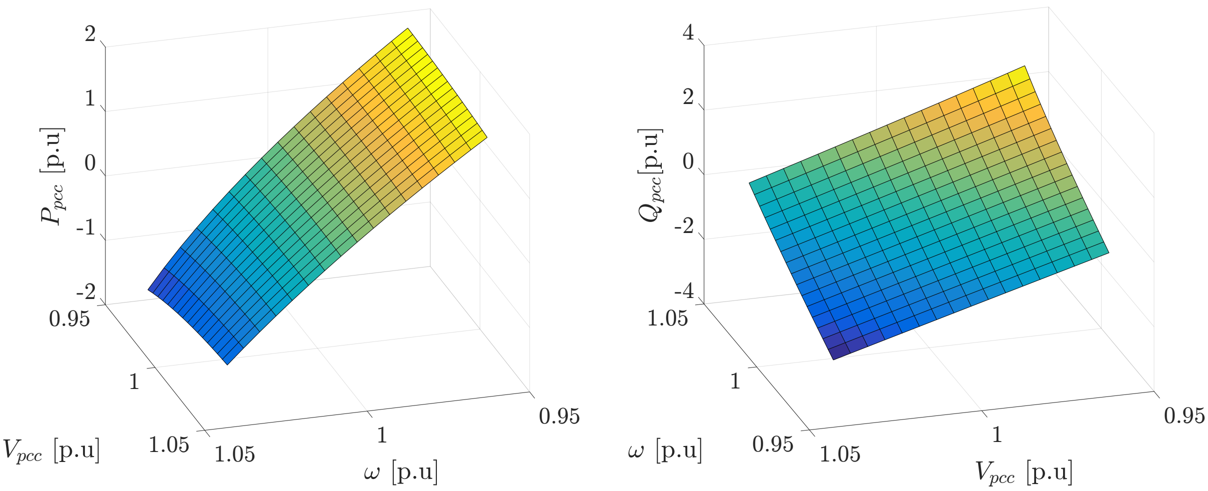

Figure 4.1: Active (left) and reactive (right) power injections at the PCC for conventional droop laws as function of the system frequency and the PCC voltage

From these figures, the conclusions are twofold. First, when the frequency deviates from its reference (1 p.u), the active power response at the PCC is not linear. This can easily be explained by the quadratic nature of the line losses. Therefore, local linear regulators such as droop laws are not sufficient to enforce a droop-like behavior of the PCC.

Second, even if the reactive power modulation response to a voltage deviation is linear, the gain depends on the active power through the system frequency. In fact, the active power-frequency droop acts on the micro-grid voltage nodes, and as a consequence the reactive power is also modulated. This cross coupling of active and reactive powers is mainly due to the low $\frac{X}{R}$ ratio and has been largely studied in micro-grids. Virtual impedance and other outer loop techniques [89, 90] have been proposed to handle this issue. It is particularly interesting to point out references [91, 92] in which the complex nature of the transmission lines are used to define new $\{V,\ \omega\}$ reference frames thanks to a linear transformations so that the power injections on the line are decoupled.

Indeed, considering a complete micro-grid system it is required to consider several converters and a more complex impedance network. Therefore we propose a novel primary control mapping that is designed to (I) decouple active and reactive powers and (II) enforces a droop-like behavior at the PCC.

The idea is depicted in Figure 4.2, and the three steps are:

- **Step (1)** - based on the unitary flexibilities, the capability diagram of the micro-grid is determined, following the procedure described in Chapter 3.
- **Step (2**) - from the capability diagram at the PCC, the admissible droop coefficients are obtained, and their choice depend on Networked-Micro-grids stability criteria – this part will not be further detailed in the remainder.
- **Step (3)** - the primary control laws are determined to enforce the specific droop-like behavior at the PCC by solving a nonlinear optimization problem.

Steps (1) and (2) must be performed in a centralized way. However, the third step may be either centralized and directly embedded into the supervisor objective function, or hierarchical along with a distribution of the control effort among the levers. In the remaining, both possibilities will be explored, and the synthesis of the control will be developed.

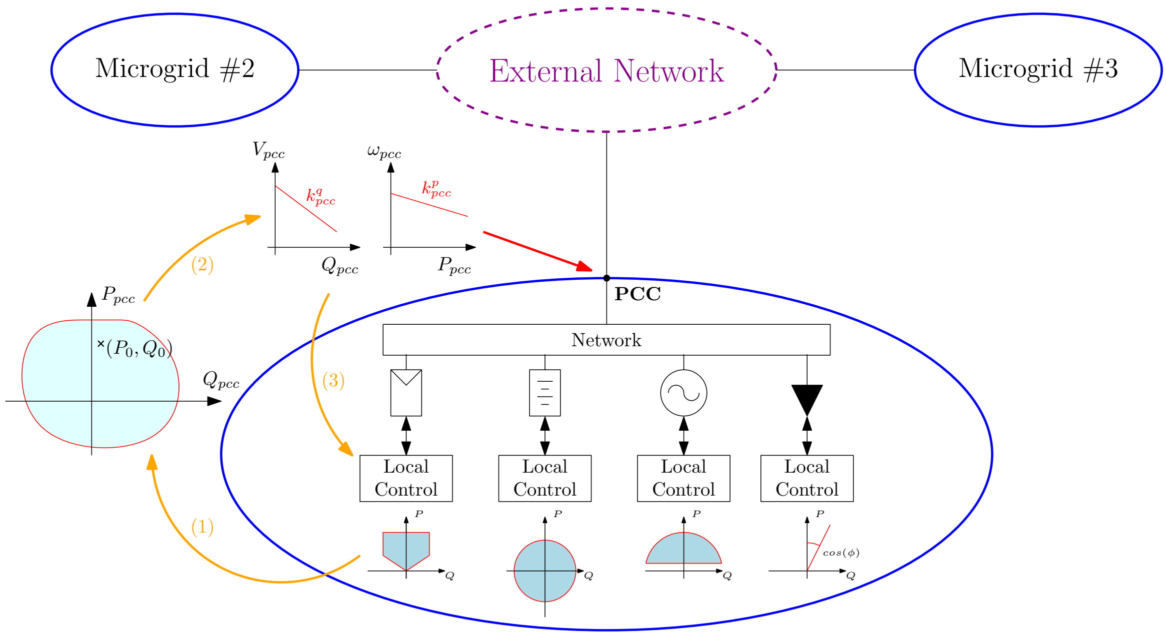

Figure 4.2: General synoptic of droop-like behavior of the PCC by optimally tuning local nonlinear primary controllers — (1) flexibility aggregation, (2) virtual PCC droop gains, (3) local control laws synthesis

4.1.2 Power margins and droop coefficient calculation

The first step of Figure 4.2 has already been developed in the previous chapter. The initial operating point of the micro-grid is given in Table 4.1. Following the methodology detailed in Chapter 3, the capability diagram at the PCC (Figure 4.3) can be inferred from the flexibility diagrams of the DERs. Therefore this section will only detail the step (2) and the calculation of the droop coefficients.

Table 4.1: Initial operating point.

Node	**Voltage [p.u]**	**Active power [p.u]**	**Reactive power [p.u]**
2	1.004	0.00	0.00
6	0.995	0.00	0.00
8	0.992	0.25	0.00
11	1.022	0.42	0.00
15	1.036	0.54	0.00
PCC	1.000	0.45	-0.01

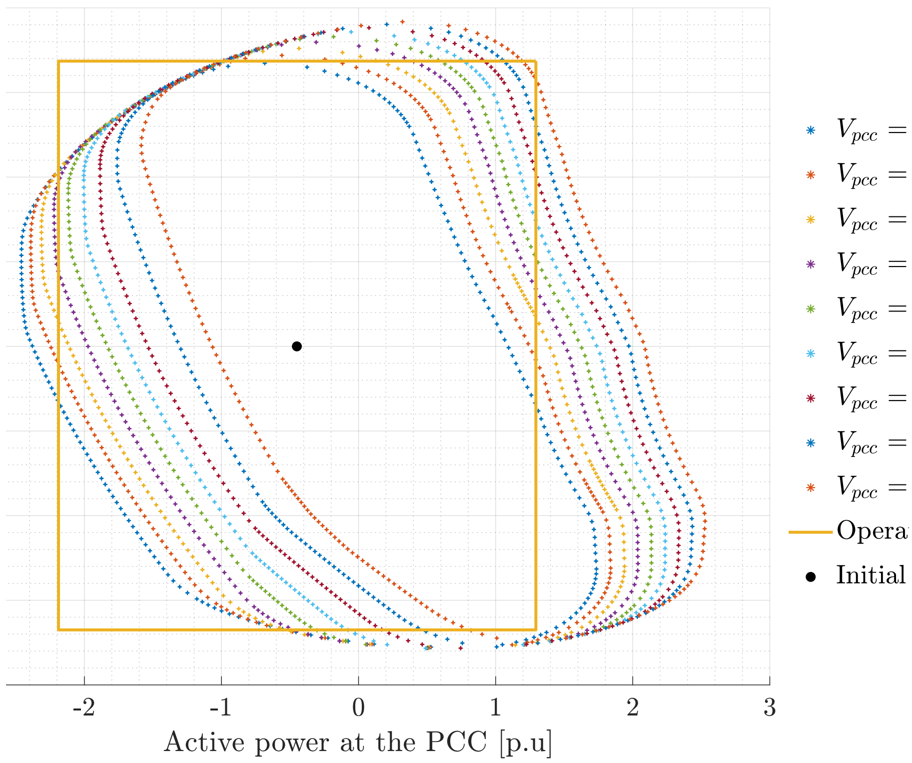

Figure 4.3: Flexibility diagram of the 18-node modified European LV benchmark network.

We need to determine the active and reactive power margins - that is the active and reactive power that the micro-grid can modulate - in order to obtain an operating region hence, the maximum droop gains. From Figure 4.3 the power margins are arbitrary and can be determined by (4.2).

$$\begin{aligned}
\Delta P^{+} &= \max(P_{pcc}|Q_{pcc} = Q^{0}_{pcc}) - P^{0}_{pcc} \\
\Delta P^{-} &= \min(P_{pcc}|Q_{pcc} = Q^{0}_{pcc}) - P^{0}_{pcc} \\
\Delta Q^{+} &= \max(Q_{pcc}|P_{pcc} = P^{0}_{pcc}) - Q^{0}_{pcc} \\
\Delta Q^{-} &= \min(Q_{pcc}|P_{pcc} = P^{0}_{pcc}) - Q^{0}_{pcc}
\end{aligned} \tag{4.2}$$

where ΔP^{+} and ΔP^{-} are the active power supports that the micro-grid is able to inject and to absorb (resp.). P^{0}_{pcc} and Q^{0}_{pcc} are the initial active and reactive power injections. For the complete PCC voltage range we determine the maximum positive and negative active and reactive powers that the micro-grid can modulate from the initial operating point. Theoretically, this gives four power margins (positive and negative modulation of the active and reactive power) and therefore leads to four different droop gains. However, practically, the droop relations are formulated with a symmetric gain for the positive and negative modulation. Without loss of generality and for the remainder of this section we make the same assumption and the choice of the droop coefficient obeys (4.3).

$$
\begin{aligned}
k^p_{pcc} &= \frac{\min(\Delta P^+, \Delta P^-)}{\underline{\omega} - \omega^n} \\
k^q_{pcc} &= \frac{\min(\Delta Q^+, \Delta Q^-)}{\underline{V_{pcc}} - V_{pcc}}
\end{aligned}
\tag{4.3}
$$

The operating region, based on the power margins are represented by the square on Figure 4.3. Some regions of the rectangle are outside of the capability diagram which means that the corresponding operating point cannot be reached. A solution would have been to reduce drastically the active and reactive power margins. This would generate a smaller rectangle that would fit into the capability diagram, thereby yielding lower maximum achievable droop coefficients and support. In addition, due to its non linearity and non convexity, and contrary to the previous chapters, the capability diagram will not be considered as a constraint in the optimization problem. Therefore, we will treat the power references obtained from this diagram as the objective of a least square problem. The next sections will present a centralized and hierarchical formulation of the optimization problem corresponding to the third step.

4.2 MPC-based centralized primary response for grid-interactive micro-grids

In the Chapter 2, a MPC-based supervisor for an islanded micro-grid has been developed. The challenge to be tackled is the difference between the models and between the objectives of the secondary and the tertiary controls. The present section focuses on the interactions of the micro-grid with an external network and the proper control in order to provide a droop-like ancillary service at the PCC.

4.2.1 Primary response outer loop

To enforce a specific behavior at the PCC, the MPC-based supervisor is upgraded with an outer loop that defines an additional objective to be tracked. Based on the voltage and frequency at the PCC, this outer loop computes the new active and reactive powers to inject or absorb with the following droop relations:

$$\begin{aligned} P_{pcc}^{*} - P_{pcc}^{genref} &= -k_{pcc}^{p}.(\omega - \omega^{*}) \\ Q_{pcc}^{*} - Q_{pcc}^{genref} &= -k_{pcc}^{q}.(V_{pcc} - {V_{pcc}}^{*}) \end{aligned} \tag{4.4}$$

where $P_{pcc}^{*}(k+1)$ and $Q_{pcc}^{*}(k+1)$ refer to the active and reactive powers to be reached at the PCC at time-step $(k+1)$. P_{pcc}^{genref} and Q_{pcc}^{genref} are the contractual active and reactive powers at the interface, ω, V_{pcc} are the frequency and voltage at the PCC, and the superscript * denotes for the voltage and frequency references.

Contrary to the formulation of the micro-grid system frequency and PCC voltage in Chapter 2 the behavior of these two states cannot be predicted. It is not possible to handle the algebraic equation (2.38) with the injection of the predicted state. Therefore, the outer loop we add will introduce a time delay between the measurement of V_{pcc} and ω in order to define the active and reactive power references for the objective function of our supervisor. Finally, the synoptic of the proposed modified MPC-supervisor is depicted in Figure 4.4 and the optimization problem can be formulated as an extension of (2.8):

$$\mathcal{C}_2 = \mathcal{C}_1 + \lambda_P \varepsilon_{P_{pcc}} + \lambda_Q \varepsilon_{Q_{pcc}} \tag{4.5}$$

where λ_P and λ_Q are the weighting factors related to the error in the active and reactive power injection at the PCC (resp. $\varepsilon_{P_{pcc}}$ and $\varepsilon_{Q_{pcc}}$).

4.2.2 External network model

As the system frequency of the networked micro-grids system depends on the contribution of each micro-grid, the model of the micro-grid detailed in Chapter 2 needs to be refined. In the previous Chapter, the inverters were controlled so that the output frequency was an image of the mismatch between the active power reference and the output power. To include the global frequency of the system (micro-grid - external system) one can use the conventional model for frequency stability studies [93]. The simplified frequency response model is based on the swing differential equation :

$$\Delta P_m(t) - \Delta P_l(t) = 2H\frac{\mathrm{d}\Delta f(t)}{\mathrm{d}t} + D\Delta f(t) \tag{4.6}$$

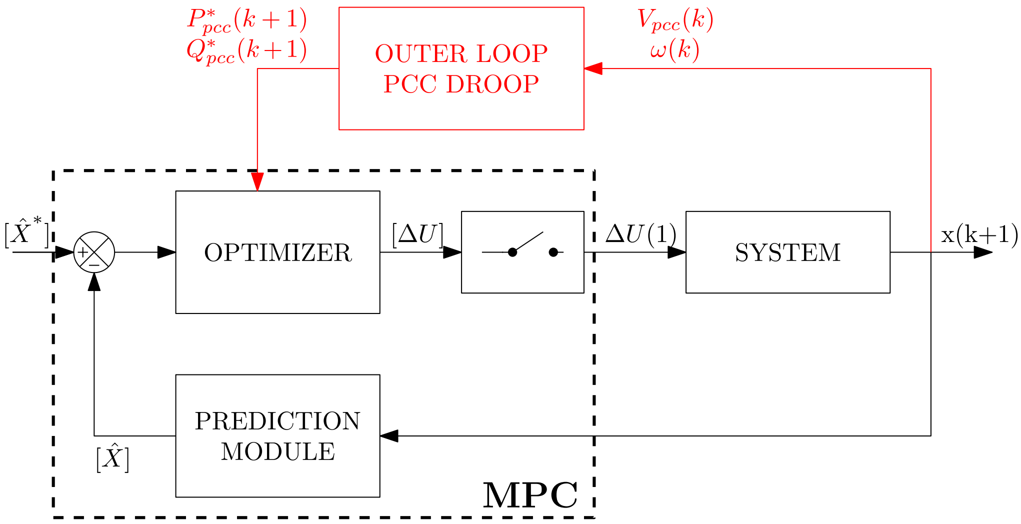

Figure 4.4: Outer loop and synoptic of upgraded MPC-based supervisor for grid-connected micro-grid

with ΔP_m, ΔP_l, Δf the mechanical, the load and the frequency deviation respectively, and H, D, are the inertia constant and the frequency dependence of the loads. The contribution of one system to the system frequency is coupled by the active power transmission through the tie-line, and is described by the DC power flow approximation :

$$P_{tie} = \frac{V_1 V_2}{X_{tie}} \sin(\delta_1 - \delta_2) \tag{4.7}$$

with X_{tie} the impedance of the tie line, V_1, δ_1, the voltage magnitude and phase angle of system 1. Once linearized, and by defining T_{tie} as the transfer coefficient, depending on the equilibrium point as

$$T_{tie} = 2\pi \frac{V_1 V_2}{X_{tie}} \cos(\delta_1^0 - \delta_2^0) \tag{4.8}$$

we obtain the following relation with the Laplace transform

$$\Delta P_{tie}(s) = \frac{T_{tie}}{s} (\Delta f_1(s) - \Delta f_2(s)) \tag{4.9}$$

and the global system can be represented as in Figure 4.5. ΔP^{pcc}, ΔP_{tie}, ΔP_{ext} are the active power mismatch at the PCC of the micro-grid, the active power deviation in the tie-line and the total active power deviation from the external system. Δf_1 and Δf_{ext} are the frequency contribution from the micro-grid and the external system to the global frequency deviation. Last, H_{ext}, H_1, D_{ext}, and D_1 are the external and micro-grid system inertia and damping coefficient.

In this figure, the feedback ΔP_{tie} represents the image of the frequency deviation, and therefore, the additional objective function of the micro-grid.

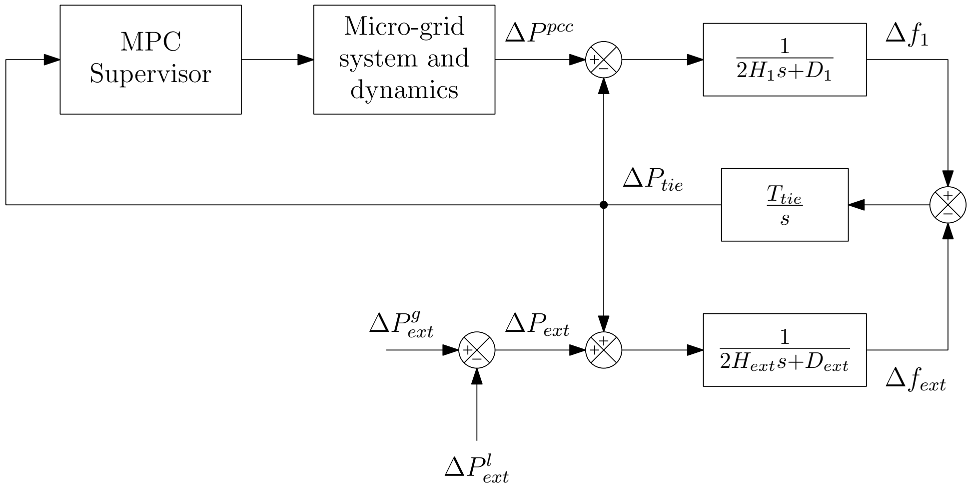

Figure 4.5: Complete model of the networked micro-grid frequency

Embedded model

Finally, it is not realistic to include the complete model of the system frequency in the embedded model of the MPC supervisor, as it does not know every parameter of the external system. Therefore, we will make the following assumptions:

(I) The complete networked micro-grids system will be described by the reduced model of the system and, due to the time step considered, and the low inertia nature of networked micro-grids systems, we neglect the impact of the system inertia (H_{sys}). This mean that, globally, the system behaves as a droop-controlled source.

(II) The voltage at the PCC depends on the local interaction of active and reactive loads, and of the network characteristics. These characteristics are unknown for the micro-grid operator, therefore we assume the voltage deviation at the PCC as a measured disturbance.

(III) The embedded model in the MPC supervisor will include the external network as an infinite bus for the considered control horizon. This means, based on the two previous assumptions that the voltage and frequency at the PCC change at the first time step of the control horizon and remain steady.

With these three assumptions, the global system is depicted in Figure 4.6. From a control point of view, this means that the MPC-based supervisor will behave as an integral control to provide the active and reactive power at the PCC specified by the enforced droop law. The assumption (III) and the mismatch between the prediction model of the external network and the real system will be tackled by the receding nature of the MPC.

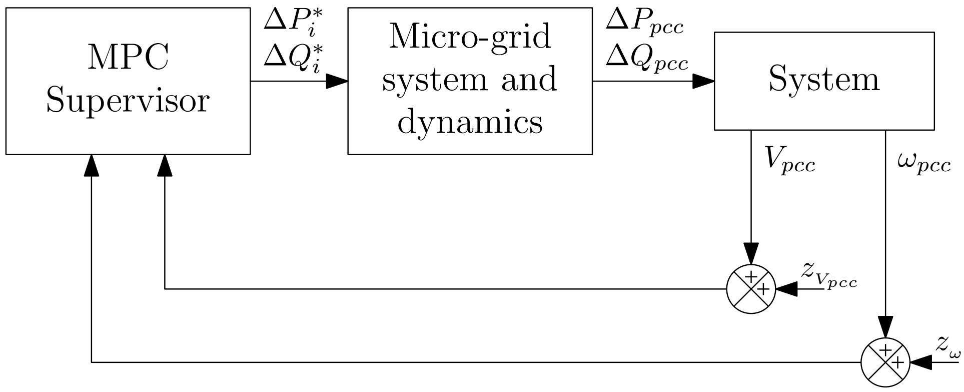

Figure 4.6: Overall synopsis of the MPC-based micro-grid supervisor with PCC control

The complete embedded model is based on the equations detailed in Chapter 2, and is further detailed in the appendix C.

4.2.3 Validation of the proposed centralized control

4.2.3.1 Hypotheses and parameters

To assess the effectiveness of the proposed extended supervisor, different test cases are simulated. Based on the routine proposed in the previous chapter to determine the maximum active and reactive power flow at the interface, and for the remainder of this section we consider the following droop coefficients at the interface :

- Active power-frequency droop $k_{pcc}^p = 10$,
- Reactive power-voltage droop $k_{pcc}^q = 7.2$.

It is worth noting that these coefficients are arbitrarily chosen but would result from a coordination mechanism and a stability assessment of the networked micro-grids system by a coordination agent of through consensus techniques which are beyond the scope of this work. For the sake of simplicity, we assume that there is no exchange planned between the micro-grid and the external system. Therefore, the droop gain represents a maximum active and reactive power at the interface of $P_{pcc} = \pm 0.5$ p.u and $Q_{pcc} = \pm 0.18$ p.u. It is worth noting that these coefficients are conservative in the way that the micro-grid can provide more active and reactive powers. The specific choice of droop gains that results in outreaching the capability diagram will be further discussed in the end of this section.

For illustrative purpose, a voltage and a frequency profile has been generated based on local measurement at the University of Lille. The frequency profile aims to emulate a fast and relatively short power mismatch, while the voltage profile has a slower dynamics with a larger amplitude. These profiles will be the base inputs for our MPC-based supervisor, and are shown in Figure 4.7.

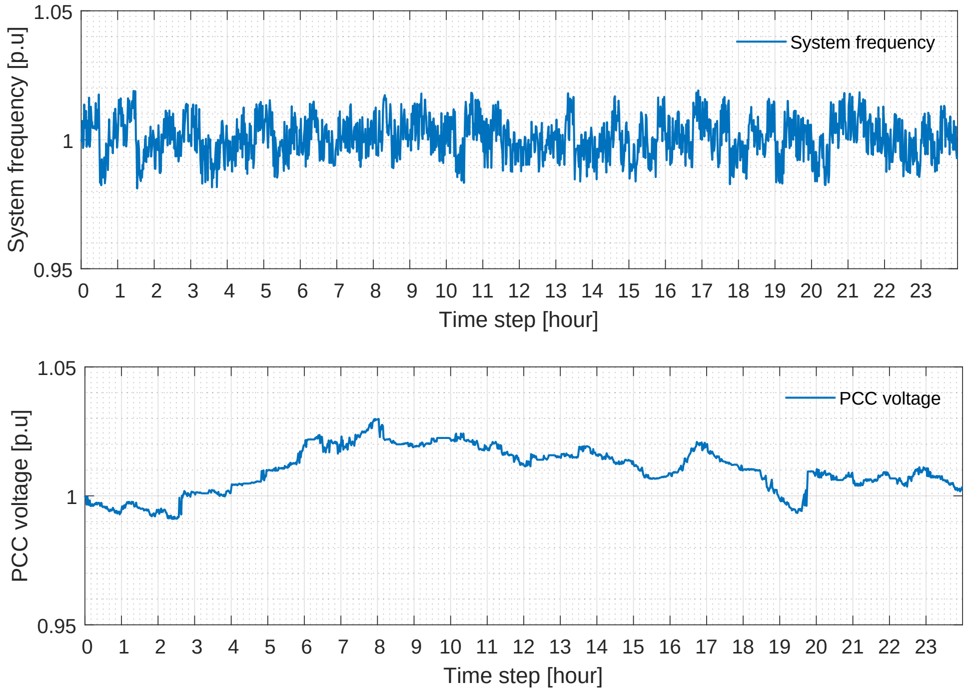

Figure 4.7: Frequency (top) and voltage (bottom) profile

4.2.3.2 Reactive power - PCC voltage response

The first case considers a voltage profile at the PCC. As previously explained, The voltage profile cannot be estimated without refined external system model. Therefore, only the first voltage deviation is considered as a step from measurements. The results are shown in Figure 4.8 and Figure 4.9 for weighting coefficients that favor the droop-like behavior of the micro-grid. The supervisor succeeded to provide the expected reactive power at the PCC (Figure 4.8), with a zero active power injection (Figure 4.9).

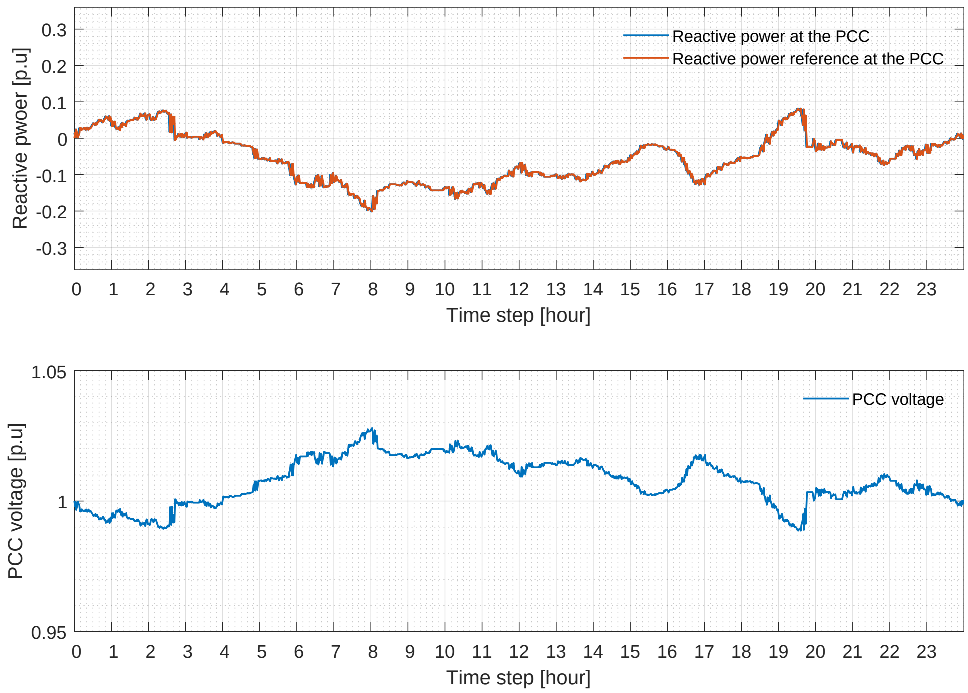

Figure 4.8: Reactive power response of the micro-grid versus PCC voltage and reactive power reference – Voltage support

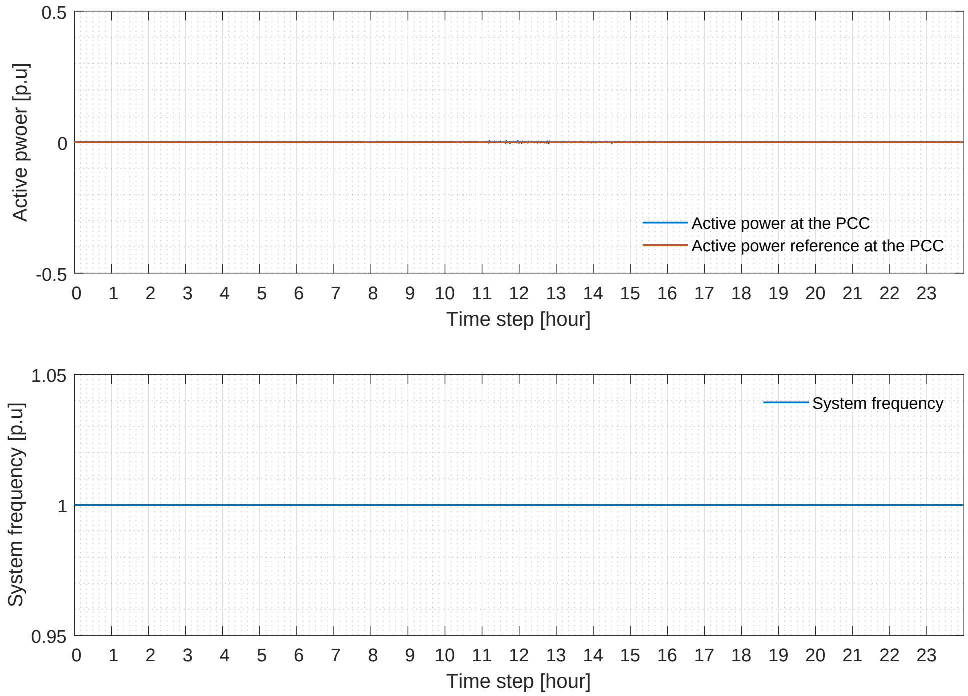

Figure 4.9: Active power response of the micro-grid versus system frequency and active power reference – Voltage support

4.2.3.3 Active power - Frequency response

This second case considers the frequency profile as the only input. As for the previous case, only the first input is taken into account ($\Delta\omega_{pcc}(1)$). The objective of the supervisor is to reach as best as possible the economic trajectory and to modulate the active power at the interface according to the frequency deviation. The results are displayed in Figure 4.10, in which the first graph shows the active power at the interface in blue, and the active power reference in red. The reference profile is based on the frequency deviation and the corresponding ideal response of the micro-grid. The second graph displays the system frequency. From these figures, two different behaviors can be observed.

First, during the first and last hours of the day, the DERs production is zero. Therefore, the supervisor is able to provide references to match very closely the required active power at the PCC. In contrast, during the fast fluctuations of the DERs production (see between 11 and 13h), the micro-grid presents larger errors in the active power at the PCC. Two effects counteract. First, the cause of the mismatched power is mainly due to the internal power balance mismatch. As the generation and load forecasts are ideal, there is no action to be taken to comply with the economical trajectory and the State of Charge of the storages will by itself converge to the optimal State of Charge. Conversely, the second objective is to provide ancillary services and requires to change the active power references. Finally, a consensus is obtained based on the weighting factors which determines the optimal control sequence.

One can favor the frequency support by adjusting the weighting factors. The simulation results with these weighting factors are shown in Figure 4.11. The system exhibits a better active power profile, at the price of a higher actuation cost (see Figure 4.12).

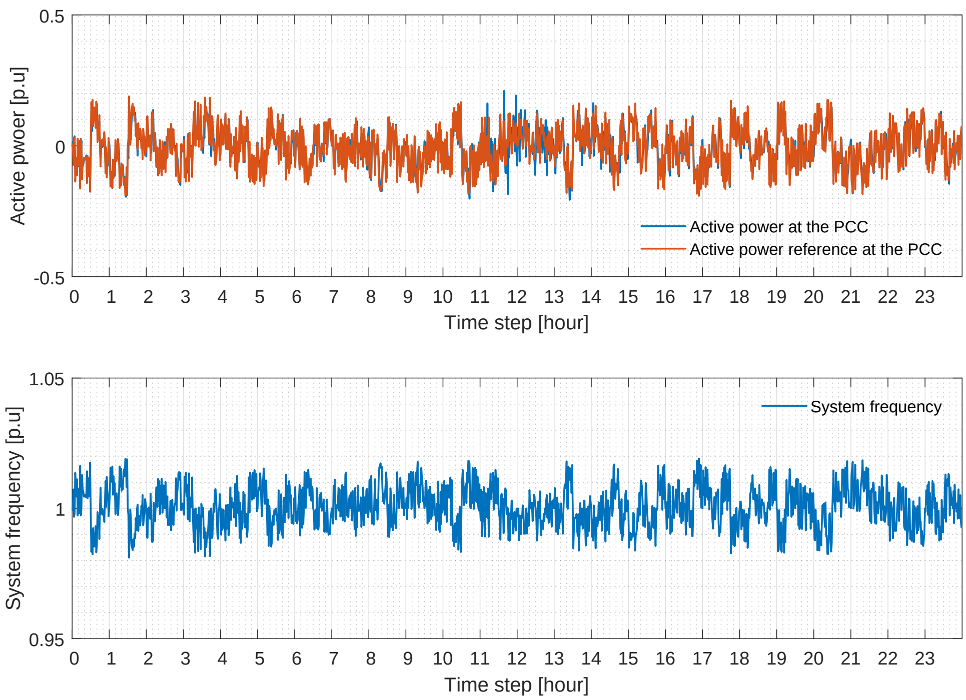

Figure 4.10: Active power response of the micro-grid versus system frequency and active power reference – Frequency support

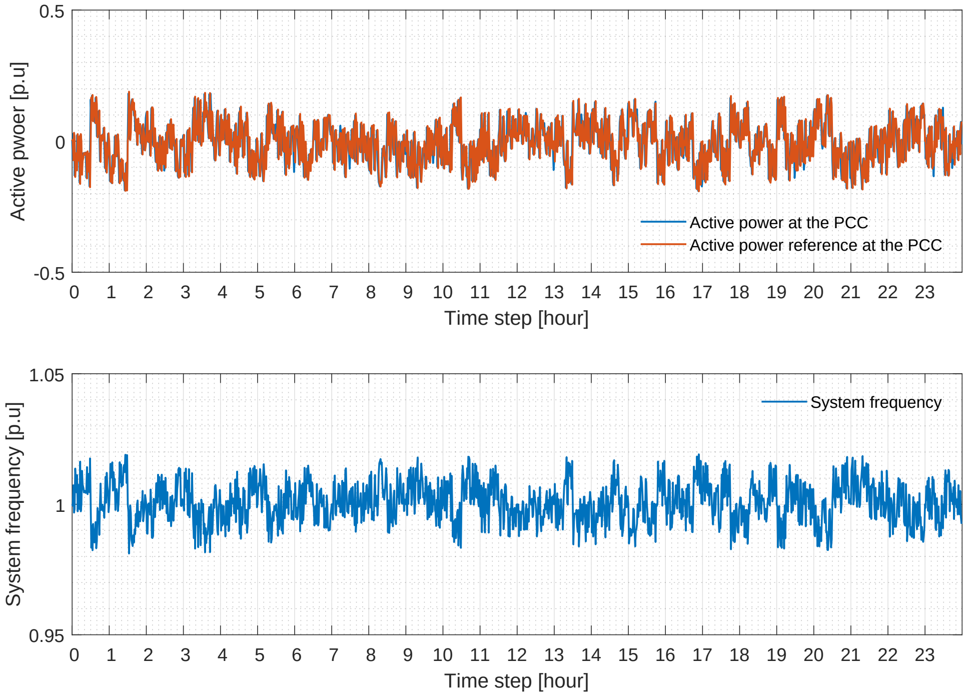

Figure 4.11: Active power response of the micro-grid versus system frequency and active power reference – Frequency support

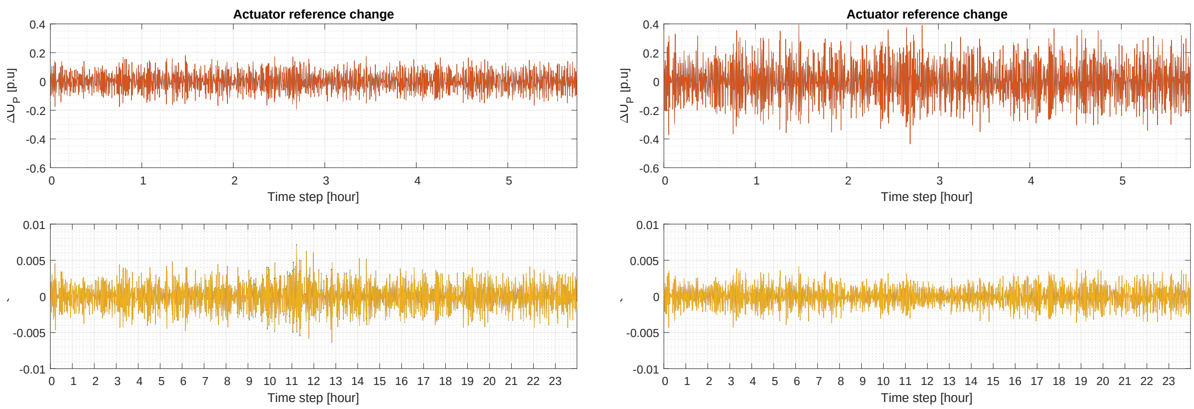

Figure 4.12: Change of references – balanced weighting factors (left) versus ancillary services focused weighting factors (right)

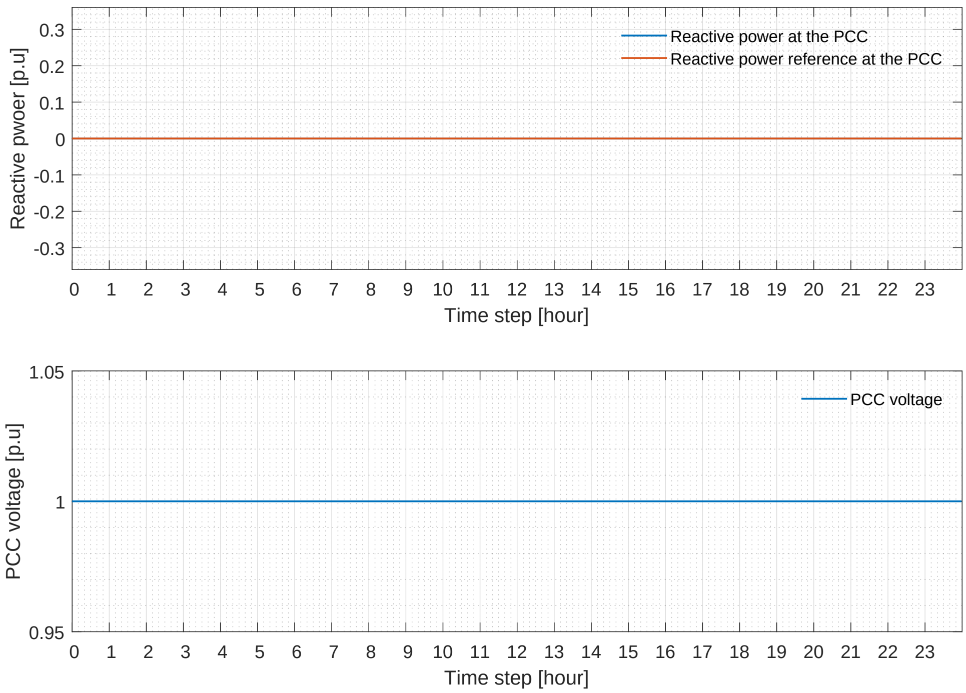

Figure 4.13: Reactive power response of the micro-grid versus PCC voltage and reactive power reference – Frequency support

An important observation in Section 4.1 and in shown in Figure 4.1 is that in a LV network, the active and reactive powers are highly coupled. Figure 4.13 displays the reactive power at the interface, and the voltage at the PCC. It can be concluded that the proposed supervisor is able to provide references that decouples the active and reactive power flows at the interface.

4.2.3.4 Full primary control of the micro-grid

The last case combines the active power and the reactive power supports at the PCC. Similar results (Figure 4.14 and Figure 4.15) are obtained for the voltage and frequency deviation profiles. The active and reactive powers match closely their references. The resulting droop gains obtained at the PCC are shwon in Figure 4.16. It can be seen that, non taking the large spikes due to numerical conditioning (mainly due to very low frequency deviations), the active and reactive power flows at the PCC are properly modulated according to the design the supervisor and of the optimization function.

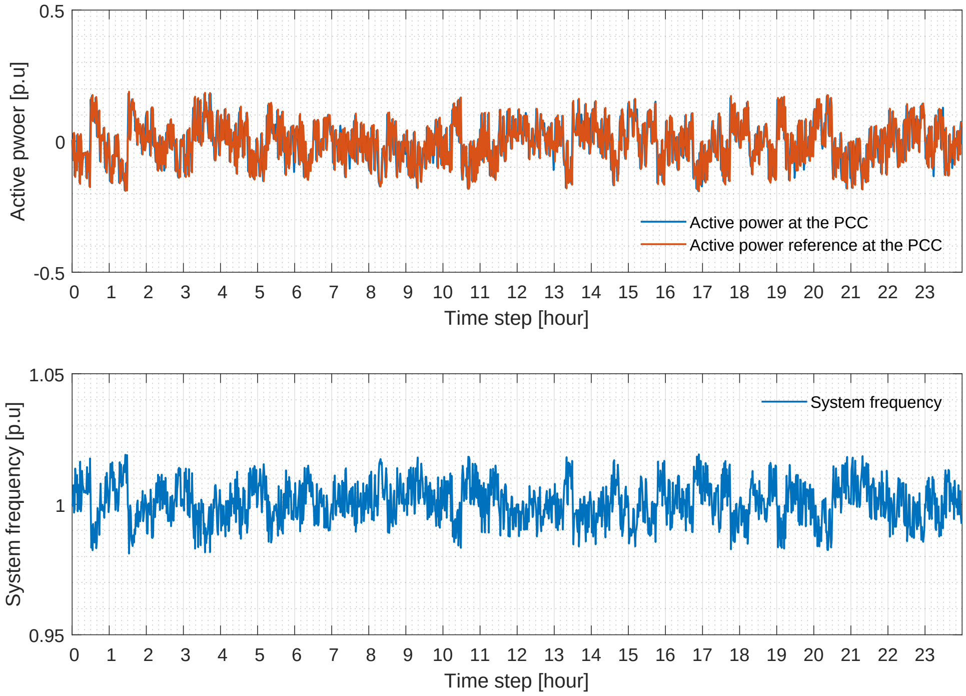

Figure 4.14: Active power response of the micro-grid versus system frequency and active power reference – Frequency and voltage support

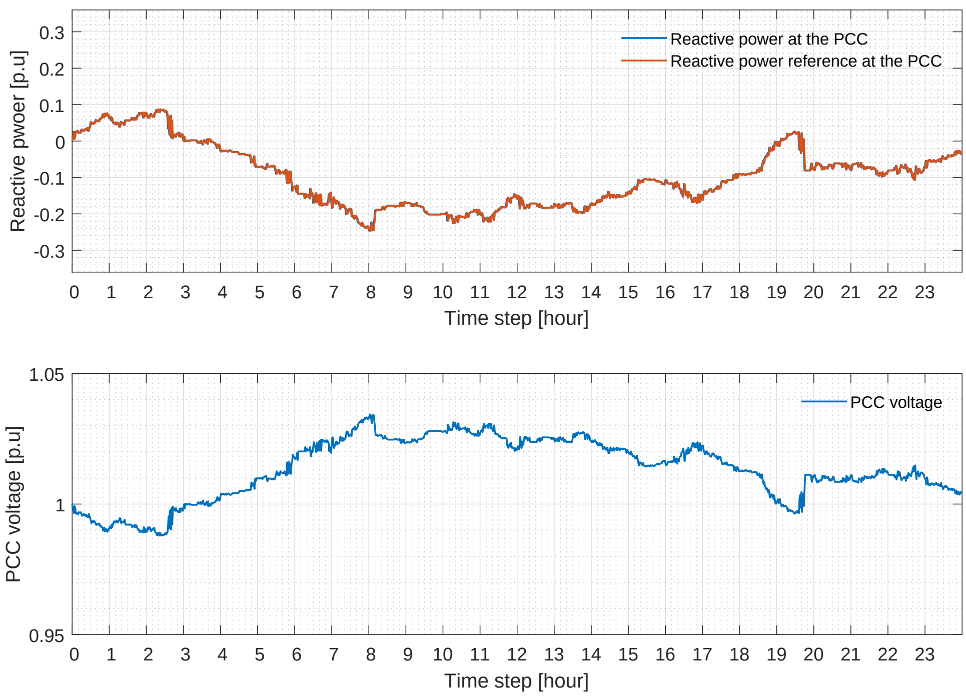

Figure 4.15: Reactive power response of the micro-grid versus PCC voltage and reactive power reference – Frequency and voltage support

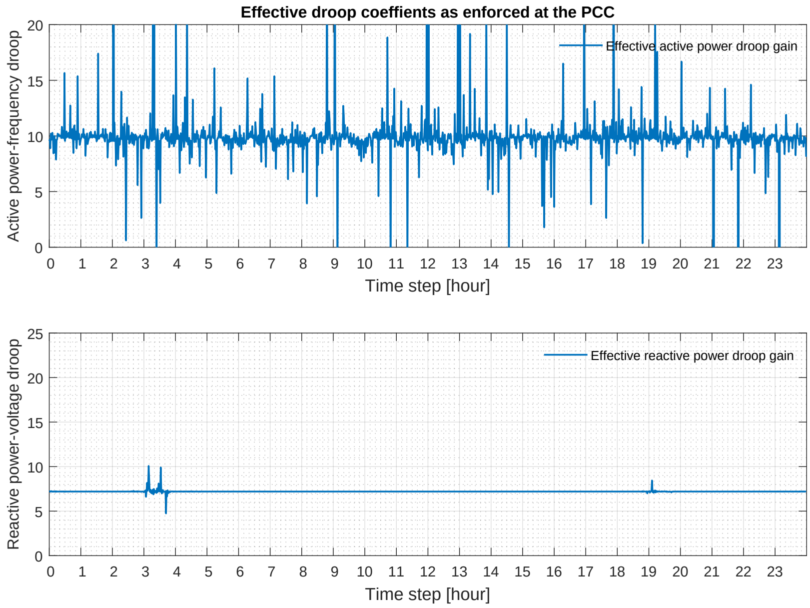

Figure 4.16: Effective droop gain enforced at the PCC

As final comment, we can discuss the hypothesis of considering the PCC as an infinite bus for a specific control horizon. The prediction model does no include the dynamics of the frequency or PCC voltage as a function of the active and reactive power injections. Therefore, in the case for which the active power flow does not precisely matches the reference, it implies that another micro-grid should be able to provide the active power mismatch. This first observation brings to light the needs of system-wide coordination, which is out of the scope of this work.

Secondly, we assumed that the lack of complete frequency dynamic model would be compensated by the accumulation action of the MPC technique. Figure 4.17 and Figure 4.18 display the responses of the micro-grid to a load change and for different weighting factors. The first figure presents the case of a supervisor that favors the provision of the ancillary services, while the second has moderate weighting factor. The initial response is similar. When the error becomes bigger, the first supervisor applies to the system large change of reference which leads to an overshoot and finally reaches the reference after 8 time steps. For the second supervisor, the active power reference is not reached at the end of the control horizon, and still presents changes of references during the whole horizon. This last observation means that higher weighting factors would also lead to a lower following error[1]. Still, at the second time step, the initial state for the optimization problem will not be steady, and the second control sequence will have to compensate the lack of the first one.

[1]The difference between commanded and actual state is the following error

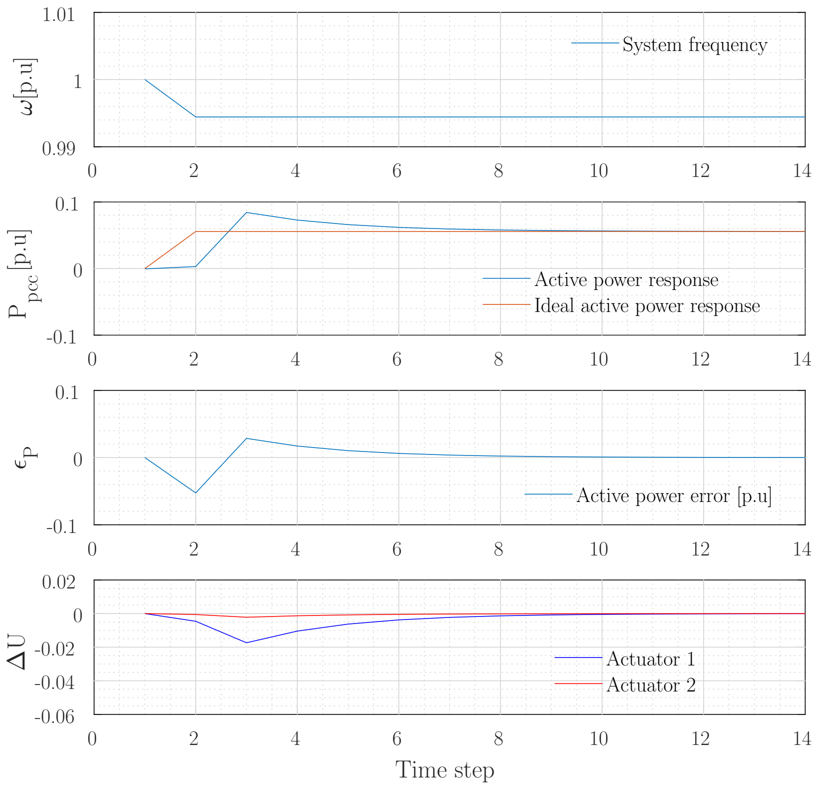

Figure 4.17: Convergence speed of a supervisor that favors the provision of frequency support

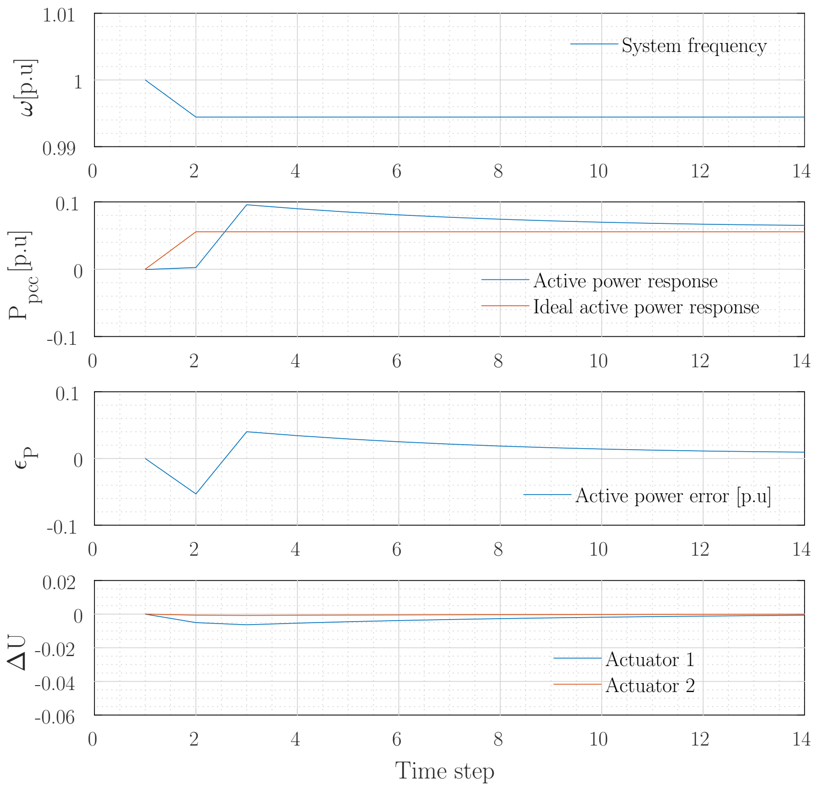

Figure 4.18: Convergence speed of a supervisor with moderate weighting factors

Finally, a first option to manage the interface between a grid-interactive micro-grid and an external power system has been proposed which is based on a extended version of the centralized MPC-based supervisor. With appropriate weighting factors and coordinated active and reactive power references, the grid-interactive micro-grid reacts to PCC voltage and frequency deviations as a droop controller. The simulations on a realistic micro-grid benchmark model have shown good results. The embedded linear model and the linear objective formulation allow the resolution of the optimization problem within a few seconds and enable its implementation for future real-time simulations with smaller time steps.

4.3 Distributed Primary response for grid-interactive micro-grids

One of the main advantages of the droop control, and more generally of the primary control is its distributed nature. The pre-defined control laws ensure a stable and coordinated reaction to voltage and frequency deviations. Theses laws, and precisely the droop gains, are defined once (or repeatedly) based on static (power limitations) and dynamic (response time, stability) considerations of the converters. In this Section, we propose a novel external droop control architecture focusing on the PCC to obtain a droop-like behavior while keeping a standard decentralized control architecture with little communication requirements.

4.3.1 Nonlinear primary control mapping

The local controllers of the flexibilities of a micro-grid are the only degrees of freedom which enable to enforce a droop-like behavior at the PCC (4.3), which only considers the frequency and PCC voltage. Hence, a new methodology is required to determine the primary control laws of the DERs, that will be based on these two variables, contrary to the traditional local droop controllers that use the local node voltages. Thus, we can reformulate the local primary control as:

$$\begin{aligned} P_i^g &= P_i^{ref} + f_i(V_{pcc}, \omega) \\ Q_i^g &= Q_i^{ref} + g_i(V_{pcc}, \omega) \end{aligned} \tag{4.10}$$

where the functions f and g are the mappings of the active and reactive powers as functions of the PCC voltage and system frequency. By combining the conventional power flow equations to the desired behavior at the PCC and the control laws at the inverter nodes, the micro-grid system can be represented by (4.11).

$$\begin{aligned}
P_{pcc} &= P_{pcc}^{ref} - k_{pcc}^{p}.(\omega - \omega^n) \\
&= V_{pcc} \sum_{j \in N} V_j (G_{pccj} \cos(\theta_{pcc} - \theta_j) + B_{pccj} \sin(\theta_{pcc} - \theta_j)) \\
Q_{pcc} &= Q_{pcc}^{ref} - k_{pcc}^{q}.(V_{pcc} - V_{pcc}^{n}) \\
&= V_{pcc} \sum_{j \in N} V_j (G_{pccj} \sin(\theta_{pcc} - \theta_j) - B_{pccj} \cos(\theta_{pcc} - \theta_j)) \\
\forall\, i \in \mathcal{N}_{\lceil} & \begin{cases} P_i^{ref} + f_i(V_{pcc}, \omega) = V_i \sum_{j \in \mathcal{N}} V_j (G_{ij} \cos(\theta_i - \theta_j) + B_{ij} \sin(\theta_i - \theta_j)) \\ Q_i^{ref} + g_i(V_{pcc}, \omega) = V_i \sum_{j \in \mathcal{N}} V_j (G_{ij} \sin(\theta_i - \theta_j) - B_{ij} \cos(\theta_i - \theta_j)) \end{cases} \\
\forall\, k \notin \mathcal{N}_{\lceil} & \begin{cases} P_k = V_k \sum_{j \in \mathcal{N}} V_j (G_{kj} \cos(\theta_k - \theta_j) + B_{kj} \sin(\theta_k - \theta_j)) \\ Q_k = V_k \sum_{j \in \mathcal{N}} V_j (G_{kj} \sin(\theta_k - \theta_j) - B_{kj} \cos(\theta_k - \theta_j)) \end{cases}
\end{aligned} \tag{4.11}$$

where $\mathcal{N}_d$ is the set of controlled nodes.

The functions f and g cannot be analytically determined as the system (4.11) is nonlinear. Therefore, we formulate an optimization problem as a least square problem to minimize the error on the provision of active and reactive power at the PCC. A first formulation of the objective function can optimize the line losses.

$$\mathcal{J} = \lambda_p \left\| P_{pcc} - P_{pcc}^{ref} \right\|^2 + \lambda_q \left\| Q_{pcc} - Q_{pcc}^{ref} \right\|^2 + P_{losses} \tag{4.12}$$

With this formulation, the primary mapping will tend to decrease the total effort at the cost of an over actuation of the levers close to the PCC. In micro-grids, line losses may not be significant. Therefore, on can prefer a second formulation that optimizes the distribution the effort among DER.

$$\begin{aligned}\mathcal{J} = \lambda_p \left\| P_{pcc} - P_{pcc}^{ref} \right\|^2 + \lambda_q \left\| Q_{pcc} - Q_{pcc}^{ref} \right\|^2 &+ \sum_{i \in \mathcal{R}_d} \left(\frac{\Delta P_i}{P_i^n} S_{base} - \Delta P_{pcc} \right)^2 \\ &+ \sum_{i \in \mathcal{R}_d} \left(\frac{\Delta Q_i}{Q_i^n} S_{base} - \Delta Q_{pcc} \right)^2\end{aligned} \tag{4.13}$$

with S_{base} the base value of the apparent power, used to scale the different basis of DER. The choice of this formulation over the first one can be justified by the cost of the active and reactive supports at the PCC. By distributing the effort, and with the assumption that each DER has an identical quadratic cost (see Section 2.4.1) the overall cost is reduced.

It is worth noting that the least square problem presents two different weighting factors for the active and reactive powers. This aims to prioritize the active or reactive power support, for the cases which are not reachable - that are references outside of the capability diagram. By using the frequency and PCC voltage variations as parameters, it is possible to determine for each DER the active and reactive power injections required. This finally leads to a primary control mapping of the active and reactive powers as functions of the PCC voltage and system frequency.

4.3.2 Validation of the proposed hierarchical control

The proposed primary control mapping is validated by simulation and for the micro-grid detailed in Appendix, with the flexibilities in Table B.1. At first, we consider a full control on the DERs and we do not penalize the derating of the renewable production (i.e decreasing the output power below the maximum power point).

The results reported in this section are scaled to a base power of 100 kVA.

4.3.2.1 Case 1: Losses minimization

For the first case, the objective is to minimize the losses of the micro-grid while providing the required active and reactive support. Figures 4.19 and 4.20 present the mapping of the active and reactive power injections at the PCC as functions of the voltage and frequency which are almost linear. The extrema, when the voltage and/or the frequency reach their bounds, present a nonlinear part due to the active and reactive powers saturation in the capability diagram (see Figure 4.3). In this test case, the weighting factors on the active and the reactive power provision are equal. Therefore, for these parts of the mapping, the optimization routine reaches the best compromise by degrading the objective function to provide a solution.

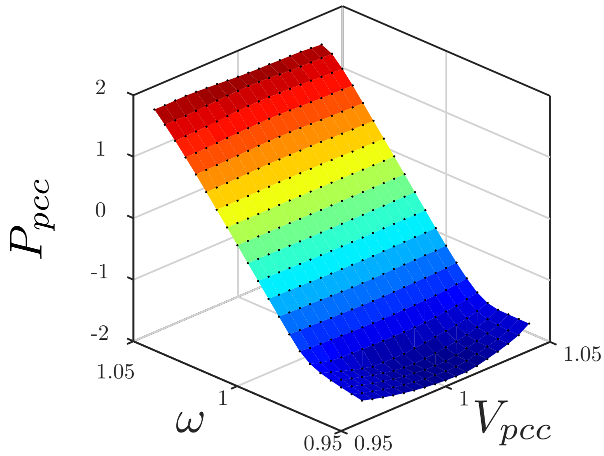

Figure 4.19: Resulting active power behavior at the point of common coupling - $P_{pcc} - \{\omega, V_{pcc}\}$ – Losses minimization

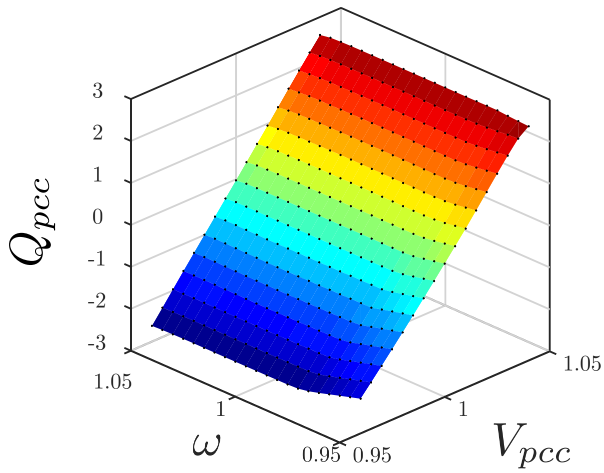

Figure 4.20: Resulting reactive power behavior at the point of common coupling - $Q_{pcc} - \{\omega, V_{pcc}\}$ – Losses minimization

It was expected that the levers close to the PCC would provide most of the effort. It can be observed that the primary mapping of node 2 presents for relatively small variations of the frequency or voltage a large modulation of the active and reactive power, while the other levers remain steady. For larger deviations, the DER at node 2 reaches its limitations, and therefore the effort is carried by the storage at node 6 and the conventional generator at node 15. It is worth noting that this generator cannot turn off and continues to provide at least 0.15 p.u of active power. Regarding the renewable production, it can be seen that the one on node 11 modulates its active power production while the second one connected on node 8 remains at its maximum power point (for sake of clarity, this mapping is not presented in Figure 4.21). Last, the reactive power of the DER on node 11 is limited for high frequency deviations and PCC voltage close to the unity because of the reduction of the active power and the constraints from the unitary diagram (cf. Appendix Figure B.2 Type 2).

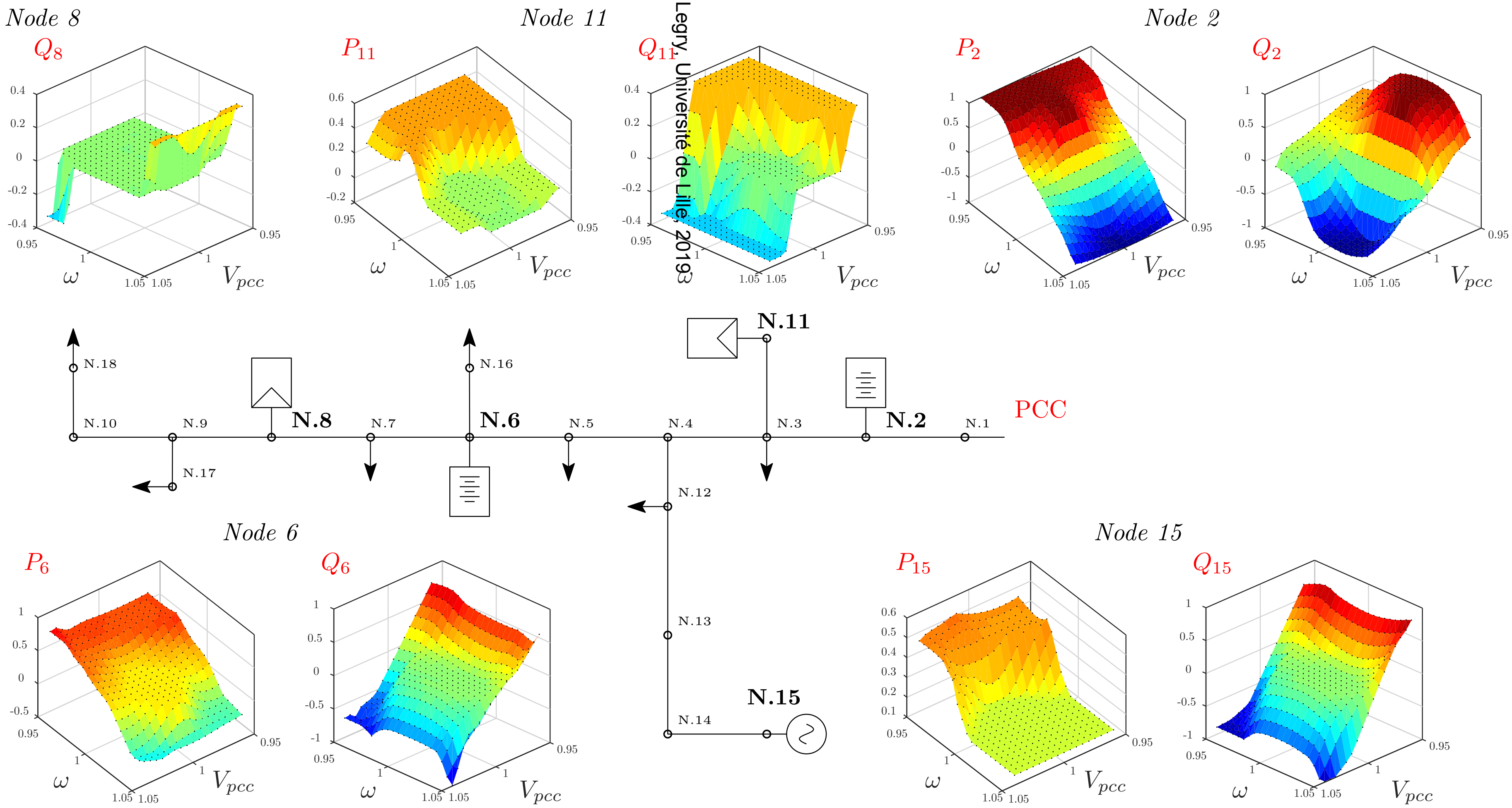

Figure 4.21: Micro-grid topology — Flexibilities and resulting primary mapping $P - \{\omega, V_{pcc}\}$ and $Q - \{\omega, V_{pcc}\}$ – Losses minimization

When the operating point is outside of the PCC capability diagram, it is interesting to focus on the impact of λ_p and λ_q on the active and reactive power provisions. λ_p and λ_q weigh respectively the priority to frequency or voltage support in the criterion defined in equation (4.13). Table 4.2 presents the active and reactive power injections at the PCC for different $\frac{\lambda_q}{\lambda_p}$ ratios and a specified operating point $P^*_{pcc} = 2.714$ p.u, $Q^*_{pcc} = 2.713$ p.u which lies outside the diagram ($\omega = 0.95$, $V_{pcc} = 0.96$). It can be seen that a high ratio (>10) generates a small reactive and a high active power error. The converse holds for a small ratio. A ratio of 1 minimizes the error on the apparent power.

Table 4.2: Influence of λ_p and λ_q on the PCC power injections – Losses minimization

λ_p	$\frac{\lambda_q}{\lambda_p}$	**Active power [p.u]**	**Reactive power [p.u]**	**Error on** P_{pcc} [%]	**Error on** Q_{pcc} [%]
1	1	1.630	2.226	39.93	17.95
1	2	1.537	2.438	43.37	10.15
1	100	1.413	2.707	47.94	0.24
1	0.5	1.760	1.920	35.18	29.24
1	0.01	2.535	-0.538	6.61	119.82

An important observation is that the form of the diagram and the weighting factors may lead to opposite reactions on the active or reactive power modulation (see Table 4.2, and $\lambda_p = 1$ and $\lambda_q = 0.01$). To highlight this point, Figure 4.22 presents the results of Table 4.2.

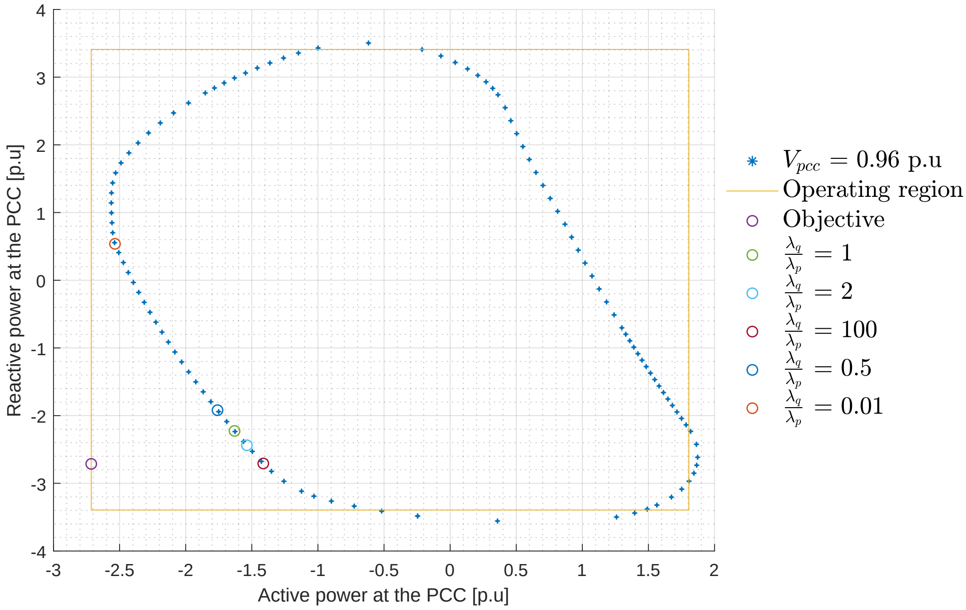

Figure 4.22: Resulting active power behavior at the point of common coupling - $P_{pcc} - \{\omega, V_{pcc}\}$ – Losses minimization

For references lying outside the capability diagram, the resulting operating point mainly depends on

- the weighting factors λ_p and λ_q,
- the gradient and the Hessian of the objective function,
- the form of the capability diagram.

4.3.2.2 Case 2: Effort distribution

Figures 4.23 and 4.24 display respectively the $P - \{\omega, V_{pcc}\}$ and $Q - \{\omega, V_{pcc}\}$ mappings obtained by the optimal tuning method presented in the previous section, which are almost linear. When the operating point is outside of the PCC capability diagram, the corresponding active power injection deviates significantly from the expected linear PCC droop control law, while the reactive power injection is barely affected. This situation occurs for under frequency and extreme PCC voltages (left part of Figure 4.3). Globally, both methods (effort distribution and line losses minimization) result in a similar behavior at the PCC.

Figure 4.25 also displays the nonlinear primary control mappings of the DERs, depending on V_{pcc} and ω. The diagrams display the active and reactive power injections scaled with a per unit PCC power. As a general rule, we can see that the control effort is shared proportionally among the levers. Each nonlinear control mapping can be interpreted consistently with the characteristics of the LV network and the operating constraints. A first remark is that the network is mainly resistive ($\frac{X}{R} < 1$). Hence, only a limited number of DERs exhibit a strong coupling between their active powers and the grid frequency. Specifically, an important share of the required active power at the PCC is allocated to node 2, and the corresponding diagrams are rather similar. This induces a strong constraint on the reactive power at node 2, which in turn drives to distribute the reactive power at the PCC among the other levers. As a result, the reactive power diagrams at nodes 6, 8, 11 and 15 exhibit a shape which is rather similar to that of the PCC reactive power diagram.

A number of saturation constraints explain the behavior at the extreme areas of some diagrams. At node 2, the reactive power is limited by the type 1 diagram constraints, which enlightens the behavior for under frequency. Conversely, the type 2 diagram at nodes 8 and 11 constrains the reactive power generation. The generator at node 15 cannot be shut down and the active power is nonzero even for frequencies over 1.04 p.u. Finally, the micro-grid voltage constraints limit the reactive power generation for the solar panels when the PCC voltage is close to 1 p.u. and extreme frequencies (note that the PV active power is not curtailed).

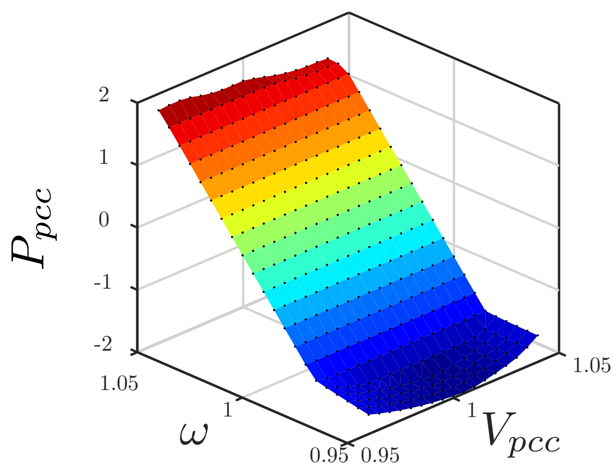

Figure 4.23: Resulting active power behavior at the point of common coupling - $P_{pcc} - \{\omega, V_{pcc}\}$ – Effort distribution.

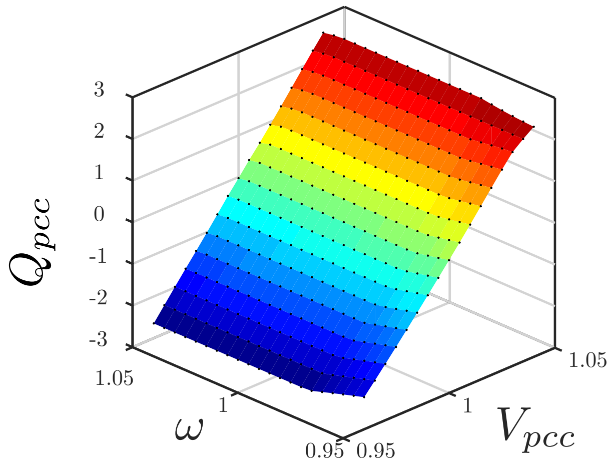

Figure 4.24: Resulting reactive power behavior at the point of common coupling - $Q_{pcc} - \{\omega, V_{pcc}\}$ – Effort distribution.

Once again, the influence of the weighting factors is reported in Table 4.3. The same conclusions as for the line losses minimization hold and λ_p and λ_q weigh respectively the priority to frequency or voltage support in the criterion defined in equation (4.13).

Table 4.3: Influence of λ_p and λ_q on the PCC power injections – Effort distribution.

λ_p	$\frac{\lambda_q}{\lambda_p}$	**Active power [p.u]**	**Reactive power [p.u]**	**Error on** P_{pcc} [%]	**Error on** Q_{pcc} [%]
1	1	1.612	2.406	40.60	11.31
1	2	1.558	2.526	42.59	6.89
1	100	1.489	2.675	45.14	1.3
1	0.5	1.688	2.232	37.81	17.72
1	0.01	2.142	1.059	21.07	60.97

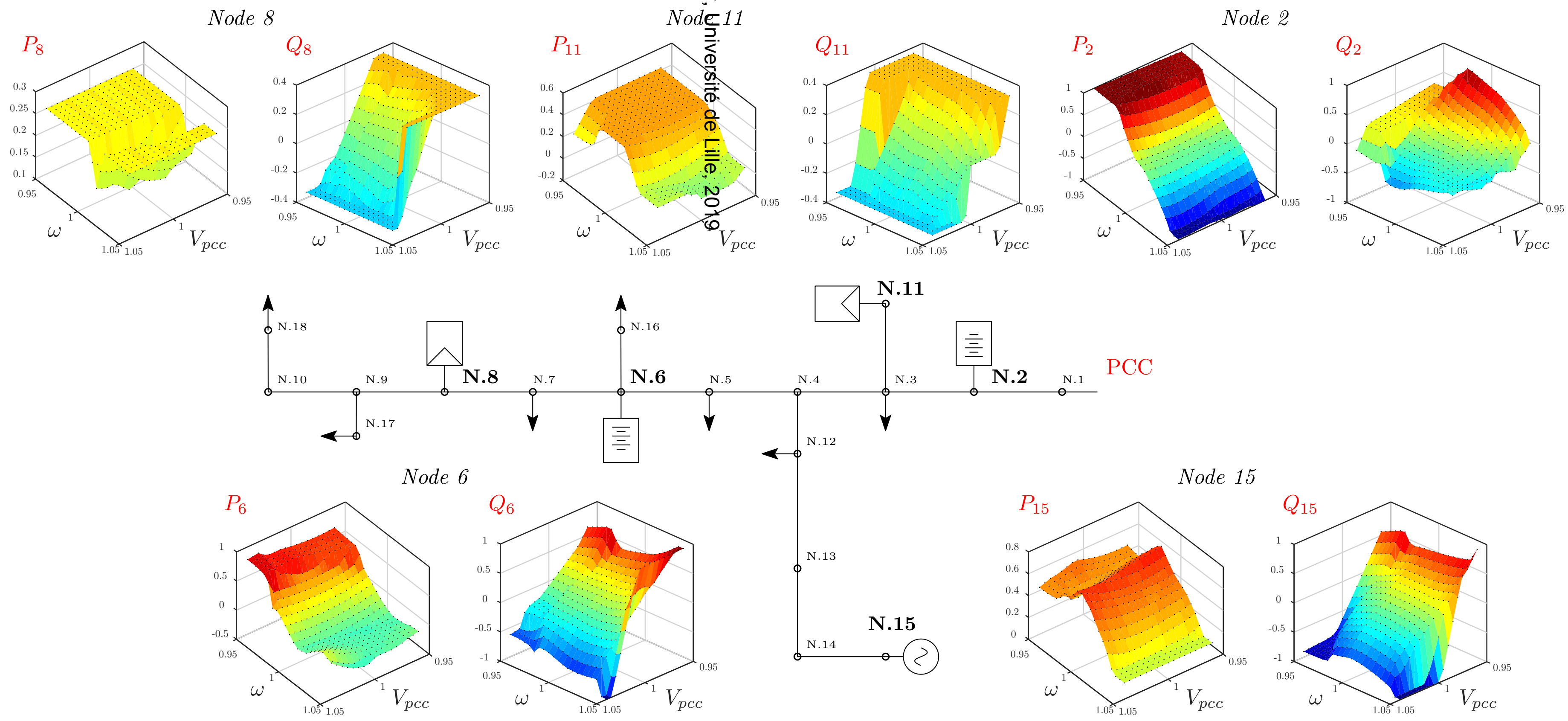

Figure 4.25: Micro-grid topology — Flexibilities and resulting primary mapping $P - \{\omega, V_{pcc}\}$ and $Q - \{\omega, V_{pcc}\}$ – Effort distribution.

4.3.2.3 Case 3: Inclusion of non-controlled DER

This last section briefly presents the case in which some of the DERs are not fully controlled, by lack of communication between the dispatch and the DER, or by inability of the inverter. To this end, the ESS at node 6 is assumed to be controlled by conventional droop mechanisms as recalled by the following equations:

$$\begin{cases} P_i^{gen} - P_i^{ref} = -k_i^p.(\omega - \omega^*) \\ Q_i^{gen} - Q_i^{ref} = -k_i^q.(V_i - V_i^*) \end{cases} \tag{4.14}$$

with

$$\begin{aligned} k_i^p &= \frac{\Delta P}{\underline{\omega} - \omega^n} \\ k_i^q &= \frac{\Delta Q}{\underline{V_i} - V_i} \end{aligned} \tag{4.15}$$

The operating point P_i^{ref}, and Q_i^{ref} are set to 0, the droop is thus assumed symmetrical. This case was not discussed in the previous section in which we determined the capability diagram of the micro-grid. Without loss of generalities, we consider in the latter the same flexibilities, and droop coefficients at the PCC as in the case 2.

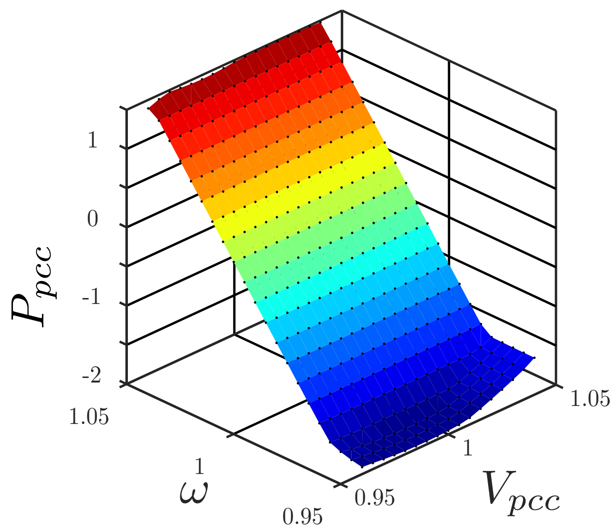

Figure 4.26: Resulting active power behavior at the point of common coupling - $P_{pcc} - \{\omega, V_{pcc}\}$ – Effort distribution with droop controlled inverter.

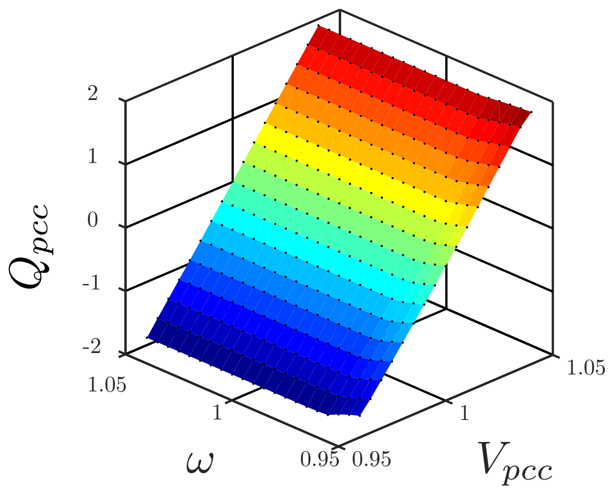

Figure 4.27: Resulting reactive power behavior at the point of common coupling - $Q_{pcc} - \{\omega, V_{pcc}\}$ – Effort distribution with droop controlled inverter.

Figures 4.26 and 4.27 present the resulting behavior of the PCC. On overall, the behavior remains linear, as expected for a droop-like PCC. The changes appear on the active and reactive power injections of the ESS at node 6. Figure 4.28 presents the voltage node 6 (left) and the resulting reactive power injection (right), according to the droop gains. It is interesting to point out that the voltage at node 6 resulting from the optimization routine is mostly dependent of the system frequency and of the active power modulation within the micro-grid. Last, the corresponding reactive power is modulated based on the local voltage which does not represent the PCC voltage. This effect can be explained by the low $\frac{X}{R}$ ratio and the inverse coupling, compared to conventional power system, for which a droop mechanism has been established. The active power injections are depicted in Figure 4.29 and obey the droop relation (4.14). It can be noted that, compared to Figure 4.25, the active power injection does significantly differ. The effort is reported proportionally to the other levers.

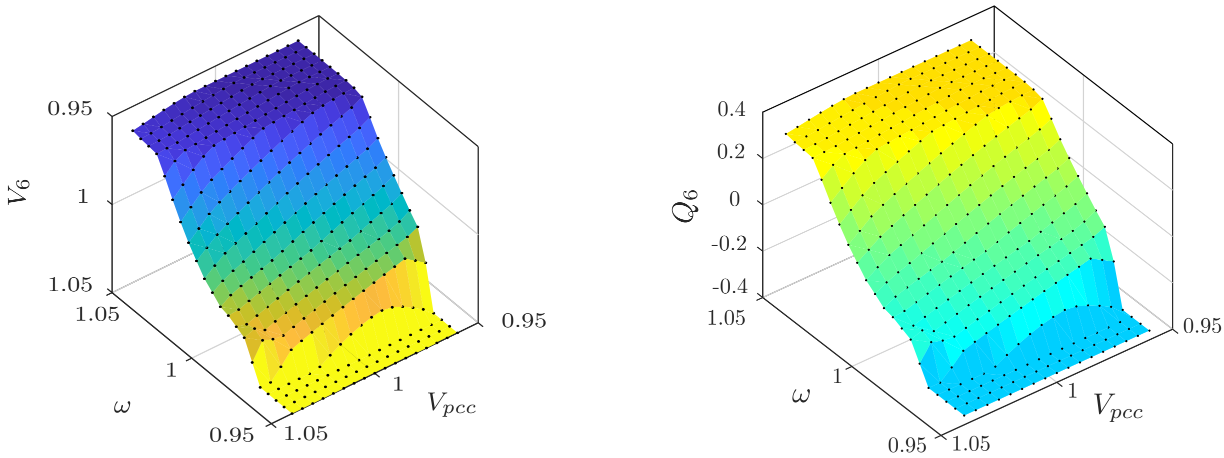

Figure 4.28: Voltage node (left) and reactive power injection (right) at node 6 as function of the system frequency and the PCC voltage

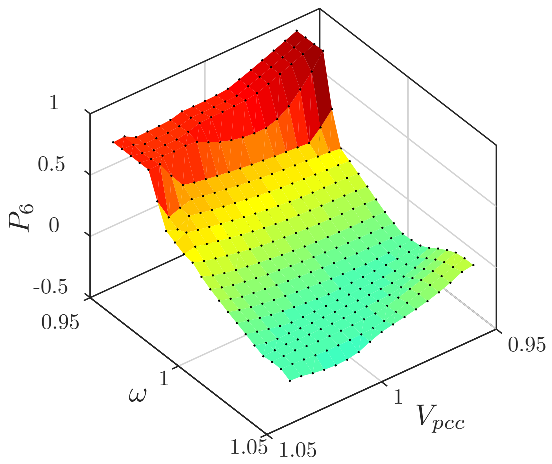

Figure 4.29: Active power primary mapping - $P_6 - \{\omega, V_{pcc}\}$ – Non-controlled DER.

4.4 Conclusion on PCC behavior of grid-interactive micro-grids

This fourth chapter was dedicated to the control and coordination of DERs in order to enforce a specific behavior at the PCC. The problematic has been highlighted by simulating the behavior of a realistic micro-grid for which the DERs are controlled by droop relations. Due to the non-linearity of the power flow equations, the linear relation of droop control cannot ensure a droop-like behavior at the PCC. With the estimation of the capability diagram of the micro-grid as detailed in Chapter 3, a methodology to determine the maximum droop relation at the PCC has been proposed.

Then, two improved coordination routines have been developed to control the micro-grid flexibilities. First, based on an extension of the MPC-based supervisor proposed in Chapter 2, a centralized solution has been introduced. The linear model of the micro-grid, and a prioritization of the ancillary services ensured a fast and suitable solution and the correction of the power and voltage references. Still, this control architecture relies on a complete and real-time communication between the central intelligence and the DERs. Eventually, to alleviate the communication infrastructure cost, a hierarchical architecture has been proposed. This solution keeps the distributed nature of the primary control as in traditional power systems, and only requires the real time communication of the PCC voltage measurements, and of the primary control mapping on the time basis of a few minutes to update the local control of DERs.

In both architectures, the heterogeneity of DERs, as well as network constraints and economical performances are ensured through the formulation of the objective function. It is worth noting that, as for every optimization problem, and more specifically for the hierarchical solution, the choice of weighting coefficients are particularly important to obtain a proper behavior of the system.

General conclusion

The continuous increase in renewable penetration at different voltage levels makes the power system more complex to control, but it can also provide solutions with the design of suitable distributed controllers. For few years now load and DER control techniques were developed to provide some of the ancillary services that make the power system operations stable. At the same time, load aggregation, VPP and micro-grid concepts tend to think power system structures anew with the emergence of 'power cells' as a sub-part of the power system. The stiffness of such power systems is also challenged, and decreases, leading to even more complex system to control. This thesis is directly related to this fundamental transformation and proposed a novel methodology to involve grid-interactive micro-grid in the ancillary services balancing mechanism.

When islanded, the micro-grid strengthens the reliability of the power system and decreases the loss of load. Yet, controlling a islanded micro-grid is a specific challenge that requires appropriate supervisor and controllers. The first part of this report has been dedicated to the supervision of micro-grids with the Model Predictive Control technique embedding a linear model of the network and the equipment. Conventional supervisor architectures consider three layers that are based on the conventional ancillary services structure. These layers have different objectives and time scales, therefore a particular attention has been given to the interface between the economical layer (tertiary layer), and the real-time management of the system (secondary layer). The use of a multi-layers MPC-based supervisor allows to combine both objectives with dedicated interface management strategies and shows good results.

Then, this thesis has addressed the challenge of providing ancillary services and particularly primary responses from a grid-interactive micro-grid in the context of weak power systems in which the network characteristics may largely vary. To avoid the saturation of the assets and possible instabilities (voltage collapse, etc.), the system operators must be able to estimate the active and reactive power flow limits at the PCC of the micro-grids. Fortunately, recent publications focused on algorithms and optimization models to determine these capabilities. Still, the proposed methodologies assume a stiff interconnection and the limitations of this hypothesis for variable voltage at the PCC has been exposed for simple realistic micro-grid. Hence, an extension of conventional methods to the nonlinear optimal power flow algorithm that determines the capability diagram of a micro-grid for variable voltages at the PCC has been proposed. This new algorithm results in a 3 dimensional graph that serves as a decision tool to design the droop-like behavior at the PCC.

Finally, two PCC management strategies have been proposed to enforce a specified droop-like behavior at the PCC. First, based on an extension of the proposed linear MPC-based supervisor, a central optimizer computes and coordinates the heterogeneous resources to enforce a droop-like behavior at the point of common coupling. This controller allows the micro-grid supervisor to balance the economical objectives with the provision of primary response. In addition, the active and reactive power at the PCC are completely decoupled, even if some power imbalance may occur if the objective function does not prioritize enough the ancillary services provision.

Secondly, considering the distributed philosophy of the primary control, another completely different strategy has been proposed, which determines new local control laws for the DERs based on a centralized optimization. The resulting nonlinear primary local control laws may be designed according to system-wide objectives such as losses minimization, voltage deviations or effort averaging.

Both strategies display good results and interesting features. In one hand, the MPC-based supervisor provides an optimal solution which considers the full potential of each flexibility and respects the network constraints. On the other hand, the design of local control laws preserves the three level hierarchical structure of a conventional micro-grid architecture, and only requires a limited communication infrastructure. Finally, the two proposed methods are scalable, and fast enough to be implemented in real-time.

Perspectives

The direct perspectives of this work are the following.

First, one of the main assumption is to consider only deterministic forecasts. Nowadays, the challenge is to include the stochastic nature of the DERs production and loads into an optimization algorithm. Therefore, the interface between economical optimization and real-time controllers is even more challenging considering realistic load and production forecasts. Yet, some works in the control literature proposed to derive optimal weightings for real time controller based on the Lagrangian multipliers from the economical optimization. The idea behind these publications lies in the use of the Lagrangian multipliers which result from the upper layer optimization solution (the EMS for micro-grids - tertiary control), in order to obtain the weighting factors of the lower layer (the PMS - secondary control). This would ensure that any real time adjustments would be the 'less costly' according to the design of the upper layer, contrary to the usual. Still, no application of such multiple layer Lagrangian-based supervisors can be found for power systems, and more specifically for micro-grid supervisors. Furthermore, even for power sharing strategies and the droop control, the inadequacy to correct optimally the power balance mismatch has been highlighted in [94]. The interface between multi-layer architecture remains one of the main challenges in controlling islanded micro-grids.

The last part of this thesis addressed and proposed novel management strategies to enforce a specific behavior at the PCC. Regarding the MPC-based solution which has been proposed, one of the assumptions is to ignore any model of the external network, and of the corresponding voltage and frequency dynamics. In the literature there exist state estimators that could be used to estimate the equivalent voltage and frequency droop, and possibly, the inertia of the system to consider faster dynamics. One of the suitable algorithms would be the well-known Kalman filter, that would adjust and correct in real time the embedded model parameters of the external network. Another solution would consist, based on a linear model of the micro-grid, to derive a linear transformation for each of the micro-grid flexibilities, that would define a new 3D frame ($P - V_{pcc} - \omega$ and $Q - V_{pcc} - \omega$) as we achieved for the nonlinear optimization problem. Such an idea has been proposed for a voltage source inverter equipped with droop control, in order to take into account the coupling of the output powers due to the transmission line [95]. This extension would generalize the linear transformation in order to be able to embed the interaction among DERs and between each DER and the PCC behavior.

The novel proposed local control laws assume that there is only a single point of common coupling to a single external network. Further works should focus on meshed system for which the micro-grid systems may exhibit multiple points of interconnection. Although the application of the MPC-based supervisor may be easily extended to such systems, the design of the distributed controllers is more challenging and will probably require to consider different aspects such as the capabilities of the micro-grid with respect to each PCC or the interactions between each PCC through the external system.

Nowadays, active power imbalance and voltage stability in the transmission system are managed in real time by TSOs through the different reserve market which is mainly provided by large conventional generators. For a distribution system, the voltage profile of the feeders are mainly managed in real time by transformers with on-load tap changer and capacitor banks. A large part of the literature of the recent years focused on the technical feasibility of integrating the DERs in a distribution system to control the voltage profile. Yet, the increasing number of DERs in the MV-network challenges even more the interface between the DSO and TSO and the commonplace practices, based on static considerations are not relevant anymore. This thesis opens this topic wide, that is on coordinating and optimizing the real-time management of the interface between TSO and DSO, or between different sub-systems as imagined within the framework of the ELECTRA project [96]. This new kind coordination also rises a challenge about policies and regulations. Beyond the ideas developed in this thesis and considering a power system consisting of several cells across multiple voltage ranges, with different capabilities and flexibilities, reserves and ancillary services, the market needs to be refined to evolve towards a more distributed and horizontal version.

Bibliography

[1] R. Lasseter, "MicroGrids," in *2002 IEEE Power Engineering Society Winter Meeting. Conference Proceedings (Cat. No.02CH37309)*, IEEE, Aug. 2002.

[2] A. Dimeas and N. Hatziargyriou, "A multiagent system for microgrids," in *IEEE Power Engineering Society General Meeting, 2004.*, IEEE, June 2004.

[3] N. Hatziargyriou, H. Asano, R. Iravani, and C. Marnay, "Microgrids," *IEEE Power and Energy Magazine*, vol. 5, pp. 78–94, July 2007.

[4] Commission de Régulation de l'Energie, "Services système et mécanisme d'ajustement." `https://www.cre.fr/Electricite/Reseaux-d-electricite/Services-systeme-et-mecanisme-d-ajustement`.

[5] Transmission and Distribution Committee of the IEEE Power Engineering Society, "IEEE guide for planning dc links terminating at ac locations having low short-circuit capacities," IEEE, 1997.

[6] North American Electric Reliability Corporation, "Integrating inverter-based resources into low short circuit strength systems," tech. rep., NERC, 2017.

[7] E. L. de Aguiar, R. Cardoso, C. M. d. O. Stein, J. P. da Costa, and E. G. Carati, "Distributed renewable power sources in weak grids — analysis and control," in *Renewable Energy - Utilisation and System Integration*, InTech, May 2016.

[8] S. Repo, H. Laaksonen, P. Jarventausta, O. Huhtala, and M. Mickelsson, "A case study of a voltage rise problem due to a large amount of distributed generation on a weak distribution network," in *2003 IEEE Bologna PowerTech Conference Proceedings,*, IEEE, June 2003.

[9] T. Sarkar and A. K. Dan, "Effect of X/R Ratio on low voltage distribution system connected with constant," in *2016 2nd International Conference on Control, Instrumentation, Energy & Communication (CIEC)*, IEEE, Sept. 2016.

[10] S. Grunau and F. W. Fuchs, "Effect of wind-energy power injection into weak grids," in *European Wind Energy Conference and Exhibition 2012, EWEC 2012*, Jan. 2012.

[11] A. Bidram and A. Davoudi, "Hierarchical structure of microgrids control system," *IEEE Transactions on Smart Grid*, vol. 3, pp. 1963–1976, Dec. 2012.

[12] O. Palizban, K. Kauhaniemi, and J. M. Guerrero, "Microgrids in active network management—part i: hierarchical control, energy storage, virtual power plants, and

market participation," *Renewable and Sustainable Energy Reviews*, vol. 36, pp. 428–439, Aug. 2014.

[13] L. Meng, E. R. Sanseverino, A. Luna, T. Dragicevic, J. C. Vasquez, and J. M. Guerrero, "Microgrid supervisory controllers and energy management systems: A literature review," *Renewable and Sustainable Energy Reviews*, vol. 60, pp. 1263–1273, July 2016.

[14] H. Han, X. Hou, J. Yang, J. Wu, M. Su, and J. M. Guerrero, "Review of power sharing control strategies for islanding operation of AC microgrids," *IEEE Transactions on Smart Grid*, vol. 7, pp. 200–215, Jan. 2016.

[15] R. R. Negenborn and J. M. Maestre, "Distributed Model Predictive Control: an overview and roadmap of future research opportunities," *IEEE Control Systems*, vol. 34, pp. 87–97, Aug. 2014.

[16] B. Robyns, A. Davigny, and C. Saudemont, "Methodologies for supervision of hybrid energy sources based on storage systems – a survey," *Mathematics and Computers in Simulation*, vol. 91, pp. 52–71, may 2013.

[17] H. Bevrani, B. Francois, and T. Ise, *Microgrid Dynamics and Control*. John Wiley & Sons, Inc., 2017.

[18] Y. Katsigiannis, P. Georgilakis, and E. Karapidakis, "Multiobjective genetic algorithm solution to the optimum economic and environmental performance problem of small autonomous hybrid power systems with renewables," *IET Renewable Power Generation*, vol. 4, p. 404, Sept. 2010.

[19] A. Baziar and A. Kavousi-Fard, "Considering uncertainty in the optimal energy management of renewable micro-grids including storage devices," *Renewable Energy*, vol. 59, pp. 158–166, Nov. 2013.

[20] J.-Y. Dieulot, F. Colas, L. Chalal, and G. Dauphin-Tanguy, "Economic supervisory predictive control of a hybrid power generation plant," *Electric Power Systems Research*, vol. 127, pp. 221–229, Oct. 2015.

[21] T. G. Hovgaard, K. Edlund, and J. B. Jorgensen, "The potential of economic MPC for power management," in *49th IEEE Conference on Decision and Control (CDC)*, IEEE, Dec. 2010.

[22] A. Parisio, E. Rikos, and L. Glielmo, "Stochastic model predictive control for economic/environmental operation management of microgrids: An experimental case study," *Journal of Process Control*, vol. 43, pp. 24–37, July 2016.

[23] F. Dörfler, J. W. Simpson-Porco, and F. Bullo, "Breaking the hierarchy: distributed control and economic optimality in microgrids," *IEEE Transactions on Control of Network Systems*, vol. 3, pp. 241–253, Sept. 2016.

[24] M. Ma, H. Chen, X. Liu, and F. Allgöwer, "Distributed model predictive load frequency control of multi-area interconnected power system," *International Journal of Electrical Power & Energy Systems*, vol. 62, pp. 289–298, Nov. 2014.

[25] A. Ouammi, H. Dagdougui, L. Dessaint, and R. Sacile, "Coordinated model predictive-based power flows control in a cooperative network of smart microgrids," *IEEE Transactions on Smart Grid*, vol. 6, pp. 2233–2244, Sept. 2015.

[26] K. Baker, J. Guo, G. Hug, and X. Li, "Distributed MPC for efficient coordination of storage and renewable energy sources across control areas," *IEEE Transactions on Smart Grid*, vol. 7, pp. 992–1001, Mar. 2016.

[27] R. Negenborn, A. Beccuti, T. Demiray, S. Leirens, G. Damm, B. D. Schutter, and M. Morari, "Supervisory hybrid model predictive control for voltage stability of power networks," in *2007 American Control Conference*, IEEE, July 2007.

[28] Q. Li, F. Chen, M. Chen, J. M. Guerrero, and D. Abbott, "Agent-based decentralized control method for islanded microgrids," *IEEE Transactions on Smart Grid*, pp. 637–649, Mar. 2015.

[29] FENIX, "Flexible electricity networks to integrate the expected energy evolution," tech. rep., 2009.

[30] A. Delavari and I. Kamwa, "Demand-side contribution to power system frequency regulation : a critical review on decentralized strategies," *International Journal of Emerging Electric Power Systems*, vol. 18, Jan. 2017.

[31] A. Molina-Garcia, F. Bouffard, and D. S. Kirschen, "Decentralized demand-side contribution to primary frequency control," *IEEE Transactions on Power Systems*, vol. 26, pp. 411–419, Feb. 2011.

[32] M. Cheng, J. Wu, S. J. Galsworthy, N. Gargov, W. H. Hung, and Y. Zhou, "Performance of industrial melting pots in the provision of dynamic frequency response in the great britain power system," *Applied Energy*, vol. 201, pp. 245–256, Sept. 2017.

[33] X. Wu, J. He, Y. Xu, J. Lu, N. Lu, and X. Wang, "Hierarchical control of residential HVAC units for primary frequency regulation," *IEEE Transactions on Smart Grid*, vol. 9, pp. 3844–3856, July 2018.

[34] Z. Li, W. Wu, and B. Zhang, "Coordinated state-estimation method for air-conditioning loads to provide primary frequency regulation service," *IET Generation, Transmission & Distribution*, vol. 11, pp. 3381–3388, Sept. 2017.

[35] C. Ziras, E. Vrettos, and G. Andersson, "Primary frequency control with refrigerators under startup dynamics and lockout constraints," in *2015 IEEE Power & Energy Society General Meeting*, IEEE, July 2015.

[36] I. Pavić, T. Capuder, and I. Kuzle, "Value of flexible electric vehicles in providing spinning reserve services," *Applied Energy*, vol. 157, pp. 60–74, Nov. 2015.

[37] K. Knezovic, S. Martinenas, P. B. Andersen, A. Zecchino, and M. Marinelli, "Enhancing the role of electric vehicles in the power grid: field validation of multiple ancillary services," *IEEE Transactions on Transportation Electrification*, vol. 3, pp. 201–209, Mar. 2017.

[38] S. Izadkhast, P. Garcia-Gonzalez, P. Frias, L. Ramirez-Elizondo, and P. Bauer, “An aggregate model of plug-in electric vehicles including distribution network characteristics for primary frequency control,” *IEEE Transactions on Power Systems*, vol. 31, pp. 2987–2998, July 2016.

[39] C. Kieny, B. Berseneff, N. Hadjsaid, Y. Besanger, and J. Maire, “On the concept and the interest of virtual power plant: Some results from the european project fenix,” in *2009 IEEE Power & Energy Society General Meeting*, IEEE, July 2009.

[40] E. Abbasi, “Coordinated primary control reserve by flexible demand and wind power through ancillary service-centered virtual power plant,” *International Transactions on Electrical Energy Systems*, vol. 27, p. e2452, Oct. 2017.

[41] L. Srinivasan, U. Markovic, M. G. Vaya, and G. Hug, “Provision of frequency control by a BESS in combination with flexible units,” in *2018 IEEE International Energy Conference (ENERGYCON)*, IEEE, June 2018.

[42] T. Zhang and H. B. Gooi, “Hierarchical MPC-based energy management and frequency regulation participation of a virtual power plant,” in *IEEE PES Innovative Smart Grid Technologies, Europe*, IEEE, Oct. 2014.

[43] M. Junhua, H. S. V. S. Kumar, and D. Srinivasan, “Congestion management in smart grids using virtual power plants as flexible resources,” in *2017 IEEE Innovative Smart Grid Technologies - Asia (ISGT-Asia)*, IEEE, Dec. 2017.

[44] J. Kim, E. Muljadi, V. Gevorgian, M. Mohanpurkar, Y. Luo, R. Hovsapian, and V. Koritarov, “Capability-coordinated frequency control scheme of a virtual power plant with renewable energy sources,” *IET Generation, Transmission & Distribution*, vol. 13, pp. 3642–3648, Aug. 2019.

[45] A. Dimeas and N. Hatziargyriou, “Operation of a multiagent system for microgrid control,” *IEEE Transactions on Power Systems*, vol. 20, pp. 1447–1455, Aug. 2005.

[46] M. Bayat, K. Sheshyekani, M. Hamzeh, and A. Rezazadeh, “Coordination of distributed energy resources and demand response for voltage and frequency support of MV microgrids,” *IEEE Transactions on Power Systems*, vol. 31, pp. 1506–1516, Mar. 2016.

[47] A. Ghafouri, J. Milimonfared, and G. B. Gharehpetian, “Coordinated control of distributed energy resources and conventional power plants for frequency control of power systems,” *IEEE Transactions on Smart Grid*, vol. 6, pp. 104–114, Jan. 2015.

[48] L. F. Costa, G. D. Carne, G. Buticchi, and M. Liserre, “The smart transformer: a solid-state transformer tailored to provide ancillary services to the distribution grid,” *IEEE Power Electronics Magazine*, vol. 4, pp. 56–67, June 2017.

[49] G. D. Carne, G. Buticchi, M. Liserre, and C. Vournas, “Real-time primary frequency regulation using load power control by smart transformers,” *IEEE Transactions on Smart Grid*, vol. 10, pp. 5630–5639, Sept. 2019.

[50] S. Qin and T. A. Badgwell, “A survey of industrial model predictive control technology,” *Control Engineering Practice*, vol. 11, pp. 733–764, July 2003.

[51] J. Richalet and D. O'Donovan, *Predictive Functional Control.* Advances in Industrial Control, London: Springer London, June 2009.

[52] E. F. Camacho and C. Bordons, *Model Predictive Control.* No. 9781852336943 in Advanced Textbooks in Control and Signal Processing, London: Springer London, 2007.

[53] B. Kouvaritakis and M. Cannon, *Model Predictive Control.* Advanced Textbooks in Control and Signal Processing, Cham: Springer International Publishing, 2016.

[54] S. M. Zanoli and C. Pepe, "The importance of cooperation and consistency in two-layer Model Predictive Control," *Proceedings of the 2016 17th International Carpathian Control Conference, ICCC 2016*, pp. 825–830, June 2016.

[55] B. Picasso, D. De Vito, R. Scattolini, and P. Colaneri, "An MPC approach to the design of two-layer hierarchical control systems," *Automatica*, vol. 46, pp. 823–831, May 2010.

[56] S. Raimondi Cominesi, M. Farina, L. Giulioni, B. Picasso, and R. Scattolini, "Two-layer predictive control of a micro-grid including stochastic energy sources," *Proceedings of the American Control Conference*, vol. 2015-July, pp. 918–923, July 2015.

[57] P. Velarde, L. Valverde, J. M. Maestre, C. Ocampo-Martinez, and C. Bordons, "On the comparison of stochastic model predictive control strategies applied to a hydrogen-based microgrid," *Journal of Power Sources*, vol. 343, pp. 161–173, Mar. 2017.

[58] P. Tatjewski, "Advanced control and on-line process optimization in multilayer structures," *IFAC Proceedings Volumes (IFAC-PapersOnline)*, vol. 11, pp. 13–26, Apr. 2007.

[59] L. Würth, R. Hannemann, and W. Marquardt, "A two-layer architecture for economically optimal process control and operation," *Journal of Process Control*, vol. 21, pp. 311–321, Mar. 2011.

[60] A. Abreu, R. Bourdais, and H. Guéguen, "Inter-layer interactions in hierarchical MPC for building energy management systems," *IFAC-PapersOnLine*, vol. 50, pp. 12027–12032, July 2017.

[61] M. N. Marwali and A. Keyhani, "Control of distributed generation systems - Part I: Voltages and currents control," *IEEE Transactions on Power Electronics*, vol. 19, pp. 1541–1550, Nov. 2004.

[62] M. Gutiérrez, T. Ixta, P. Zuniga, E. Barocio, and F. Uribe, "Droop controller comparison for AC microgrids," *2016 IEEE International Autumn Meeting on Power, Electronics and Computing, ROPEC 2016*, Nov. 2017.

[63] M. Chen and G. Rincon-Mora, "Accurate electrical battery model capable of predicting runtime and i–v performance," *IEEE Transactions on Energy Conversion*, vol. 21, pp. 504–511, June 2006.

[64] L. Gao, S. Liu, and R. Dougal, "Dynamic lithium-ion battery model for system simulation," *IEEE Transactions on Components and Packaging Technologies*, vol. 25, pp. 495–505, Sept. 2002.

[65] W. van Ackooij, I. D. Lopez, A. Frangioni, F. Lacalandra, and M. Tahanan, "Large-scale unit commitment under uncertainty: an updated literature survey," *Annals of Operations Research*, vol. 271, pp. 11–85, Sept. 2018.

[66] B. Marti, *Emissions of power delivery systems.* PhD thesis, Swiss Federal Institute of Technology (ETH) Zurich, 2005.

[67] S. Soliman and A. Mantawy, *Modern optimization techniques with applications in electric power systems.* Springer New York, Aug. 2012.

[68] C. Deckmyn, T. L. Vandoorn, J. van de Vyver, J. Desmet, and L. Vandevelde, "A microgrid multilayer control concept for optimal power scheduling and voltage control," *IEEE Transactions on Smart Grid*, vol. 9, pp. 4458–4467, Sept. 2018.

[69] T. Bocklisch, "Hybrid energy storage approach for renewable energy applications," *Journal of Energy Storage*, vol. 8, pp. 311–319, Nov. 2016.

[70] K. Strunz, E. Abbasi, C. Abbey, C. Andrieu, U. Annakkage, S. Barsali, R. C. Campbell, R. Fletcher, F. Gao, T. Gaunt, A. Gole, N. Hatziargyriou, R. Iravani, G. Joos, H. Konishi, M. Kuschke, E. Lakervi, C.-C. Liu, J. Mahseredjian, F. Mosallat, D. Muthumuni, A. Orths, S. Papathanassiou, K. Rudion, Z. Styczynski, and S. C. Verm, "Benchmark systems for network integration of renewable energy resources," Tech. Rep. 273, 2014.

[71] J. Lofberg, "YALMIP : a toolbox for modeling and optimization in MATLAB," *2004 IEEE International Conference on Robotics and Automation*, pp. 284–289, Sept. 2004.

[72] P. Kundur, *Power system stability and control.* New York: McGraw-Hill, 1994.

[73] T. Lund, P. Sørensen, and J. Eek, "Reactive power capability of a wind turbine with doubly fed induction generator," *Wind Energy*, vol. 10, pp. 379–394, July 2007.

[74] European Commission, "Network code on requirements for grid connection of generators," no. July 2009, 2016.

[75] Enedis, "Modalités du contrôle de performances des installations de production raccordées en haute tension (HTA) au réseau public de distribution géré par ERDF," 2012.

[76] S. Kundu, K. Kalsi, and S. Backhaus, "Approximating flexibility in distributed energy resources: a geometric approach," in *2018 Power Systems Computation Conference (PSCC)*, IEEE, June 2018.

[77] L. Zhao, W. Zhang, H. Hao, and K. Kalsi, "A geometric approach to aggregate flexibility modeling of thermostatically controlled loads," *IEEE Transactions on Power Systems*, vol. 32, pp. 4721–4731, Nov. 2017.

[78] J. Silva, J. Sumaili, R. J. Bessa, L. Seca, M. A. Matos, V. Miranda, M. Caujolle, B. Goncer, and M. Sebastian-Viana, "Estimating the active and reactive power flexibility area at the TSO-DSO interface," *IEEE Transactions on Power Systems*, vol. 33, pp. 4741–4750, Sept. 2018.

[79] D. A. Contreras and K. Rudion, "Improved assessment of the flexibility range of distribution grids using linear optimization," *20th Power Systems Computation Conference, PSCC 2018*, June 2018.

[80] J. Silva, J. Sumaili, R. J. Bessa, L. Seca, M. Matos, and V. Miranda, "The challenges of estimating the impact of distributed energy resources flexibility on the TSO/DSO boundary node operating points," *Computers and Operations Research*, vol. 96, pp. 294–304, Sept. 2018.

[81] M. Heleno, R. Soares, J. Sumaili, R. J. Bessa, L. Seca, and M. A. Matos, "Estimation of the flexibility range in the transmission-distribution boundary," *2015 IEEE Eindhoven PowerTech Conference Proceedings*, Sept. 2015.

[82] Z. Yang, H. Zhong, Q. Xia, A. Bose, and C. Kang, "Optimal power flow based on successive linear approximation of power flow equations," *IET Generation, Transmission & Distribution*, vol. 10, pp. 3654–3662, Oct. 2016.

[83] G. B. Dantzig, "1. The Linear Programming Concept," in *Linear Programming and Extensions*, pp. 1–11, Princeton: Princeton University Press, Jan. 1963.

[84] J. Nocedal and S. J. Wright, *Numerical optimization*, vol. 46 of *Springer Series in Operations Research and Financial Engineering*. Boston, MA: Springer New York, oct 2006.

[85] G. Allaire, *Numerical analysis and optimization*. Oxford university press, 2007.

[86] S. Low, "Convex relaxation of optimal power flow—Part I: formulations and equivalence," *IEEE Transactions on Control of Network Systems*, vol. 1, pp. 15–27, Mar. 2014.

[87] L. Qi, K. Teo, and X. Yang, *Optimization and control with applications*, vol. 96 of *Applied Optimization*. Boston, MA: Springer US, 2005.

[88] F. Mumtaz, M. H. Syed, M. A. Hosani, and H. H. Zeineldin, "A novel approach to solve power flow for islanded microgrids using modified newton raphson with droop control of DG," *IEEE Transactions on Sustainable Energy*, vol. 7, pp. 493–503, Apr. 2016.

[89] J. M. Guerrero, L. G. de Vicuna, J. Matas, M. Castilla, and J. Miret, "Output impedance design of parallel-connected UPS inverters with wireless load-sharing control," *IEEE Transactions on Industrial Electronics*, vol. 52, pp. 1126–1135, Aug. 2005.

[90] J. M. Guerrero, J. Matas, L. G. de Vicuna, M. Castilla, and J. Miret, "Decentralized control for parallel operation of distributed generation inverters using resistive output impedance," *IEEE Transactions on Industrial Electronics*, vol. 54, pp. 994–1004, Apr. 2007.

[91] Y. Li and Y. W. Li, "Power management of inverter interfaced autonomous microgrid based on virtual frequency-voltage frame," *IEEE Transactions on Smart Grid*, vol. 2, pp. 30–40, Mar. 2011.

[92] K. D. Brabandere, B. Bolsens, J. V. den Keybus, A. Woyte, J. Driesen, and R. Belmans, "A voltage and frequency droop control method for parallel inverters," *IEEE Transactions on Power Electronics*, vol. 22, pp. 1107–1115, July 2007.

[93] H. Bevrani, *Robust power system frequency control.* Springer International Publishing, 2014.

[94] P. P. Vergara, J. C. Lopez, L. C. P. da Silva, and M. J. Rider, "Economic impact of the active power droop gain in droop-based islanded microgrids," in *2019 IEEE Milan PowerTech Conference Proceedings*, IEEE, Aug. 2019.

[95] Y. Li and Y. W. Li, "Decoupled power control for an inverter based low voltage microgrid in autonomous operation," in *IEEE 6th International Power Electronics and Motion Control Conference*, IEEE, May 2009.

[96] A. Z. Morch, S. H. Jakobsen, K. Visscher, and M. Marinelli, "Future control architecture and emerging observability needs," in *2015 IEEE 5th International Conference on Power Engineering, Energy and Electrical Drives (POWERENG)*, IEEE, May 2015.

Appendices

Appendix A

Analytical formulation of the Jacobian Matrix

The following appendix will develop the analytical calculation of the Jacobian matrix. We first recall the BIM and Equation 2.19

$$\begin{cases} P_i\left(\delta_1, .., \delta_n, V_1, .., V_n, \omega\right) = V_i \sum\limits_{j \in \mathcal{N}} V_j \left|Y_{ij}\right| \cos(\delta_i - \delta_j - \theta_{ij}) \\ Q_i\left(\delta_1, .., \delta_n, V_1, .., V_n, \omega\right) = V_i \sum\limits_{j \in \mathcal{N}} V_j \left|Y_{ij}\right| \sin(\delta_i - \delta_j - \theta_{ij}) \end{cases}$$

and after linearization, it comes:

$$\begin{bmatrix} P_1^{ref} - P_1\left(\delta_1^0, .., \delta_1^0, V_1^0, .., V_1^0, \omega^0\right) \\ \vdots \\ P_i^{ref} - P_i\left(\delta_1^0, .., \delta_1^0, V_1^0, .., V_1^0, \omega^0\right) \\ Q_1^{ref} - Q_1\left(\delta_1^0, .., \delta_1^0, V_1^0, .., V_1^0, \omega^0\right) \\ \vdots \\ Q_i^{ref} - Q_i\left(\delta_1^0, .., \delta_1^0, V_1^0, .., V_1^0, \omega^0\right) \end{bmatrix} = \mathbf{J} \begin{bmatrix} \Delta\delta_1 \\ \vdots \\ \Delta\delta_i \\ \Delta V_1 \\ \vdots \\ \Delta V_i \\ \Delta\omega \end{bmatrix} \tag{A.1}$$

with the Jacobian:

$$\mathbf{J_{PV}} = \begin{bmatrix} \frac{\partial P_1}{dV_1}\Big|_{\mathbf{X^0}} & \cdots & \frac{\partial P_1}{dV_i}\Big|_{\mathbf{X^0}} \\ \vdots & & \vdots \\ \frac{\partial P_i}{dV_1}\Big|_{\mathbf{X^0}} & \cdots & \frac{\partial P_i}{dV_i}\Big|_{\mathbf{X^0}} \end{bmatrix} \quad \mathbf{J_{P\delta}} = \begin{bmatrix} \frac{\partial P_1}{d\delta_1}\Big|_{\mathbf{X^0}} & \cdots & \frac{\partial P_1}{d\delta_i}\Big|_{\mathbf{X^0}} \\ \vdots & & \vdots \\ \frac{\partial P_i}{d\delta_1}\Big|_{\mathbf{X^0}} & \cdots & \frac{\partial P_i}{d\delta_i}\Big|_{\mathbf{X^0}} \end{bmatrix} \quad \mathbf{J_{P\omega}} = \begin{bmatrix} \frac{\partial P_1}{d\omega}\Big|_{\mathbf{X^0}} \\ \vdots \\ \frac{\partial P_i}{d\omega}\Big|_{\mathbf{X^0}} \end{bmatrix}$$

$$\mathbf{J_{QV}} = \begin{bmatrix} \frac{\partial Q_1}{dV_1}\Big|_{\mathbf{X^0}} & \cdots & \frac{\partial Q_1}{dV_i}\Big|_{\mathbf{X^0}} \\ \vdots & & \vdots \\ \frac{\partial Q_i}{dV_1}\Big|_{\mathbf{X^0}} & \cdots & \frac{\partial Q_i}{dV_i}\Big|_{\mathbf{X^0}} \end{bmatrix} \quad \mathbf{J_{Q\delta}} = \begin{bmatrix} \frac{\partial Q_1}{d\delta_1}\Big|_{\mathbf{X^0}} & \cdots & \frac{\partial Q_1}{d\delta_i}\Big|_{\mathbf{X^0}} \\ \vdots & & \vdots \\ \frac{\partial Q_i}{d\delta_1}\Big|_{\mathbf{X^0}} & \cdots & \frac{\partial Q_i}{d\delta_i}\Big|_{\mathbf{X^0}} \end{bmatrix} \quad \mathbf{J_{Q\omega}} = \begin{bmatrix} \frac{\partial Q_1}{d\omega}\Big|_{\mathbf{X^0}} \\ \vdots \\ \frac{\partial Q_i}{d\omega}\Big|_{\mathbf{X^0}} \end{bmatrix}$$

The conventional expression of the Jacobian matrix for the powerflow equations are as follow:

$$\forall i \neq j, \qquad \frac{\partial P_i}{\partial \delta_j} = -V_i V_j \left|Y_{ij}\right| \sin(\delta_i - \delta_j - \theta_{ij})$$

$$\frac{\partial P_i}{\partial \delta_i} = V_i \sum_{\substack{j=1 \\ j \neq i}} V_j \left| Y_{ij} \right| \sin(\delta_i - \delta_j - \theta_{ij})$$

$$\forall i \neq j, \qquad \frac{\partial P_i}{\partial V_j} = -V_i \left| Y_{ij} \right| \cos(\delta_i - \delta_j - \theta_{ij})$$

$$\frac{\partial P_i}{\partial V_i} = -V_i \left| Y_{ii} \right| \cos(\theta_{ij}) - \sum_{\substack{j=1 \\ j \neq i}} V_j \left| Y_{ij} \right| \cos(\delta_i - \delta_j - \theta_{ij})$$

$$\forall i \neq j, \qquad \frac{\partial Q_i}{\partial \delta_j} = V_i V_j \left| Y_{ij} \right| \cos(\delta_i - \delta_j - \theta_{ij})$$

$$\frac{\partial Q_i}{\partial \delta_i} = -V_i \sum_{\substack{j=1 \\ j \neq i}} V_j \left| Y_{ij} \right| \cos(\delta_i - \delta_j - \theta_{ij})$$

$$\forall i \neq j, \qquad \frac{\partial Q_i}{\partial V_j} = -V_i \left| Y_{ij} \right| \sin(\delta_i - \delta_j - \theta_{ij})$$

$$\frac{\partial Q_i}{\partial V_i} = V_i \left| Y_{ii} \right| \sin(\theta_{ij}) - \sum_{\substack{j=1 \\ j \neq i}} V_j \left| Y_{ij} \right| \sin(\delta_i - \delta_j - \theta_{ij})$$

$$\frac{\partial P_i}{\partial \omega} = -V_i \sum_{\substack{j=1 \\ j \neq i}} V_j \left[\frac{\partial Y_{ij}}{\partial \omega} \cos(\delta_i - \delta_j - \theta_{ij}) + \frac{\partial \theta_{ij}}{\partial \omega} \left| Y_{ij} \right| \sin(\delta_i - \delta_j - \theta_{ij}) \right]$$

$$\frac{\partial Q_i}{\partial \omega} = -V_i \sum_{\substack{j=1 \\ j \neq i}} V_j \left[\frac{\partial Y_{ij}}{\partial \omega} \sin(\delta_i - \delta_j - \theta_{ij}) - \frac{\partial \theta_{ij}}{\partial \omega} \left| Y_{ij} \right| \cos(\delta_i - \delta_j - \theta_{ij}) \right]$$

with

$$\frac{\partial Y_{ij}}{\partial \omega} = -\frac{\frac{X_{ij}^2}{\omega}}{(R_{ij}^2 + X_{ij}^2)^{3/2}} = -\frac{L_{ij}^2 \omega}{(R_{ij}^2 + L_{ij}^2 \omega^2)^{3/2}}$$

$$\frac{\partial \theta_{ij}}{\partial \omega} = -\frac{\frac{X_{ij}}{R_{ij}\omega}}{1 + \left(\frac{X_{ij}}{R_{ij}}\right)^2} = -\frac{\frac{L_{ij}}{R_{ij}}}{1 + \frac{L_{ij}^2 \omega^2}{R_{ij}}}$$

In addition, droop controller induces modification on the Jacobian, and therefore, the partial derivative of the active power with respect to the system frequency, and of the reactive power with respect to the node voltage should be updated as follows:

$$\frac{\partial P_i}{\partial \omega} = -K_i^p - V_i \sum_{\substack{j=1 \\ j \neq i}} V_j \left[\frac{\partial Y_{ij}}{\partial \omega} \cos(\delta_i - \delta_j - \theta_{ij}) + \frac{\partial \theta_{ij}}{\partial \omega} \left| Y_{ij} \right| \sin(\delta_i - \delta_j - \theta_{ij}) \right]$$

$$\frac{\partial Q_i}{\partial V_i} = -K_i^q + V_i\,|Y_{ii}|\sin(\theta_{ij}) - \sum_{\substack{j=1\\ j\neq i}} V_j\,|Y_{ij}|\sin(\delta_i - \delta_j - \theta_{ij})$$

Appendix B

Micro-grid test-bench topology and parameters

The following appendix presents the topology of the radial micro-grid used for simulations and comparison through this thesis. The network topology is presented in Figure B.1, and the characteristics of the lines and DER on Table B.1, B.2 and B.3. The flexibilities of DER and associated capability diagram are depicted in Figure B.2.

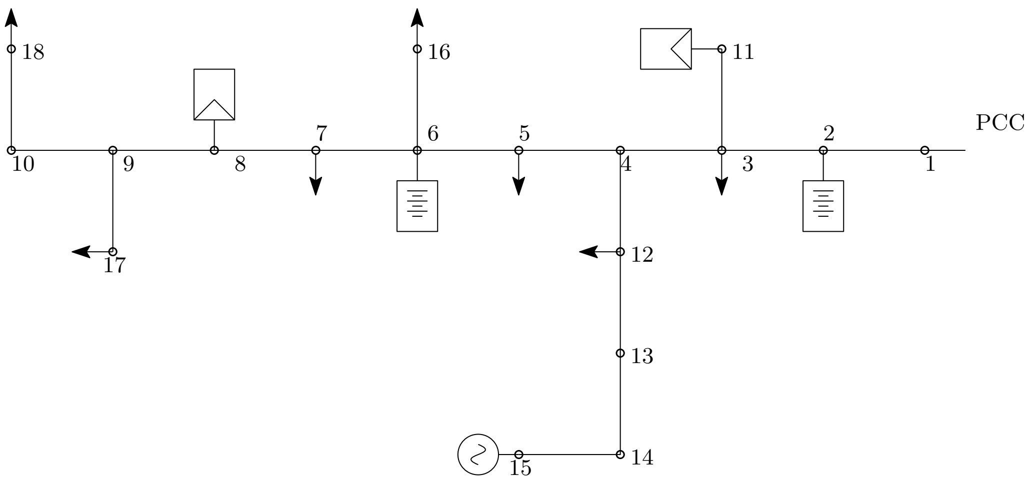

Figure B.1: Microgrid network topology and DER positions

Table B.1: DER parameters

Type	**Node**	P_{nom} **[kW]**	**Flexibility**
PV	8	100	3
PV	11	50	3
ESS	2	100	1
ESS	17	100	1
Genset	15	100	2

Table B.2: Line parameters

Type	R [Ohm]	X [Ohm]
1	0.170	0.087
2	0.280	0.087
3	0.353	0.091

Table B.3: Line characteristics

Line		Type	Length [m]
From	To		
1	2	3	45
2	3	3	50
3	4	3	50
4	5	3	75
5	6	3	75
6	7	3	85
7	8	3	45
8	9	2	95
9	10	2	35
3	11	2	30
4	12	3	20
12	13	3	25
13	14	2	125
14	15	2	85
6	16	2	125
10	18	1	45
17	9	2	85

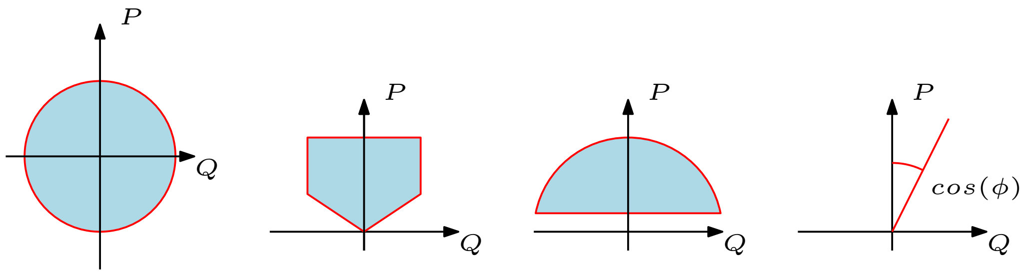

Figure B.2: DER flexibilities and capability diagrams

Appendix C

Network model with PCC interactions

Notations

$\mathbf{J}$ is the inverse Jacobian matrix of the network, $\mathbf{J_{slack}}$ is the matrix of the partial derivatives of the angles and voltage magnitudes with respect the the PCC voltage[1] and $\mathbf{J_{pcc}}$ is the aggregation of the partial derivatives of the active and reactive power at the PCC with respect to the angles and voltage magnitudes. The bold variables denote a matrix or vector. For the sake of simplicity, we also introduce the notations for part of the Jacobian matrix, as $\mathbf{J}(1,1)$, $\mathbf{J}(1,2)$, $\mathbf{J}(2,1)$, $\mathbf{J}(2,2)$ for the upper left, upper right, lower left and lower right part of the Jacobian $\mathbf{J}$ respectively,

$$\mathbf{J} = \begin{bmatrix} \mathbf{J}(1,1) & \mathbf{J}(1,2) \\ \mathbf{J}(2,1) & \mathbf{J}(2,2) \end{bmatrix} \tag{C.1}$$

The same holds for $\mathbf{J_{slack}}$ with $\mathbf{J_{slack}}(1)$ and $\mathbf{J_{slack}}(2)$, the upper and lower part of $\mathbf{J_{slack}}$

$$\mathbf{J_{slack}} = \begin{bmatrix} \mathbf{J_{slack}}(1) \\ \mathbf{J_{slack}}(2) \end{bmatrix} \tag{C.2}$$

and for $\mathbf{J_{pcc}}$

$$\mathbf{J_{pcc}} = \begin{bmatrix} \mathbf{J_{pcc}}(1) \\ \mathbf{J_{pcc}}(2) \end{bmatrix} \tag{C.3}$$

Last, a bold variable denotes a vector (i.e $\mathbf{\Delta V}$ denote the voltage deviation for the micro-grid nodes).

Model development

Let's recall the non linear formulation of the power flow equations:

$$\begin{aligned} P_i &= V_i \sum_{j \in N} V_j \, |Y_{ij}| \cos(\delta_i - \delta_j - \theta_{ij}) \\ Q_i &= V_i \sum_{j \in N} V_j \, |Y_{ij}| \sin(\delta_i - \delta_j - \theta_{ij}) \end{aligned} \tag{C.4}$$

[1]This matrix is obtain numerically, by the resolution of successive load flows

With the first order Taylor expansion of C.4, and by adding the impact of a change in the PCC voltage magnitude, we obtain

$$\begin{bmatrix} \Delta V \\ \Delta \delta \end{bmatrix} = \mathbf{J^{-1}} \begin{bmatrix} \Delta P \\ \Delta Q \end{bmatrix} + \mathbf{J_{slack}} \Delta V_{pcc} \tag{C.5}$$

with ΔP and ΔQ, the combined deviations of the load and generation power respectively. In our model, ΔV_{pcc} is considered as a disturbance. Therefore we can reformulate C.5

$$\begin{bmatrix} \Delta V \\ \Delta \delta \end{bmatrix} = \mathbf{J} \begin{bmatrix} \Delta P \\ \Delta Q \end{bmatrix}_{load} + \mathbf{J} \begin{bmatrix} \Delta P \\ \Delta Q \end{bmatrix}_{gen} \tag{C.6}$$

without loss of generalities, we consider in the remainder that the diesel generators or conventional generators can be modeled as the droop converter with a null droop gain. The equations of the droop-controlled converter are

$$\begin{cases} P_i^{gen}(k+1) - P_i^{ref}(k+1) = -k_i^p.(\omega(k+1) - \omega^*) \\ Q_i^{gen}(k+1) - Q_i^{ref}(k+1) = -k_i^q.(V_i(k+1) - V_i^*) \end{cases} \tag{C.7}$$

which gives,

$$\begin{aligned} \Delta P_i^{gen} &= P_i^{gen}(k+1) - P_i^{gen}(k) \\ &= P_i^{ref}(k+1) - P_i^{ref}(k) - k_i^p.(\omega(k+1) - \omega^*) + k_i^p.(\omega(k) - \omega^*) \end{aligned} \tag{C.8}$$

$$\begin{aligned} \Delta Q_i^{gen} &= Q_i^{gen}(k+1) - Q_i^{gen}(k) \\ &= Q_i^{ref}(k+1) - Q_i^{ref}(k) - k_i^q.(V_i(k+1) - V_i^*) + k_i^q.(V_i(k) - V_i^*) \end{aligned} \tag{C.9}$$

and finally,

$$\Delta P_i^{gen} = \Delta P_i^{ref}(k) - k_i^p \Delta\omega \tag{C.10a}$$

$$\Delta Q_i^{gen} = \Delta Q_i^{ref}(k) - k_i^q \Delta V_i \tag{C.10b}$$

considering

$$\begin{cases} \Delta P_i^{ref}(k) = P_i^{ref}(k+1) - P_i^{ref}(k) \\ \Delta Q_i^{ref}(k) = Q_i^{ref}(k+1) - Q_i^{ref}(k) \end{cases} \tag{C.11}$$

and

$$\Delta\omega = \omega(k+1) - \omega(k) \tag{C.12}$$

In our model, $\Delta\omega$ is considered as a disturbance. Reinjecting C.10b into C.5, we obtain for the voltage

$$\mathbf{\Delta V} = [\mathbf{J}(1,1)\ \mathbf{J}(1,2)] \begin{bmatrix} \mathbf{\Delta P} \\ \mathbf{\Delta Q} \end{bmatrix}_{load} + [\mathbf{J}(1,1)\ \mathbf{J}(1,2)] \begin{bmatrix} \mathbf{\Delta P} \\ \mathbf{\Delta Q} \end{bmatrix}_{gen} + \mathbf{J_{slack}}(1) \Delta V_{pcc} \tag{C.13}$$

which becomes

$$\begin{aligned} \mathbf{\Delta V} = [\mathbf{J}(1,1)\ \mathbf{J}(1,2)] \begin{bmatrix} \mathbf{\Delta P} \\ \mathbf{\Delta Q} \end{bmatrix}_{load} + [\mathbf{J}(1,1)\ \mathbf{J}(1,2)] \begin{bmatrix} \mathbf{\Delta P^{ref}} \\ \mathbf{\Delta Q^{ref}} \end{bmatrix} \\ - \mathbf{J}(1,1)[\mathbf{k^p}]\Delta\omega - \mathbf{J}(1,2)[\mathbf{k^q}]\mathbf{\Delta V} + \mathbf{J_{slack}}(1)\Delta V_{pcc} \end{aligned} \tag{C.14}$$

with $[\mathbf{k^p}]$ the column vector of the active power droop coefficient (0 if the node is not a droop-controlled converter) and $[\mathbf{k^q}]$, a diagonal matrix of the reactive droop coefficients. Finally, the voltage is expressed by

$$\begin{aligned}\mathbf{\Delta V} = &(\mathbb{1} + \mathbf{J}(1,2)[\mathbf{k^q}])^{-1}\left[\mathbf{J}(1,1)\ \mathbf{J}(1,2)\right]\begin{bmatrix}\mathbf{\Delta P}\\ \mathbf{\Delta Q}\end{bmatrix}_{load}\\ &+ (\mathbb{1} + \mathbf{J}(1,2)[\mathbf{k^q}])^{-1}\left[\mathbf{J}(1,1)\ \mathbf{J}(1,2)\right]\begin{bmatrix}\mathbf{\Delta P^{ref}}\\ \mathbf{\Delta Q^{ref}}\end{bmatrix}_{load}\\ &- (\mathbb{1} + \mathbf{J}(1,2)[\mathbf{k^q}])^{-1}\mathbf{J}(1,1)[\mathbf{k^p}]\Delta\omega\\ &+ (\mathbb{1} + \mathbf{J}(1,2)[\mathbf{k^q}])^{-1}\mathbf{J_{slack}}(1)\Delta V_{pcc}\end{aligned} \tag{C.15}$$

Next, we can formulate the evolution of the angle a function of the power deviations and of the PCC voltage and frequency deviations,

$$\begin{aligned}\mathbf{\Delta}\delta = &\left[\mathbf{J}(2,1)\ \mathbf{J}(2,2)\right]\begin{bmatrix}\mathbf{\Delta P}\\ \mathbf{\Delta Q}\end{bmatrix}_{load} + \left[\mathbf{J}(2,1)\ \mathbf{J}(2,2)\right]\begin{bmatrix}\mathbf{\Delta P^{ref}}\\ \mathbf{\Delta Q^{ref}}\end{bmatrix}\\ &- \mathbf{J}(2,1)[\mathbf{k^p}]\Delta\omega + \mathbf{J_{slack}}(2)\Delta V_{pcc}\\ &- \mathbf{J}(2,2)[\mathbf{k^q}](\mathbb{1} + \mathbf{J}(1,2)[\mathbf{k^q}])^{-1}\left[\mathbf{J}(1,1)\ \mathbf{J}(1,2)\right]\begin{bmatrix}\mathbf{\Delta P}\\ \mathbf{\Delta Q}\end{bmatrix}_{load}\\ &- \mathbf{J}(2,2)[\mathbf{k^q}](\mathbb{1} + \mathbf{J}(1,2)[\mathbf{k^q}])^{-1}\left[\mathbf{J}(1,1)\ \mathbf{J}(1,2)\right]\begin{bmatrix}\mathbf{\Delta P^{ref}}\\ \mathbf{\Delta Q^{ref}}\end{bmatrix}\\ &+ \mathbf{J}(2,2)[\mathbf{k^q}](\mathbb{1} + \mathbf{J}(1,2)[\mathbf{k^q}])^{-1}\left[\mathbf{J}(1,1)\right][\mathbf{k^p}]\Delta\omega\\ &- \mathbf{J}(2,2)[\mathbf{k^q}](\mathbb{1} + \mathbf{J}(1,2)[\mathbf{k^q}])^{-1}\mathbf{J_{slack}}(1)\Delta V_{pcc}\end{aligned} \tag{C.16}$$

With these expressions, we can remove the algebraic relation in the reactive power droop equation C.10b,

$$\begin{aligned}\mathbf{\Delta Q^{gen}} =&\mathbf{\Delta Q^{ref}}\\ &- [\mathbf{k^q}](\mathbb{1} + \mathbf{J}(1,2)[\mathbf{k^q}])^{-1}\left[\mathbf{J}(1,1)\ \mathbf{J}(1,2)\right]\begin{bmatrix}\mathbf{\Delta P}\\ \mathbf{\Delta Q}\end{bmatrix}_{load}\\ &- [\mathbf{k^q}](\mathbb{1} + \mathbf{J}(1,2)[\mathbf{k^q}])^{-1}\left[\mathbf{J}(1,1)\ \mathbf{J}(1,2)\right]\begin{bmatrix}\mathbf{\Delta P^{ref}}\\ \mathbf{\Delta Q^{ref}}\end{bmatrix}\\ &+ [\mathbf{k^q}](\mathbb{1} + \mathbf{J}(1,2)[\mathbf{k^q}])^{-1}\mathbf{J}(1,1)\Delta\omega\\ &- [\mathbf{k^q}](\mathbb{1} + \mathbf{J}(1,2)[\mathbf{k^q}])^{-1}\mathbf{J_{slack}}(1)\Delta V_{pcc}\end{aligned} \tag{C.17a}$$

$$\mathbf{\Delta P^{gen}} = \mathbf{\Delta P^{ref}} - [\mathbf{k^p}]\Delta\omega \tag{C.17b}$$

The last element to model is the behavior of the PCC. We assume the angle to be constant, and equals to zero, and the voltage magnitude as

$$V_{pcc}(k+1) = V_{pcc}(k) + \Delta V_{pcc} \tag{C.18}$$

The active and reactive power at the interface can be derived by the first order Taylor expansion of the power flow equations, and by replacing the voltage magnitudes and angles deviations within the micro-grid by their analytical expressions C.15 and C.16, to obtain

$$\begin{bmatrix} \Delta P \\ \Delta Q \end{bmatrix}_{pcc} = \mathbf{J_{pcc}} \begin{bmatrix} \Delta V \\ \Delta \delta \end{bmatrix} \tag{C.19}$$

Finally, we obtain the linear model as,

$$\begin{bmatrix} \mathbf{\Delta V} \\ \mathbf{\Delta} \delta \\ \omega \\ \mathbf{P^{ref}} \\ \mathbf{Q^{ref}} \\ \mathbf{P} \\ \mathbf{Q} \end{bmatrix} (k+1) = \mathbf{A} \begin{bmatrix} \mathbf{\Delta V} \\ \mathbf{\Delta} \delta \\ \omega \\ \mathbf{P^{ref}} \\ \mathbf{Q^{ref}} \\ \mathbf{P} \\ \mathbf{Q} \end{bmatrix} (k) + \mathbf{B} \begin{bmatrix} \mathbf{\Delta P^{ref}} \\ \mathbf{\Delta Q^{ref}} \end{bmatrix} (k) + \mathbf{C} \begin{bmatrix} \mathbf{\Delta P_{load}} \\ \mathbf{\Delta Q_{load}} \\ \mathbf{V}^* \\ \omega^* \\ \Delta V_{pcc} \\ \Delta \omega \end{bmatrix} (k) \tag{C.20}$$

with matrices **A**, **B** and **C** from Equations (C.15), (C.16), (C.17a), (C.17b) and (C.19).

Control of distributed energy resources for primary response of grid interactive micro-grid

Ces travaux portent sur la commande d'un micro-réseau interactif pour fournir des services système à un réseau électrique faible, et plus particulièrement une réponse primaire en fréquence et en tension au point d'interconnection (PCC). Le premier objectif de cette thèse est de superviser un micro-réseau afin d'assurer un fonctionnement stable tout en respectant les objectifs économiques définis par un optimiseur externe.
Dans un second temps, une nouvelle méthodologie en trois étapes a été mise au point. Premièrement, pour fournir les services auxiliaires au PCC, il est nécessaire d'estimer et de coordonner les flexibilités des différents équipements tels que les générateurs d'energie distribués, les énergies renouvelables, les stockages, etc. Un algorithme d'optimisation est proposé pour l'agrégation de ces flexibilités afin de déterminer les flux de puissance active et réactive maximum que le micro-réseau peut fournir. La deuxième étape détermine le comportement possible du micro-réseau à son PCC. Enfin, deux nouveaux algorithmes de contrôle ont été développés pour assurer un comportement de type statisme au PCC. Une première solution, basée sur un superviseur centralisé et la commande prédictive, assure un ajustement en temps réel des points de consigne. La seconde est une solution distribuée qui détermine de nouvelles lois de contrôle locales primaires pour les différents actionneurs. L'efficacité des deux architectures de contrôle a été validée par simulation sur un modèle de micro-réseau de référence.

Mots-clés

«Micro-réseau interactif», «Control primaire», «Contrôle prédictif», «Contrôle primaire non linéaire»

Control of distributed energy resources for primary response of grid interactive micro-grid

This work focuses on the control of a grid-interactive micro-grid to provide ancillary services to a weak power system, and more particularly a primary frequency and voltage response at the point of common coupling (PCC). The first objective of this thesis is to supervise a micro-grid in order to ensure stable operation while enforcing the economic objectives defined by an external optimizer.
Then, a novel three-step methodology has been developed.First, to provide the ancillary services at the PCC, it is necessary to estimate and coordinate the flexibility of heterogeneous equipment such as distributed generators, renewables, storages, etc. An optimization algorithm is proposed for the aggregation of these flexibilities to deduce the maximum active and reactive power flows that the micro-grid can provide. The second step determines the possible behavior of the micro-grid at its PCC. Finally, two new control algorithms have been developed to ensure a droop-like behavior at the PCC. A first solution, based on a centralized Model Predictive Control based supervisor, ensures a real-time adjustment of the set-points. The second one is a distributed solution that determines new primary local control laws for DERs. The effectiveness of the two control architectures has been validated by simulation with a benchmark micro-grid model.

Keywords

«Grid-interactive Micro-grid», «DER Primary Control», «Model Predictive Control», «Nonlinear Primary Control».

